



**HAL**  
open science

## The Hyades: distance, structure, dynamics, and age

M. Perryman, A. Brown, Y. Lebreton, A. Gomez, C. Turon, G. Cayrel de Strobel, J. Mermilliod, N. Robichon, J. Kovalevsky, F. Crifo

► **To cite this version:**

M. Perryman, A. Brown, Y. Lebreton, A. Gomez, C. Turon, et al.. The Hyades: distance, structure, dynamics, and age. *Astronomy and Astrophysics - A&A*, 1998, 331, pp.81-120. 10.48550/arXiv.astro-ph/9707253 . hal-04639027

**HAL Id: hal-04639027**

**<https://hal.science/hal-04639027>**

Submitted on 9 Jul 2024

**HAL** is a multi-disciplinary open access archive for the deposit and dissemination of scientific research documents, whether they are published or not. The documents may come from teaching and research institutions in France or abroad, or from public or private research centers.

L'archive ouverte pluridisciplinaire **HAL**, est destinée au dépôt et à la diffusion de documents scientifiques de niveau recherche, publiés ou non, émanant des établissements d'enseignement et de recherche français ou étrangers, des laboratoires publics ou privés.

# The Hyades: distance, structure, dynamics, and age<sup>\*</sup>

M.A.C. Perryman<sup>1,2</sup>, A.G.A. Brown<sup>1</sup>, Y. Lebreton<sup>3</sup>, A. Gómez<sup>3</sup>, C. Turon<sup>3</sup>, G. Cayrel de Strobel<sup>3</sup>, J.C. Mermilliod<sup>4</sup>, N. Robichon<sup>3</sup>, J. Kovalevsky<sup>5</sup>, and F. Crifo<sup>3</sup>

<sup>1</sup> Sterrewacht Leiden, Postbus 9513, 2300 RA Leiden, The Netherlands

<sup>2</sup> Astrophysics Division, European Space Agency, ESTEC, Noordwijk 2200 AG, The Netherlands

<sup>3</sup> DASGAL/URA CNRS 335, Section d'Astrophysique, Observatoire de Paris, F-92195 Meudon Cedex, France

<sup>4</sup> Université de Lausanne, Chavannes-des-Bois, CH-1290, Switzerland

<sup>5</sup> Observatoire de la Côte d'Azur, CERGA, Avenue Copernic, F-06130 Grasse, France

Received 20 March 1997 / Accepted 16 July 1997

**Abstract.** We use absolute trigonometric parallaxes from the Hipparcos Catalogue to determine individual distances to members of the Hyades cluster, from which the 3-dimensional structure of the cluster can be derived. Inertially-referenced proper motions are used to rediscuss distance determinations based on convergent-point analyses. A combination of parallaxes and proper motions from Hipparcos, and radial velocities from ground-based observations, are used to determine the position and velocity components of candidate members with respect to the cluster centre, providing new information on cluster membership: 13 new candidate members within 20 pc of the cluster centre have been identified. Farther from the cluster centre there is a gradual merging between certain cluster members and field stars, both spatially and kinematically. Within the cluster, the kinematical structure is fully consistent with parallel space motion of the component stars with an internal velocity dispersion of about  $0.3 \text{ km s}^{-1}$ . The spatial structure and mass segregation are consistent with  $N$ -body simulation results, without the need to invoke expansion, contraction, rotation, or other significant perturbations of the cluster. The quality of the individual distance determinations permits the cluster zero-age main sequence to be accurately modelled. The helium abundance for the cluster is determined to be  $Y = 0.26 \pm 0.02$  which, combined with isochrone modelling including convective overshooting, yields a cluster age of  $625 \pm 50 \text{ Myr}$ . The distance to the observed centre of mass (a concept meaningful only in the restricted context of the cluster members contained in the Hipparcos Catalogue) is  $46.34 \pm 0.27 \text{ pc}$ , corresponding to a distance modulus  $m - M = 3.33 \pm 0.01 \text{ mag}$  for the objects within 10 pc of the cluster centre (roughly corresponding to the tidal radius). This distance modulus is close to, but significantly better determined than, that derived from recent high-precision radial velocity studies, somewhat larger than that indicated by recent ground-

based trigonometric parallax determinations, and smaller than those found from recent studies of the cluster convergent point. These discrepancies are investigated and explained.

**Key words:** astrometry – parallaxes – HR Diagram – Hyades – distance scale

---

## 1. Introduction

The considerable importance of the Hyades cluster in studies of Galactic structure, in the understanding of the chemical evolution of the Galaxy, and in the determination of the Population I distance scale, is well documented in the literature. The nearest moderately rich cluster, with some 300 possible members, a total mass of some 300–400  $M_{\odot}$ , and an age of around 600–800 Myr, it has an extension in the sky of about 20 degrees. Although uncertainty in the distances of individual members has limited the definition of the cluster's main sequence, and thereby its helium content and corresponding evolutionary sequence, it has nevertheless been used as the basic observational material for several fundamental relationships in astrophysics, including the location of the main sequence in the Hertzsprung-Russell diagram and the mass-luminosity relationship, as well as forming the basis for the determination of luminosities of supergiants, OB stars, and peculiar stars in clusters. Determinations of the distance to the cluster have provided the zero-point for distances within our Galaxy and, indirectly through the Cepheids, one of the foundations on which the extragalactic distance scale ultimately rests.

At 40–50 pc, the Hyades cluster is somewhat beyond the distance where the parallaxes of individual stars are easily measured, or generally considered as fully reliable, from ground-based observations. Over almost a century, considerable effort using a wide variety of indirect methods has therefore been brought to bear on the problem of establishing the distance to

---

\* Based on observations made with the ESA Hipparcos astrometry satellite. Table 2 is also available in electronic form at the CDS via anonymous ftp to cdsarc.u-strasbg.fr (130.79.128.5) or via <http://cdsweb.u-strasbg.fr/Abstract.html>

the cluster. Distance estimates have been based on a variety of geometrical manifestations of a cluster of stars participating in a uniform space motion, while other estimates have been based on the average trigonometric parallax for a number of cluster stars, dynamical parallaxes for binaries, and photometric parallaxes using a variety of photometric systems. Nevertheless, the details of the HR and mass-luminosity diagrams remain imprecisely established due to limitations in the accuracy of the parallaxes of the individual members, while the distance of the cluster is still open to debate: recent estimates of the distance modulus range from 3.16 based on trigonometric parallaxes (Gatewood et al. 1992), 3.40 based on convergent-point analyses using proper motions from the FK5 and PPM Catalogues (Schwan 1991), and 3.42 based on recent Hubble Space Telescope FGS observations (van Altena et al. 1997a).

The present work is inspired by the availability of the final results of the Hipparcos astrometry mission, which provide a radical improvement in astrometric data on all stars in the Hipparcos observing programme, including approximately 240 candidate Hyades members. The Hipparcos results offer the following principal improvements: (1) standard errors of the annual proper motions of typically 1 milliarcsec (mas) with respect to an inertial (extragalactic) reference frame; (2) absolute trigonometric parallaxes with standard errors of order 1 mas; (3) systematic errors of the astrometric parameters below around 0.1 mas (or mas/yr); (4) parameter determination, or indications, of double or multiple systems for component separations larger than about 0.1 arcsec and  $\Delta m \lesssim 3$  mag; (5) precise photometry and detailed variability indicators based on the Hipparcos broad-band magnitude  $H_p$ ; (6) homogeneous  $B - V$  and  $V - I$  colour indices.

Literature on the Hyades distance determination is considerable: this paper is intended neither as a comprehensive review nor a critical evaluation of the previous estimates in the light of the Hipparcos results. Neither does it aim to answer unambiguously the question ‘what is the distance to the Hyades’, a somewhat nebulous problem given the resolution in radial distance provided by the Hipparcos parallaxes, and the sensitivity of the results to the precise qualification of distance: if the distance of the centre of mass is the objective, membership criteria, selection effects, and M/L relationships become critical. Rather, our objective is to reconcile previous distance estimates based on the availability of reliable absolute trigonometric parallaxes, assign improved membership probabilities, and thereafter probe both the cluster dynamics and the assumptions on which previous distance determinations have rested. Finally, we will define the observational main sequence based on a subset of objects for which membership is secure and observational data particularly reliable, and compare this with theoretical determinations of the Hyades zero-age main sequence based on knowledge of the cluster’s metallicity.

In order to establish the complexities of the problem, Sect. 2 provides a summary of (some of) the distance determinations discussed in the literature to date, with particular reference to the agreement or disagreement between the results of the various convergent-point analyses and distance estimates derived

by other means. Sect. 3 summarises the data, both from the Hipparcos Catalogue and from the published literature, used for the present study. Selection effects entering the list of candidates for this study are also discussed.

The development of the paper then proceeds as follows. In Sect. 4, we examine the improvement brought by the Hipparcos proper motions (and their connection to an inertial frame) which, as we shall demonstrate, permit a significant advance in the understanding of the systematic effects entering previous evaluations of the distance to the Hyades based on convergent-point analyses. New insights and the limitations of this approach applied to the Hyades are discussed. In Sect. 5 we use the Hipparcos absolute trigonometric parallaxes to determine a statistically significant distance estimate for each candidate member, eventually permitting a provisional mean cluster distance to be defined. This is carried out in parallel with a combination of the parallaxes and proper motions with published and unpublished radial velocities to determine the position and velocity components of candidate members with respect to a reference cluster centre. In Sect. 6 we discuss the Hipparcos parallaxes: first we combine the information coming from the Hipparcos parallaxes and proper motions, and demonstrate their mutual consistency. Then we examine the differences between ground-based and Hipparcos parallaxes. Finally, we examine effects (in particular ‘Lutz-Kelker’ type corrections) which complicate the direct interpretation of the Hipparcos parallaxes.

In Sects. 7 and 8 we examine the spatial distribution and dynamics of the cluster, looking at the question of mass segregation, and comparing our present results with published  $N$ -body simulations. We examine the velocity residuals of each member, which can be fully explained on the basis of the observational errors. We also examine the consistency of these results with previous estimates of the rotation, flattening, and internal velocity dispersion of the system.

Finally, in Sect. 9, we restrict our list of Hyades candidates to those showing no existing evidence for multiplicity, and construct the resulting observational main-sequence, comparing it with new models for the zero-age main sequence. From this, the cluster helium abundance is estimated, and this information is used to construct isochrones from which an estimate of the cluster age is determined.

## 2. Distance determinations to date

Under certain conditions which are at least reasonably well represented in the Hyades, the common proper motion of stars in a cluster can be used in the well-established, but nonetheless ingenious ‘convergent-point’ method of distance determination. Since all distance determinations employed for the Hyades have either been based on this method, or have been judged according to their agreement or otherwise with it, a short review of its theoretical basis and a comparison between its results and those obtained by other methods over the years is in order. Reviews of the various distance determination methods include those by van Altena (1974), Hanson (1980), and Turner et al. (1994). We will not discuss details of distance estimates based on photomet-

**Table 1.** Distance determinations ordered by date (... indicates one or more co-authors). The distance modulus (D.M.) is taken or derived from the original reference, occasionally with some uncertainty as to a definitive value (and not necessarily in agreement with values referred to in subsequent compilations).

D.M.	Year	Author	Method
2.75	1939	Smart	Convergent point
2.91	1945	Seares	Convergent point
3.03±0.06	1952	van Bueren	Convergent point (GC, N30, NWZC)
2.85	1955	Pearce	Convergent point
3.08	1956	Heckmann...	Convergent point
3.04	1965	Wayman...	Convergent point
3.23±0.12	1967	Wallerstein...	Dynamical parallaxes
3.14±0.19	1967	Eggen	Trigonometric parallaxes (Yale)
3.37	1967	Iben	Stellar interiors
3.08±0.07	1969	Sears...	Stebbins photometric parallaxes
3.10±0.06	1969	Eggen	R-I photometric parallaxes
3.25±0.20	1969	Helfer	Wilson-Bappu
3.09±0.06	1970	Upton	pm gradient (FK4, N30, Yale, SAO)
3.23±0.25	1970	Lutz	Wilson-Bappu
3.19±0.06	1971	Upton	UBV photometric parallaxes
3.25±0.20	1972	Golay	Geneva photometric parallaxes
3.30	1972	Iben...	Stellar interiors
3.23	1973	Koester...	Stellar interiors
3.21	1974	van Altena	Mean of secondary indicators
3.29±0.20	1974	Uppgren	Trigonometric parallaxes (van Vleck)
3.29±0.08	1975	Hanson	Compilation of methods to date
3.19±0.15	1975	Klemola...	Trigonometric parallaxes (Lick)
3.19±0.04	1975	Corbin...	Proper motions from meridian circles
3.42±0.20	1975	Hanson	Absolute pm's wrt extragalactic
3.18±0.16	1977	McAllister	Absolute pm's corrected
3.10±0.17	1977	Buchholz	GCTSP + systematic corrections
3.32±0.06	1977	Hanson	Proper motion gradients
3.30±0.04	1980	Hanson	Weighted mean of geometric methods
3.25±0.08	1980	Hanson	Trigonometric parallaxes
3.40±0.29	1981	Hauck	Gliese/field + Lutz-Kelker correction
3.30	1981	Hardorp	Masses of visual binaries
3.47±0.05	1982	McClure	Masses of visual binaries
3.20	1982	Eggen	Photoelectric photometry of 72 stars
3.30	1983	Morris...	Convergent point
3.45±0.05	1984	VandenBerg...	Stellar evolution theory
3.23	1984	Detweiler...	Revised radial velocity
3.26±0.11	1985	Cameron	Main sequence versus Gliese stars
3.33	1985	Stefanik...	Vrad (212 stars) + Hanson pm
3.42±0.10	1987	Loktin...	Proper motion geometry in FK4
3.36±0.05	1987	Peterson...	McClure data plus new photometry
3.28±0.10	1988	Gunn...	Vrad from Griffin + bulk Hanson pm
3.35±0.07	1988	Heintz	5 binaries
3.42±0.10	1989	Loktin...	Proper motion gradient
3.37±0.07	1990	Schwan	Proper motions from 44 FK5
3.30±0.10	1990	Uppgren...	Parallaxes (van Vleck, 23 stars)
3.18±0.09	1991	Patterson...	Parallaxes (McCormick, 10 stars)
3.40±0.04	1991	Schwan	Proper motions from 145 FK5/PPM
3.45±0.06	1992	Morris	Convergent point
3.16±0.10	1992	Gatewood...	Parallax of 51 Tauri
3.20±0.06	1992	Gatewood...	Mean parallaxes to date
3.2 ±0.1	1994	Turner...	Combined methods
3.40±0.07	1997a	Torres...	Orbital parallax 51 Tau (propagated)
3.38±0.11	1997b	Torres...	Orbital parallax 70 Tau (propagated)
3.39±0.08	1997c	Torres...	Orbital parallax 78 Tau (propagated)
3.42±0.09	1997a	van Altena...	HST FGS observations of 7 objects
3.32±0.06	1997b	van Altena...	Mean ground parallaxes to date

ric parallaxes (see, e.g., van Altena 1974, Turner et al. 1994). A summary is given in Table 1.

From simple dynamical arguments it can be shown that, for an open cluster of a few hundred stars within a volume of a few parsecs in radius, moving together under their mutual gravitation, the internal velocity dispersion is of the order of  $1 \text{ km s}^{-1}$  or less, and thus small compared with the typical linear veloc-

ity of the cluster as a whole relative to the Sun,  $\mathbf{v}$  (the Hyades cluster has a space motion of approximately  $45 \text{ km s}^{-1}$  with respect to the Sun, presumably reflecting the velocity of the cloud in which the cluster formed). Provided that the cluster is sufficiently nearby to extend over an area of, say, several degrees, the parallel motions of the stars in space yield, on the celestial sphere, directions of proper motions that appear to converge on a unique point – the direction of the unit vector  $\langle \mathbf{v} \rangle$  is known as the convergent point. If  $\mathbf{b}$  is the barycentric coordinate vector to a cluster member, and  $\langle \mathbf{b} \rangle$  its coordinate direction then, neglecting the internal velocity dispersion, the radial velocity is  $\rho = \langle \mathbf{b} \rangle' \mathbf{v}$  (the prime symbol associated with matrices and vectors will be used to denote transposition, so that  $\mathbf{x}'\mathbf{y}$  denotes the scalar product of the two vectors). With  $\lambda$  denoting the angular distance between the star and the convergent point, and  $\boldsymbol{\mu}$  the proper motion vector:

$$\langle \mathbf{b} \rangle' \langle \mathbf{v} \rangle = \cos \lambda \quad (1)$$

and:

$$|\boldsymbol{\mu}| = \pi |\mathbf{v}| \sin \lambda / A_v \quad (2)$$

where  $\pi$  is the parallax of the cluster member.  $A_v = 4.74047... \text{ km yr s}^{-1}$  is the astronomical unit expressed in the appropriate form when  $\pi$  and  $\mu$  are expressed in mas and  $\text{mas yr}^{-1}$  respectively. For the Hyades,  $\lambda \simeq 33^\circ$ , the radial velocity  $v_{\text{rad}} \simeq 40 \text{ km s}^{-1}$  in the cluster centre,  $|\mathbf{v}| \simeq 45 \text{ km s}^{-1}$ , and  $|\boldsymbol{\mu}| \sim 100 \text{ mas yr}^{-1}$ .

Although  $\mathbf{v}$  can in principle be determined from the radial velocity measurements alone, its resulting direction is generally not well determined because of the limited angular extent of the cluster; the usual procedure has therefore been to determine  $\langle \mathbf{v} \rangle$  from proper motions, and  $|\mathbf{v}|$  from radial velocities, from which  $\lambda$  is obtained from Eq. (1) and  $\pi$  from Eq. (2).

Although the method is conceptually simple, its application in practice is not so straightforward. Errors in the individual proper motions resulting from measurement errors, or defects in the proper motion system, lead to accidental errors in  $\pi$ , to an error in  $\langle \mathbf{v} \rangle$  and, ultimately, to a systematic bias in  $\lambda$  depending on  $\langle \mathbf{b} \rangle$ . For the Hyades, the streaming motion differs by only 60–70 degrees from that of local field stars towards the solar antapex, so that observational scatter in the proper motions of member stars, and the random motions of field stars, complicates membership selection based only on proper motions.

In the basic convergent-point method it is assumed that the cluster is neither expanding, contracting, or rotating, that the motion of the cluster with respect to the field is large enough to permit accurate membership discrimination, and that the system of proper motions is inertial and without systematic errors. In his review, van Altena (1974) considered that the first two criteria were adequately satisfied, but that information on the proper motion system was incomplete. Hanson (1975) considered the possibility of random motions contributing significantly to the stars' space velocities, as well as the effects of expansion, contraction, or rotation, concluding that any resulting deviations from parallel motion are insignificant at levels affecting the distance determination by the convergent point method. Gunn et

**Table 2.** Data on the membership of the Hyades for the 282 stars in our sample, listed by various authors. Membership or non-membership inferred by the relevant authors are indicated by ‘1’ or ‘0’ in the corresponding column respectively (see text). Entries with ‘-’ in columns (b–m) inclusive are new candidates proposed in this paper. Columns have the following meaning: **(a)** Hipparcos Catalogue (HIP) number; **(b)** van Bueren number (1952, BAN, 11, 385); **(c)** Membership according to van Bueren; **(d)** van Altena number (1969, AJ, 74, 2); **(e)** Membership according to van Altena; **(f)** Hanson number (1975, AJ, 80, 379); **(g)** Membership according to Hanson; **(h)** Pels et al. (Leiden) number (1975, A&A, 43, 423); van Bueren stars have the vB number + 1000; **(i)** Membership according to Pels et al.; **(j)** Sequential number in Table 4 of Griffin et al. (1988, AJ, 96, 172); **(k)** Membership according to Griffin et al.; **(l)** Schwan number (1991, A&A, 243, 386); **(m)** Membership according to Schwan; **(n)** Hipparcos parallax (mas); **(o)** Hipparcos parallax standard error (mas); **(p)** Radial velocity (km s<sup>-1</sup>); **(q)** Error in radial velocity (km s<sup>-1</sup>; # preceding the error indicates SB/RV (column s) with undetermined  $\gamma$  velocity); **(r)** Source of radial velocity; **(s)** SB = spectroscopic binary, RV = radial velocity (possibly) variable; **(t)** H, I, M = star was previously known, or classified by Hipparcos, to have resolved components (from Field H56); this may overlap with the column u flag, but may also indicate visual or wide binary (see text for details); **(u)** C, G, O, V, or X = relevant part of the Hipparcos Double and Multiple Systems Annex, from Field H59, supplemented by S = suspected binary in Hipparcos Catalogue, from Field H61 (see text for details); **(v)** distance,  $d$  (pc), from the cluster centre defined by the 134 stars within  $r < 10$  pc (see Table 3); **(w)** kinematic statistic  $c = \mathbf{z}'\Sigma^{-1}\mathbf{z}$  ( $c = 14.16$  corresponding to  $3\sigma$ ); **(x)** Final membership assigned in this paper (0, 1); ‘?’ indicates possible new members unclassifiable due to unknown radial velocities. Sources of radial velocities: **(0)** Radial velocity unknown; **(1)** Griffin et al. AJ, 96, 172 (1988); AJ, 90, 609 (1985); AJ, 86, 588 (1981); AJ, 83, 1114 (1978); AJ, 82, 176 (1977); A&A, 106, 221 (1982); **(2)** Hipparcos Input Catalogue (mainly from R.E. Wilson, 1953); **(3)** Weighted mean of ref. 2 ( $39.6 \pm 1.2$ ) and Kraft, ApJ, 142, 681 (1965,  $38.4 \pm 1.5$ ); **(4)** Kraft, ApJ, 142, 681 (1965,  $37.4 \pm 0.4$  and  $36.5 \pm 0.5$ ); Cheriguene, A&A, 13, 447 (1971,  $37.3 \pm 0.7$ ); **(5)** McClure, ApJ, 254, 606 (1982); **(6)** Torres et al., ApJ, 474, 256 (1997); **(7)** Mayor & Mazeh, A&A, 171, 157 (1987); **(8)** Kraft, ApJ, 142, 681 (1965); **(9)** Margoni et al., A&AS, 93, 545 (1992); **(10)** Lucy & Sweeney, AJ, 76, 544 (1971); **(11)** Abt & Levy, ApJS, 59, 229; **(12)** Griffin, MNRAS, 155, 1 (1971); **(13)** Andersen & Nordstrom, A&A, 122, 23 (1983); **(14)** Morse et al., AJ, 101, 1495 (1991); **(15)** Detweiler et al., AJ, 89, 1038 (1984); **(16)** Weighted mean of data from Palmer et al., Roy. Obs. Bull., 135 (1968) and Stillwell, PDAO, 7, 337 (1949); **(17)** Tomkin et al., AJ, 109, 780 (1995); **(18)** Heintz, ApJS, 46, 247 (1981); **(19)** Abt, ApJS, 11, 429 (1965); **(20)** Fekel, PASP, 92, 785 (1980); **(21)** Perraud, Journal des Observateurs, 45, 361 (1962); **(22)** Fouts & Sandage, AJ, 91, 1189 (1986; star G83–18); **(23)** Strassmeier et al., A&AS, 72, 291 (1988); **(24)** New Coravel observations provided by J.C. Mermilliod; **(25)** Woolley et al., Royal Obs. Annals, 14, 1; **(26)** Hanson & Vasilevskis, AJ, 88, 844; **(27)** Evans, Bull. Inf. CDS, 15, 121 (1978); **(28)** Orbit recomputed by Mermilliod with period =  $490 \pm 1$  days (from Batten).

HIP	vB		vA		Hanson		Pels		Griffin		Schwan		Parallax		Radial Velocity			Multiplicity			Membership		
	#		#		#		#		#		#		$\pi$	$\sigma_\pi$	$V_r$	$\sigma_V$	s	$V_r$	H56	H59	$d$ (pc)	c	S
(a)	(b)	(c)	(d)	(e)	(f)	(g)	(h)	(i)	(j)	(k)	(l)	(m)	(n)	(o)	(p)	(q)	(r)	(s)	(t)	(u)	(v)	(w)	(x)
10540	157	0	*	-	*	-	*	-	*	-	*	-	24.93	0.88	+26.0	1.2	2	*	*	*	24.6	43.09	0
10672	-	-	-	-	-	-	-	-	-	-	-	-	15.37	1.29	+26.40	0.32	24	*	*	*	37.1	9.81	1
12031	-	-	-	-	-	-	-	-	-	-	-	-	13.44	3.62	*	*	0	*	*	*	41.8	1.11	?
12709	*	-	*	-	*	-	*	-	1	0	*	-	53.89	1.27	+32.15	0.15	1	SB	*	O	30.5	13.10	1
13042	-	-	-	-	-	-	-	-	-	-	-	-	11.18	17.11	*	*	0	*	I	C	51.5	5.40	?
13117	-	-	-	-	-	-	-	-	-	-	-	-	29.67	9.34	+26.6	0.49	24	*	H	C	23.8	4.26	1
13600	-	-	-	-	-	-	-	-	-	-	-	-	18.89	1.29	+30.41	0.23	24	*	*	*	20.1	7.75	1
13684	*	-	*	-	*	-	*	-	3	0	*	-	5.84	0.92	+30.67	0.13	1	*	*	*	130.5	37.89	0
13806	153	0	*	-	*	-	*	-	4	1	*	-	25.77	1.39	+26.62	0.21	1	*	*	*	19.4	0.30	1
13834	154	0	*	-	*	-	*	-	*	-	5	1	31.41	0.84	+28.1	1.2	2	*	*	*	20.5	0.26	1
13976	-	-	-	-	-	-	-	-	-	-	-	-	42.66	1.22	+28.35	0.18	24	*	*	*	26.5	0.38	1
14792	133	1	*	-	*	-	*	-	5	0	177	0	5.13	2.22	+25.99	0.17	1	*	*	*	152.2	11.74	0
14838	-	-	-	-	-	-	-	-	-	-	-	-	19.44	1.23	+24.70	0.50	2	*	*	S	16.4	8.05	1
14976	-	-	-	-	-	-	-	-	-	-	-	-	23.73	1.18	+27.27	0.22	24	*	*	*	18.4	0.68	1
15206	158	0	*	-	*	-	*	-	*	-	*	-	10.74	1.12	+42.8	#0.9	24	SB	*	*	51.1	60.38	0
15300	*	-	*	-	*	-	*	-	6	1	*	-	29.49	4.70	+29.84	0.29	1	*	I	C	18.1	0.79	1
15304	1	1	*	-	*	-	1001	1	8	1	141	1	20.20	1.18	+32.44	0.21	1	*	I	*	16.5	9.27	1
15310	2	1	*	-	*	-	1002	1	9	1	149	0	21.64	1.33	+33.00	0.13	1	*	I	*	15.6	7.12	1
15368	-	-	-	-	-	-	-	-	-	-	-	-	13.76	5.62	*	*	0	*	H	C	32.6	3.66	?
15374	-	-	-	-	-	-	-	-	-	-	-	-	24.54	3.95	*	*	0	*	*	*	15.1	11.05	?
15532	*	-	*	-	*	-	2	1	13	0	*	-	4.48	2.24	+47.27	0.22	1	*	*	*	179.4	107.93	0
15563	*	-	*	-	*	-	*	-	*	-	158	0	34.18	1.70	+30.45	0.26	24	*	*	*	20.7	0.51	1
15720	-	-	-	-	-	-	-	-	-	-	-	-	29.75	2.73	+28.9	0.45	24	*	*	*	17.9	0.47	1
16329	3	1	*	-	*	-	3	1	14	0	164	0	21.61	1.48	+26.67	0.09	1	*	I	G	11.3	36.71	0
16377	-	-	-	-	-	-	-	-	-	-	-	-	10.48	1.61	*	*	0	*	*	*	55.2	11.41	?
16529	4	1	*	-	*	-	1004	1	16	1	46	1	22.78	1.26	+32.72	0.17	1	*	*	*	11.8	0.27	1
16548	-	-	-	-	-	-	-	-	-	-	-	-	17.20	3.36	+26.6	0.34	24	*	*	*	20.0	10.22	1
16896	159	0	*	-	*	-	*	-	20	0	*	-	11.73	1.33	+47.83	0.22	1	*	*	*	41.1	70.94	0
16908	5	1	*	-	*	-	1005	1	21	1	47	1	25.23	1.58	+33.56	0.21	1	*	*	*	11.7	3.86	1
17128	134	1	*	-	*	-	*	-	*	-	178	0	2.47	1.59	+62.4	0.4	26	*	*	*	360.7	163.77	0
17324	*	-	*	-	*	-	*	-	24	0	*	-	1.46	1.13	+31.88	0.26	1	*	*	*	640.1	5.75	0
17605	*	-	*	-	*	-	*	-	28	0	*	-	6.63	1.68	+92.10	0.65	1	*	*	*	106.3	710.47	0
17609	-	-	-	-	-	-	-	-	-	-	-	-	68.62	1.78	+32.20	2.50	2	*	*	*	32.4	8.39	1
17766	*	-	*	-	*	-	*	-	30	1	*	-	24.02	2.27	+35.40	0.25	1	*	*	*	11.4	1.21	1
17779	136	1	*	-	*	-	*	-	31	0	180	0	7.65	0.95	-1.48	0.17	1	*	*	*	86.1	299.33	0
17950	-	-	-	-	-	-	-	-	-	-	-	-	22.22	0.97	*	*	0	*	I	C	16.3	7.53	?
17962	-	-	-	-	-	-	-	-	-	-	-	-	21.37	1.62	+40.00	5.00	2	*	*	*	7.3	0.98	1
18018	170	0	*	-	*	-	6	1	33	1	*	-	24.72	4.62	+35.30	0.12	1	*	*	X	10.3	0.08	1
18096	-	-	-	-	-	-	-	-	-	-	-	-	11.19	1.65	+40.02	0.24	24	*	*	*	44.1	11.14	1
18170	6	1	*	-	*	-	1006	1	*	-	6	1	24.14	0.90	+35.0	2.5	2	*	*	*	8.1	0.27	1

Table 2. Hyades membership compilation summary (2/4)

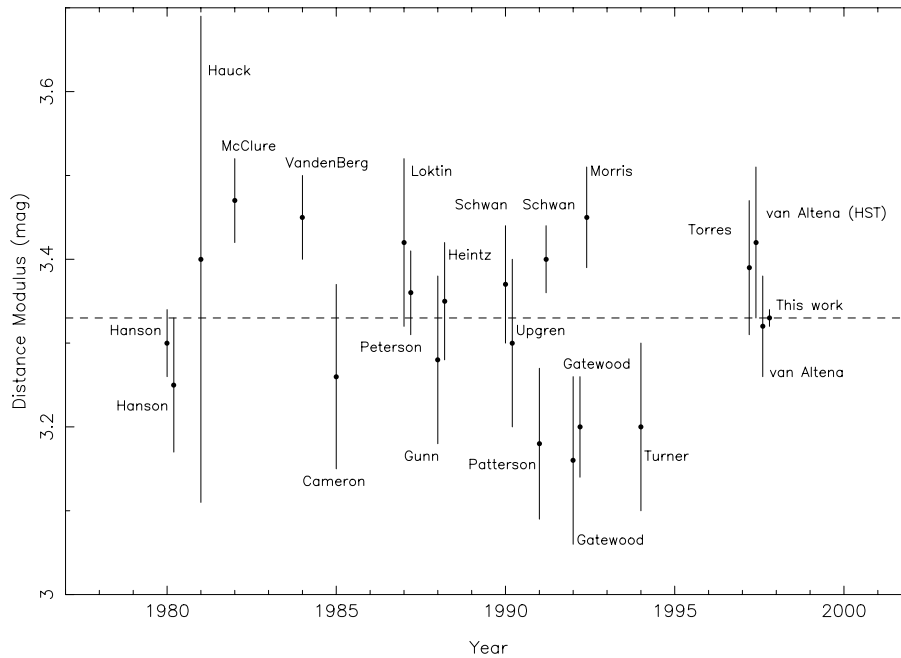
HIP	vB	vA	Hanson	Pels	Griffin	Schwan	Parallax	Radial	Velocity	Multiplicity	Membership												
#	#	#	#	#	#	#	$\pi$	$V_r$	$\sigma_V$	$V_r$ H56 H59	d (pc)												
(a)	(b)	(c)	(d)	(e)	(f)	(g)	(h)	(i)	(j)	(k)	(l)	(m)	(n)	(o)	(p)	(q)	(r)	(s)	(t)	(u)	(v)	(w)	(x)
18322	*	-	*	-	*	-	8	1	36	1	155	0	26.49	1.98	+37.18	0.22	1	*	*	*	10.8	3.82	1
18327	7	1	*	-	*	-	1007	1	37	1	65	1	24.16	1.40	+36.79	0.13	1	*	*	*	7.8	0.21	1
18617	-	-	*	-	*	-	-	-	-	-	-	-	10.38	2.61	*	*	0	*	M	C	54.6	9.52	?
18658	8	1	*	-	*	-	1008	1	*	-	19	1	25.42	1.05	+39.1	1.1	3	*	*	G	9.9	2.97	1
18692	*	-	*	-	*	-	*	-	46	0	*	-	10.93	1.19	+37.94	0.18	1	*	*	*	45.9	13.67	1
18719	9	1	*	-	*	-	1009	1	*	-	*	-	16.04	1.33	+37.0	#2.5	2	SB	*	*	17.5	47.25	0
18735	137	1	*	-	*	-	1137	1	*	-	162	0	21.99	0.81	+31.7	#1.1	2	SB	I	*	5.4	2.84	1
18946	*	-	*	-	*	-	11	1	55	1	146	0	23.07	2.12	+36.93	0.26	1	*	*	*	5.8	0.70	1
18975	160	0	*	-	*	-	*	-	*	-	*	-	27.80	0.95	+34.4	1.5	13	*	*	*	12.7	14.75	0
19082	*	-	*	-	*	-	12	1	57	1	*	-	14.56	3.17	+38.33	0.22	1	*	*	*	23.1	2.20	1
19098	*	-	*	-	*	-	10	1	58	1	*	-	19.81	1.39	+37.61	0.05	1	*	*	*	6.2	1.10	1
19117	*	-	*	-	*	-	*	-	60	0	*	-	29.02	2.12	+37.28	0.13	1	*	*	*	12.9	19.85	0
19148	10	1	*	-	*	-	1010	1	62	1	66	1	21.41	1.47	+38.04	0.17	1	*	*	*	4.3	0.36	1
19207	*	-	*	-	*	-	15	1	65	1	*	-	23.57	2.26	+38.95	0.23	1	*	*	*	5.6	1.01	1
19261	11	1	*	-	*	-	1011	1	68	1	67	1	21.27	1.03	+36.35	0.26	1	*	I	C	4.2	0.71	1
19263	*	-	*	-	*	-	16	1	70	1	*	-	19.70	1.68	+38.72	0.05	1	*	*	*	6.0	0.92	1
19316	*	-	*	-	*	-	14	1	75	1	*	-	24.90	2.59	+38.43	0.28	1	*	*	*	7.9	1.81	1
19365	*	-	*	-	*	-	*	-	79	0	*	-	10.68	1.43	+37.92	0.15	1	*	I	*	49.7	4.75	1
19386	-	-	-	-	-	-	-	-	-	-	-	-	15.37	0.97	+33.6	0.39	24	*	*	*	24.9	6.62	1
19441	*	-	*	-	*	-	*	-	84	1	*	-	29.78	1.90	+39.24	0.16	1	*	*	*	14.1	0.47	1
19449	-	-	-	-	-	-	-	-	-	-	-	-	12.14	2.03	*	*	0	*	*	*	38.7	3.82	?
19472	*	-	14	0	18	0	*	-	*	-	*	-	29.88	2.67	*	*	0	*	M	C	13.2	55.80	0
19481	*	-	19	0	23	0	*	-	*	-	*	-	23.85	1.26	+38.0	4.5	25	*	*	G	6.5	175.60	0
19504	13	1	*	-	*	-	1013	1	*	-	68	1	23.22	0.92	+37.1	0.3	4	*	*	*	4.8	0.14	1
19554	14	1	*	-	*	-	1014	1	*	-	11	1	25.89	0.95	+36.6	#1.2	2	SB	I	*	11.7	0.69	1
19572	138	1	*	-	*	-	1138	1	85	0	165	0	12.91	1.19	+78.24	0.27	1	*	*	S	34.2	401.51	0
19591	*	-	*	-	*	-	20	1	86	1	*	-	27.21	2.11	+36.90	0.26	1	SB	M	C	11.2	0.41	1
19641	*	-	*	-	*	-	*	-	87	0	*	-	11.42	1.27	+26.97	0.15	1	*	*	*	41.4	22.37	0
19696	*	-	51	1	89	1	*	-	90	0	*	-	11.33	1.61	-5.92	0.33	1	*	*	*	42.1	414.42	0
19767	*	-	59	0	100	0	*	-	*	-	*	-	27.98	1.18	+53.4	7.2	25	*	*	*	11.3	98.78	0
19781	17	1	*	-	101	1	1017	1	93	1	69	1	21.91	1.27	+39.24	0.06	1	*	*	*	3.2	1.15	1
19786	18	1	60	1	105	1	1018	1	94	1	70	1	22.19	1.45	+39.32	0.14	1	*	*	*	4.5	0.74	1
19789	16	1	*	-	*	-	1016	1	*	-	48	1	18.12	0.92	+38.4	1.2	2	*	*	*	10.6	0.75	1
19793	15	1	*	-	*	-	1015	1	92	1	49	1	21.69	1.14	+38.21	0.23	1	*	*	*	6.1	0.35	1
19796	19	1	*	-	*	-	1019	1	97	1	71	1	21.08	0.97	+38.50	0.15	1	*	*	*	5.7	0.51	1
19808	*	-	68	1	111	1	23	1	98	1	*	-	22.67	2.30	+40.51	0.15	1	*	*	*	4.4	1.21	1
19834	*	-	72	1	115	1	24	1	99	1	*	-	31.94	3.74	+38.79	0.36	1	*	*	*	15.2	7.86	1
19862	*	-	75	1	119	1	*	-	100	1	*	-	31.11	2.76	+38.96	0.17	1	*	*	*	14.4	7.74	1
19870	162	0	*	-	*	-	1162	1	101	1	50	1	19.48	0.99	+38.46	0.12	1	SB	*	*	6.6	0.50	1
19877	20	1	79	1	122	1	1020	1	*	-	20	1	22.51	0.82	+36.4	1.2	2	*	I	*	3.2	0.44	1
19934	21	1	*	-	*	-	1021	1	103	1	51	1	19.48	1.17	+38.46	0.19	1	*	*	*	7.1	0.11	1
19981	*	-	*	-	*	-	28	1	106	0	*	-	30.56	1.52	+28.82	0.20	1	*	I	*	14.3	21.14	0
20019	22	1	108	1	167	0	1022	1	111	1	72	1	21.40	1.24	+38.18	0.13	1	SB	*	*	2.1	0.83	1
20056	23	1	123	1	178	1	1023	1	*	-	73	1	21.84	1.14	+37.7	0.4	5	SB	*	*	2.4	0.00	1
20082	25	1	133	1	185	1	1025	1	117	1	74	1	20.01	1.91	+39.64	0.08	1	*	*	*	4.1	2.00	1
20086	*	-	135	1	187	1	30	1	118	1	*	-	19.57	1.86	+40.53	0.04	1	*	*	S	5.2	5.45	1
20087	24	1	*	-	*	-	1024	1	*	-	12	1	18.25	0.82	+37.78	0.12	6	SB	I	O	9.7	0.08	1
20130	26	1	*	-	*	-	1026	1	120	1	75	1	23.53	1.25	+39.58	0.06	1	*	*	*	4.9	1.10	1
20146	27	1	156	1	198	1	1027	1	122	1	76	1	21.24	1.32	+38.80	0.08	1	*	*	*	2.0	0.07	1
20187	*	-	171	0	210	0	*	-	125	0	*	-	20.13	2.02	+37.99	0.06	1	*	*	*	5.0	10.97	1
20197	*	-	174	0	*	-	*	-	*	-	*	-	12.93	1.06	-19.10	1.3	12	*	*	*	31.2	657.25	0
20205	28	1	175	1	*	-	1028	1	127	1	1	1	21.17	1.17	+39.28	0.11	1	*	*	*	2.0	0.22	1
20215	29	1	179	1	212	1	1029	1	129	1	77	1	23.27	1.14	+39.21	#0.27	1	SB	I	C	3.7	1.85	1
20219	30	1	182	1	213	1	1030	1	*	-	21	1	22.31	0.92	+42.0	2.5	2	*	I	*	3.0	1.23	1
20226	*	-	*	-	*	-	*	-	130	0	*	-	4.91	0.88	+8.78	0.19	1	*	*	*	157.8	182.99	0
20237	31	1	*	-	*	-	1031	1	132	1	78	1	22.27	0.93	+38.81	0.18	1	*	*	*	2.9	0.21	1
20255	32	1	*	-	*	-	1032	1	*	-	79	1	21.12	0.77	+42.0	#1.2	2	SB	*	*	2.5	8.65	1
20261	33	1	*	-	*	-	1033	1	*	-	22	1	21.20	0.99	+36.2	1.2	2	*	*	*	2.1	0.65	1
20284	34	1	201	1	230	1	1034	1	*	-	23	1	21.80	0.85	+39.2	0.3	7	SB	*	*	2.7	0.53	1
20319	-	-	-	-	-	-	-	-	-	-	-	-	11.64	3.73	*	*	0	*	*	*	41.3	9.00	?
20349	35	1	*	-	*	-	1035	1	*	-	52	1	19.55	0.89	+37.1	1.2	2	*	*	*	6.2	0.23	1
20350	36	1	*	-	*	-	1036	1	*	-	80	1	19.83	0.89	+40.8	2.4	24	*	*	*	4.5	1.43	1
20357	37	1	215	1	246	1	1037	1	137	1	81	1	19.46	1.02	+39.20	0.21	1	*	*	*	5.6	0.54	1
20400	38	1	229	1	257	1	1038	1	*	-	24	1	21.87	0.96	+37.8	2.3	9	SB	I	*	2.5	0.24	1
20415	139	1	*	-	*	-	*	-	139	0	163	0	15.44	1.28	+26.77	0.20	1	*	*	*	22.6	28.11	0
20419	*	-	*	-	*	-	33	1	142	1	82	1	19.17	1.93	+40.77	#0.20	1	SB	*	*	7.5	1.63	1
20440	40	1	249	1	271	1	1040	1	*	-	83	1	21.45	2.76	+37.4	2.9	10	SB	I	C	1.7	0.21	1
20441	39	1	248	0	270	1	1039	1	*	-	25	1	26.96	1.40	+34.8	#2.6	24	SB	*	G	9.3	12.16	1
20455	41	1	256	1	*	-	1041	1	148	1	2	1	21.29	0.93	+39.65	0.08	1	SB	I	*	1.4	0.17	1
20480	42	1	*	-	*	-	1042	1	149	1	53	1	20.63	1.34	+39.24	0.24	1	*	*	*	4.5	0.28	1
20482	43	1	*	-	*	-	1043	1	150	1	84	1	15.82	1.44	+39.90	0.09	1	SB	*	O	17.1	2.57	1
20484	45	1	272	1	288	1	1045	1	*	-	26	1	21.17	0.80	+37.7	0.3	11	SB	*	*	1.3	0.17	1
20485	173	0	276	1	290	1	35																

Table 2. Hyades membership compilation summary (3/4)

HIP	vB	vA	Hanson	Pels	Griffin	Schwan	Parallax	Radial	Velocity	Multiplicity	Membership													
#	#	#	#	#	#	#	$\pi$	$V_r$	$\sigma_V$	$V_r$ H56 H59	d (pc)													
(a)	(b)	(c)	(f)	(h)	(j)	(l)	(n)	(p)	(q)	(s)	(v)													
			(g)	(i)	(k)	(m)	$\sigma_\pi$	$V_r$	$\sigma_V$	(t) (u)	(w)													
										(x)														
20563	174	0	310	1	312	1	39	1	164	1	*	*	*	5.5	1.33	1								
20567	51	1	315	1	316	1	1051	1	*	-	89	1	18.74	1.17	+40.1	0.6	8	*	*	*	7.1	0.81	1	
20577	52	1	319	1	320	1	1052	1	165	1	90	1	20.73	1.29	+38.80	#0.08	1	RV	*	*	*	2.0	0.40	1
20601	140	1	*	-	*	-	1140	1	167	0	142	1	14.97	1.51	+42.20	0.12	1	SB	*	*	*	23.5	8.76	1
20605	*	-	334	1	336	1	*	-	*	-	*	-	24.41	6.94	+40.2	0.36	24	*	H	C	5.4	1.10	1	
20614	53	1	*	-	*	-	1053	1	*	-	28	1	20.40	0.74	+36.6	1.2	2	*	*	*	3.4	1.05	1	
20626	-	-	-	-	-	-	-	-	-	-	-	-	15.92	1.00	*	*	0	*	*	*	18.6	11.59	?	
20635	54	1	*	-	*	-	1054	1	*	-	29	1	21.27	0.80	+38.6	1.2	27	*	I	*	4.7	0.11	1	
20641	55	1	*	-	*	-	1055	1	*	-	30	1	22.65	0.84	+32.0	2.5	2	*	I	*	4.9	3.27	1	
20648	56	1	355	1	*	-	1056	1	*	-	31	1	22.05	0.77	+38.7	1.3	14	*	I	C	1.5	0.05	1	
20661	57	1	360	1	357	1	1057	1	*	-	32	1	21.47	0.97	+39.1	#0.5	15	SB	I	C	0.8	0.56	1	
20679	176	0	363	1	361	1	1176	1	*	-	*	-	20.79	1.83	+37.0	#7.5	21	SB	M	C	2.1	0.82	1	
20686	58	1	*	-	*	-	1058	1	172	1	91	1	23.08	1.22	+40.72	#0.47	1	SB	I	C	3.5	1.04	1	
20693	61	1	*	-	*	-	1061	1	177	0	181	0	22.03	0.90	+29.67	0.30	1	*	*	*	9.3	17.54	0	
20711	60	1	*	-	*	-	1060	1	*	-	13	1	21.07	0.80	+35.6	0.6	16	*	I	*	5.2	1.28	1	
20712	62	1	*	-	*	-	1062	1	178	1	56	1	21.54	0.97	+38.77	0.14	1	SB	*	*	3.9	1.01	1	
20713	141	1	388	1	*	-	1141	1	*	-	93	1	20.86	0.84	+40.8	4.26	19	SB	*	*	1.8	3.65	1	
20719	63	1	389	1	382	1	1063	1	179	1	94	1	21.76	1.46	+39.39	#0.31	1	SB	*	*	0.5	3.35	1	
20741	64	1	400	1	388	1	1064	1	180	1	95	1	21.42	1.54	+40.23	0.28	1	*	*	*	0.4	0.24	1	
20745	*	-	404	1	392	1	48	1	182	1	*	-	28.27	3.17	+41.38	0.18	1	*	M	C	11.3	1.24	1	
20751	*	-	*	-	*	-	59	1	183	1	96	1	23.03	1.66	+41.12	#0.20	1	SB	*	*	5.4	1.32	1	
20762	*	-	407	1	394	1	49	1	184	1	*	-	21.83	2.29	+41.22	0.21	1	*	*	*	2.9	0.43	1	
20810	188	0	444	1	413	1	*	-	190	0	*	-	8.66	2.61	+60.94	0.06	1	*	*	*	69.1	87.60	0	
20815	65	1	446	1	415	1	1065	1	191	1	97	1	21.83	1.01	+39.32	0.24	1	*	*	*	1.0	0.14	1	
20826	66	1	*	-	*	-	1066	1	193	1	98	1	21.18	1.04	+40.22	0.21	1	*	*	*	4.1	0.30	1	
20827	179	0	459	1	417	1	52	1	192	1	*	-	17.29	2.23	+40.46	0.07	1	*	*	*	11.7	1.17	1	
20842	67	1	*	-	*	-	1067	1	*	-	33	1	20.85	0.86	+37.5	3.3	11	*	I	*	4.4	0.12	1	
20850	178	0	472	1	420	1	50	1	196	1	100	1	21.29	1.91	+40.94	0.08	1	*	*	*	2.4	0.27	1	
20873	68	1	485	1	429	1	1068	1	*	-	101	1	18.42	1.93	+40.6	0.3	24	*	*	X	8.1	2.10	1	
20885	71	1	489	1	*	-	1071	1	200	1	34	1	20.66	0.85	+40.17	#0.08	1	SB	I	*	2.1	3.31	1	
20889	70	1	*	-	*	-	1070	1	199	1	3	1	21.04	0.82	+39.37	0.06	1	*	I	*	2.4	0.25	1	
20890	69	1	*	-	*	-	1069	1	198	1	102	1	20.09	1.11	+39.91	0.08	1	SB	*	*	4.3	0.78	1	
20894	72	1	491	1	*	-	1072	1	*	-	35	1	21.89	0.83	+38.9	0.2	17	SB	I	*	0.9	0.05	1	
20899	73	1	495	1	439	1	1073	1	201	1	103	1	21.09	1.08	+39.99	0.16	1	*	*	*	1.2	0.14	1	
20901	74	1	504	1	*	-	1074	1	*	-	14	1	20.33	0.84	+39.9	4.1	11	*	*	*	4.1	0.26	1	
20916	75	1	511	1	448	0	1075	1	*	-	104	1	20.58	1.74	+45.0	#2.5	2	SB	I	C	2.3	3.93	1	
20935	77	1	536	1	461	1	1077	1	209	1	105	1	23.25	1.04	+39.90	0.11	1	SB	*	O	3.4	0.77	1	
20948	78	1	544	1	469	1	1078	1	210	1	106	1	21.59	1.09	+38.62	0.24	1	*	I	*	1.0	0.04	1	
20949	76	1	*	-	*	-	1076	1	208	1	57	1	17.08	1.18	+39.02	0.17	1	*	*	*	15.2	0.47	1	
20951	79	1	547	1	470	1	1079	1	211	1	107	1	24.19	1.76	+40.70	0.06	1	*	I	*	5.1	0.84	1	
20952	*	-	550	0	474	0	*	-	*	-	*	-	7.68	1.27	+96.3	1.2	2	*	*	*	83.9	512.19	0	
20978	180	0	560	1	478	1	56	1	215	1	108	1	24.71	1.27	+40.97	0.06	1	*	*	*	5.9	1.69	1	
20995	80	1	569	1	481	0	1080	1	*	-	171	0	22.93	1.25	+29.3	5.00	18	SB	I	C	2.9	3.30	1	
21008	81	1	*	-	*	-	1081	1	*	-	109	1	19.94	0.93	+38.0	#2.5	2	SB	*	*	4.7	1.28	1	
21019	*	-	*	-	*	-	*	-	216	0	*	-	3.52	1.98	+47.89	0.26	1	*	*	*	237.8	15.22	0	
21029	82	1	584	1	*	-	1082	1	*	-	36	1	22.54	0.77	+41.0	1.8	13	*	I	*	2.1	0.75	1	
21036	84	1	591	1	*	-	1084	1	*	-	38	1	21.84	0.89	+38.8	1.2	2	*	I	*	2.5	0.14	1	
21039	83	1	589	1	493	0	1083	1	*	-	37	1	22.55	1.09	+39.56	0.23	24	SB	I	*	2.2	0.35	1	
21053	85	1	597	1	496	1	1085	1	*	-	111	1	24.28	0.79	+40.9	1.3	8	*	I	*	5.2	3.77	1	
21066	86	1	*	-	*	-	1086	1	220	1	112	1	22.96	0.99	+41.35	0.26	1	*	*	*	5.4	1.03	1	
21092	-	-	-	-	-	-	-	-	-	-	-	-	19.64	9.61	*	*	0	*	H	C	13.3	0.95	?	
21099	87	1	*	-	*	-	1087	1	222	1	58	1	21.81	1.25	+40.62	0.08	1	*	*	*	2.9	0.38	1	
21112	88	1	625	1	507	1	1088	1	224	1	172	0	19.46	1.02	+40.98	0.31	1	*	*	*	5.6	0.44	1	
21123	*	-	627	1	509	1	63	1	225	1	*	-	23.41	1.65	+40.38	0.11	1	SB	*	O	3.8	0.41	1	
21137	89	1	644	1	516	1	1089	1	*	-	39	1	22.25	1.14	+36.0	#2.5	2	SB	*	*	1.7	2.23	1	
21138	191	0	645	1	517	1	62	1	228	1	*	-	15.11	4.75	+41.28	0.21	1	*	*	*	19.9	1.08	1	
21152	90	1	*	-	*	-	1090	1	*	-	143	1	23.13	0.92	+39.8	1.0	24	*	*	*	9.4	0.20	1	
21179	*	-	677	1	532	1	60	1	*	-	*	-	17.55	2.97	+41.70	#1.0	24	SB	*	*	11.1	2.01	1	
21194	*	-	682	0	541	0	*	-	*	-	*	-	9.42	2.76	*	*	0	*	*	*	60.1	69.56	0	
21256	*	-	*	-	*	-	66	1	235	1	*	-	24.98	1.95	+41.39	0.20	1	*	*	*	7.2	1.19	1	
21261	*	-	*	-	*	-	65	1	237	1	*	-	21.06	2.21	+41.43	0.15	1	*	*	*	2.5	0.42	1	
21267	94	1	724	1	574	1	1094	1	*	-	116	1	22.80	0.98	+36.9	0.9	8	*	*	*	3.8	1.38	1	
21273	95	1	725	1	*	-	1095	1	*	-	7	1	21.39	1.24	+37.7	0.9	28	SB	*	O	1.9	1.18	1	
21280	96	1	727	1	578	1	1096	1	*	-	117	1	24.02	1.68	+37.6	#1.2	2	SB	M	C	5.0	2.83	1	
21306	*	-	741	0	593	0	*	-	*	-	*	-	12.62	1.96	-81.8	6.9	22	*	*	*	33.2	375.20	0	
21317	97	1	748	1	598	1	1097	1	241	1	119	1	23.19	1.30	+40.78	0.16	1	*	*	*	3.6	0.53	1	
21332	*	-	751	1	600	1	*	-	*	-	*	-	9.87	1.02	*	*	0	*	*	*	55.0	19.28	0	
21353	98	1	*	-	*	-	*	-	242	0	*	-	6.81	1.34	+28.95	0.19	1	*	*	*	101.9	47.17	0	
21395	*	-	771	1	611	0	*	-	245	0	*	-	13.51	1.32	+40.37	0.24	1	SB	*	*	28.1	14.28	0	
21459	100	1	*	-	*	-	1100	1	*	-	59	1	22.60	0.76	+43.3	1.2	2	*	*	*	5.9	3.40	1	
21474	101	1	*	-	*																			

Table 2. Hyades membership compilation summary (4/4)

HIP	vB	vA	Hanson	Pels	Griffin	Schwan	Parallax	Radial Velocity	Multiplicity	Membership											
#	#	#	#	#	#	#	$\pi$ $\sigma_\pi$	$V_r$ $\sigma_V$ $s$	$V_r$ H56 H59	$d$ (pc) $c$ $S$											
(a)	(b) (c)	(d) (e)	(f) (g)	(h) (i)	(j) (k)	(l) (m)	(n) (o)	(p) (q) (r)	(s) (t) (u)	(v) (w) (x)											
21683	108	1	*	*	1108	1	20.51	0.82	+35.6	2.5	19	*	I	*	3.4	2.91	1				
21684	*	*	*	*	*	*	9.56	1.73	+30.69	0.20	1	*	*	*	58.7	63.17	0				
21723	*	*	*	*	80	1	266	1	24	1	23.95	1.63	+42.50	0.19	1	*	*	5.9	0.53	1	
21741	109	1	*	*	1109	1	267	1	60	1	15.96	1.36	+41.34	0.16	1	*	*	17.7	0.52	1	
21762	185	0	*	*	82	1	269	1	125	1	23.65	2.53	+40.90	0.17	1	SB	M	C	4.7	0.76	1
21788	110	1	*	*	1110	1	270	0	166	0	19.48	1.26	+35.85	0.05	1	*	*	8.3	7.85	1	
21829	163	0	*	*	*	*	*	*	*	*	5.88	0.97	+35.7	1.2	2	*	*	126.7	47.56	0	
21923	*	*	*	*	278	0	*	*	23.23	1.25	*	*	+13.57	0.20	1	*	I	*	4.6	211.77	0
21946	*	*	*	*	279	0	*	*	21.10	2.22	*	*	+14.49	0.23	1	SB	*	*	3.5	178.36	0
21983	*	*	*	*	94	1	281	0	*	*	21.48	1.84	+24.47	0.34	1	SB	*	*	5.4	82.06	0
22044	111	1	*	*	1111	1	*	*	20.73	0.88	+39.6	0.5	2	*	I	*	*	5.9	1.18	1	
22105	*	*	*	*	*	*	282	0	*	*	9.08	1.79	+25.94	0.11	1	*	*	64.1	71.72	0	
22157	112	1	*	*	1112	1	*	*	18	1	12.24	0.86	+43.0	1.0	11	SB	I	*	36.1	4.32	1
22176	164	0	*	*	*	*	283	0	*	*	10.81	0.94	+44.11	0.10	1	SB	*	*	46.5	62.75	0
22177	*	*	*	*	119	1	285	1	*	*	22.45	2.32	+43.16	0.25	1	*	*	11.1	0.36	1	
22203	142	1	*	*	1142	1	284	1	126	1	19.42	1.09	+42.42	#0.71	1	SB	*	*	6.5	0.76	1
22221	113	1	*	*	1113	1	286	1	144	1	26.26	1.04	+42.47	#0.11	1	SB	*	G	10.5	5.44	1
22224	*	*	*	*	92	1	*	*	127	1	24.11	1.72	+40.32	#0.09	1	SB	*	*	6.0	0.38	1
22253	*	*	*	*	93	1	290	1	*	*	15.74	1.98	+41.78	0.23	1	*	*	18.7	1.09	1	
22265	114	1	*	*	1114	1	*	*	128	1	19.81	1.43	+39.8	#0.4	15	SB	*	*	5.9	1.79	1
22271	*	*	*	*	291	0	*	*	22.07	2.03	+40.30	0.17	1	*	*	8.5	4.18	1			
22350	115	1	*	*	1115	1	296	1	61	1	19.30	1.67	+41.84	#0.44	1	SB	*	G	7.9	0.72	1
22380	116	1	*	*	1116	1	298	1	129	1	21.38	1.46	+41.62	0.15	1	*	*	4.4	0.97	1	
22394	117	0	*	*	*	*	299	1	62	1	18.96	1.62	+40.60	0.31	1	SB	*	*	10.4	0.34	1
22422	118	1	*	*	1118	1	300	1	130	1	19.68	0.96	+42.04	0.14	1	*	*	6.3	0.53	1	
22446	165	0	*	*	*	*	301	0	*	*	13.26	1.11	+31.84	0.14	1	*	*	30.3	35.59	0	
22496	119	1	*	*	1119	1	*	*	131	1	22.96	1.17	+41.40	0.16	24	SB	*	G	5.1	1.31	1
22505	120	1	*	*	1120	1	305	1	132	1	23.64	0.99	+42.34	#0.33	1	SB	*	S	6.0	1.75	1
22524	121	1	*	*	1121	1	307	1	133	1	19.30	0.95	+42.74	0.17	1	SB	*	*	7.2	0.80	1
22550	122	1	*	*	1122	1	312	1	134	1	20.15	1.14	+42.44	#0.17	1	SB	I	C	7.4	0.83	1
22565	123	1	*	*	1123	1	*	*	8	1	17.27	0.82	+36.8	1.2	2	*	I	*	12.8	4.10	1
22566	143	1	*	*	1143	1	313	1	135	1	17.14	1.00	+42.92	0.19	1	*	*	13.1	1.19	1	
22607	124	1	*	*	1124	1	*	*	136	1	23.91	1.04	+39.83	0.24	1	SB	I	C	6.7	1.87	1
22654	*	*	*	*	98	1	318	1	*	*	18.93	2.02	+42.88	0.25	1	*	*	8.4	0.58	1	
22684	145	1	*	*	1145	1	319	0	167	0	12.14	2.22	+48.53	0.08	1	*	I	C	36.7	17.34	0
22751	125	1	*	*	*	*	325	0	168	0	11.62	1.95	+48.72	0.18	1	*	*	40.9	16.84	0	
22782	146	1	*	*	1146	1	327	0	174	0	14.82	0.88	+57.10	0.23	1	*	*	22.0	95.20	0	
22805	166	0	*	*	*	*	328	0	*	*	5.52	1.29	+19.14	0.33	1	SB	*	*	135.2	114.49	0
22850	126	1	*	*	1126	1	*	*	137	1	14.67	0.95	+38.4	2.0	8	*	*	22.9	1.27	1	
22893	147	1	*	*	*	*	331	0	175	0	9.66	1.43	-30.57	0.26	1	*	*	58.3	993.75	0	
23044	149	1	*	*	1149	1	336	0	*	*	12.62	1.89	+37.96	0.17	1	*	I	C	37.6	13.12	1
23056	148	1	*	*	*	*	335	0	169	0	14.29	1.48	+60.93	0.17	1	*	*	26.8	109.89	0	
23069	127	1	*	*	1127	1	337	1	138	1	19.66	1.62	+43.68	0.16	1	*	*	7.9	0.80	1	
23205	*	*	*	*	*	*	*	*	*	*	10.73	1.66	*	*	0	*	I	C	50.5	8.53	?
23214	128	1	*	*	1128	1	*	*	44	1	23.09	0.83	+42.5	1.5	24	*	I	*	6.7	0.30	1
23312	*	*	*	*	*	*	*	*	160	0	16.77	1.79	+42.21	0.40	24	*	*	18.7	1.18	1	
23409	*	*	*	*	105	1	341	0	*	*	11.39	1.66	+78.64	0.36	1	*	*	45.5	358.75	0	
23497	129	1	*	*	1129	1	*	*	4	1	20.01	0.91	+38.0	1.7	8	*	*	8.9	1.29	1	
23498	187	0	*	*	107	1	345	1	139	1	18.44	1.66	+43.51	0.19	1	*	*	11.1	0.08	1	
23574	150	1	*	*	1150	1	346	0	176	0	2.26	1.27	+30.22	0.19	1	*	*	396.8	31.53	0	
23589	*	*	*	*	347	0	*	*	5.30	0.81	+49.35	0.21	1	*	*	143.2	40.64	0			
23599	*	*	*	*	348	0	*	*	3.98	1.61	+111.51	0.37	1	*	*	205.9	855.75	0			
23662	*	*	*	*	*	*	*	*	16.69	1.12	*	*	0	*	O	*	*	18.6	4.30	?	
23701	151	1	*	*	1151	1	349	0	145	1	13.78	2.08	+42.92	#0.16	1	SB	*	G	29.7	2.37	1
23750	*	*	*	*	*	*	140	1	17.78	1.40	+42.31	0.18	24	*	*	10.6	0.15	1			
23772	*	*	*	*	*	*	*	*	12.00	1.87	+35.38	#0.93	24	RV	H	C	39.7	11.47	1		
23983	130	1	*	*	1130	1	*	*	10	1	18.54	0.83	+44.16	0.14	24	SB	I	*	13.0	0.55	1
24019	131	1	*	*	1131	1	*	*	9	1	18.28	1.30	+44.90	0.52	24	*	I	C	15.5	5.84	1
24020	132	1	*	*	1132	1	353	1	64	1	18.28	1.30	+45.00	0.19	1	*	I	C	15.5	36.00	0
24021	*	*	*	*	*	*	*	*	21.39	1.21	*	*	0	*	*	*	*	11.3	9.56	?	
24035	152	1	*	*	1152	1	354	0	170	0	25.67	1.53	+16.48	#0.39	1	SB	I	*	13.1	175.91	0
24046	*	*	*	*	*	*	*	*	24.88	1.06	*	*	0	*	I	*	*	12.6	54.92	0	
24116	*	*	*	*	*	*	*	*	11.56	1.19	+45.30	1.20	2	*	*	41.9	1.87	1			
24923	*	*	*	*	*	*	*	*	18.26	1.58	+43.70	0.23	24	*	*	14.7	0.17	1			
25141	167	0	*	*	*	*	361	0	9.40	1.48	+34.54	0.24	1	*	*	63.7	24.65	0			
25639	*	*	*	*	*	*	*	*	11.58	1.13	+42.1	0.43	24	*	*	46.3	14.11	?			
25694	*	*	*	*	*	*	*	*	11.17	1.28	*	*	0	*	*	46.4	11.21	?			
25871	*	*	*	*	*	*	*	*	11.55	0.91	*	*	0	*	*	45.0	1.32	?			
25929	155	0	*	*	*	*	366	0	6.74	1.40	+33.22	0.34	1	*	*	104.9	30.90	?			
26159	*	*	*	*	*	*	*	*	11.13	1.39	*	*	0	*	*	47.3	10.82	?			
26227	156	0	*	*	367	0	*	*	0.72	1.90	+46.64	0.24	1	*	*	1345.6	4.57	0			
26382	168	0	*	*	*	*	*	*	18.56	0.86	+41.1	1.2	2	*	*	16.2	2.07	1			
26795	*	*	*	*	*	*	161	0	6.93	1.13	+27.1	0.27	23	SB	*	*	102.9	66.29	0		
26844	*	*	*	*	*	*	*	*	46.51	2.35	*	*	0	*	*	26.7	2.78	?			
27431	*	*	*	*	*	*	*	*	13.11	0.87	*	*	0	*	*	37.4	8.89	?			
27502	*	*	*	*	*	*	147	0	6.15	1.25	*	*	0	*	*	120.0	10.01	0			
27791	*	*	*	*	*	*	*	*	11.50	6.04	*	*	0	*	I	X/S	49.7	1.46	?		
27933	*	*	*	*	*	*	148	0	12.76	0.94	*	*	0	*	*	39.2	33.71	0			
28356	*	*	*	*	*	*	*	*	14.87	0.98	+45.00	2.50	2	*	*	33.1	0.53	1			
28469	*	*	*	*	*	*	*	*	10.52	0.99	+48.00	5.00	2	*	*	56.3	10.27	1			
28614	169	0	*	*	*	*	*	*	21.49	0.82	+40.9	0.3	20	SB	I	C	19.3	26.99	0		
28774	*	*	*	*	*	*	*	*	12.81	12.80	*	*	0	*	I	C	41.6	11.50	?		



**Fig. 1.** Distance modulus (given by  $m - M = -5 \log \pi - 5$ , where  $\pi$  is the parallax in arcsec) for the distance determinations, with errors, since 1980 given in Table 1. The ‘Torres’ determination refers to Torres et al. (1997c).

al. (1988) presented weak evidence for rotation at the levels of  $\lesssim 1 \text{ km s}^{-1} \text{ rad}^{-1}$  (projected), not inconsistent with these conclusions.

The convergent point method was first applied to the Hyades cluster by Boss (1908), using the proper motions of 41 suspected cluster members supplemented by three radial velocities. The classical convergent-point method was further developed and discussed by Smart (1938), Brown (1950), and others. A systematic regression error arising from the quadratic form of the proper motion component coefficients in the normal equations, and leading to an upward revision of 7 per cent in the distance to the cluster, was identified by Seares (1944, 1945).

Subsequent distance determinations using the convergent-point method initially appeared to be in close agreement, although the correspondence between the van Bueren (1952) and Wayman et al. (1965) results was later attributed in part to the use of the same proper motion system (van Altena 1974). Hodge & Wallerstein (1966) suggested that the cluster was 20 per cent farther than indicated by the proper motions – given the previous standard distance, binary stars in the Hyades would have been overluminous with respect to their masses, both as compared to normal stars like the Sun, and as compared to models derived from stellar structure theory (Wallerstein & Hodge 1967).

In the classical convergent-point method, the determination of  $\langle v \rangle$  depends only on the directions of proper motions, and not on their absolute values. Upton (1970) derived a procedure for calculating the distance directly from the proper motion gradients across the cluster, dispensing with the intermediate step of locating the convergent point – the cluster distance is then given by the ratio of the mean cluster radial velocity to the proper motion gradient in either coordinate. Use of this method, whose relevant equations can be derived by differentiating the basic convergent-point equation (Eq. 2), has the advantage that more

complete use is made of the proper motion data, while the two independently measured gradients yield two distance estimates whose comparison provides an indication of the systematic and accidental errors involved.

The accepted distance to the Hyades was revised from about 40 pc to about 44 pc around 1978 based on models of the chemical composition (Koester & Weidemann 1973), and independent astrometric and photometric results (van Altena 1974, Hanson 1975, Eggen 1982). Hanson (1975) applied different formulations of the convergent-point method to new proper motion and cluster membership data, concluding that the errors due to different formulations of the method appeared to be quite small, with systematic errors in previous meridian circle proper motions implicated as the cause of the discrepancies which seemed to exist between distances derived from earlier proper motion analyses and those resulting from a broad variety of other observational methods.

Taking into account systematic magnitude effects in the Hanson proper motions, McAlister (1977) revised Hanson’s distance of 48 pc downward to 43 pc, close to the value of 43.5 pc given by Corbin et al. (1975). Murray & Harvey (1976) showed how all measurements of proper motion and radial velocity of the cluster members could be combined into a general solution for the cluster motion and the parallaxes of individual stars. A review of astrometric results by Hanson (1980) concluded that 45.6 pc (distance modulus  $3.30 \pm 0.04$ ) was indicated by the best of current data; being a weighted mean of classical convergent-point methods and trigonometric parallaxes. Meanwhile, dynamical parallaxes from visual and eclipsing binaries have traditionally yielded slightly higher values: McClure (1982) found 49 pc, but a reanalysis of that and other data by Peterson & Solensky (1987) gave 47 pc (distance modulus  $3.36 \pm 0.05$ ) still slightly higher than the astrometric results.

Determination of the convergent point from radial velocities was applied to the Hyades by Stefanik & Latham (1985), Detweiler et al. (1984), and Gunn et al. (1988), based on the methodology applied by Thackeray (1967) to Sco-Cen.

Schwan (1990, 1991) presented the most recent determinations of the convergent point based on proper motions of 44 and 145 stars from the FK5 and FK5/PPM respectively, and derived a distance modulus of  $3.40 \pm 0.04$ .

Individual trigonometric parallaxes have been published for certain candidate Hyades members, most recently by Patterson & Ianna (1991), by Gatewood et al. (1992), and in the Fourth Edition of the General Catalogue of Trigonometric Stellar Parallaxes (van Altena et al. 1995). Recent determinations of a mean cluster distance have been given by Turner et al. (1994), and van Altena et al. (1997b). High-precision orbital parallaxes have recently been determined for 51 Tau (vB24), 70 Tau (vB57), and 78 Tau (vB72) by Torres, Stefanik & Latham (1997a,b,c). In each case, however, their extrapolation to a mean cluster distance involves the use of relative ground-based proper motions, so that the high intrinsic accuracy of their orbital parallax determinations does not propagate through to a corresponding accuracy on the mean distance.

A weighted mean distance modulus of  $3.42 \pm 0.09$  mag, based on Hubble Space Telescope FGS observations of seven cluster members, has been given by van Altena et al. (1997a).

These recent determinations are shown, with their published errors, in Fig. 1. It is evident that the Hyades distance may still not be considered as a conventional astronomical constant. It is this uncertainty, and its attendant implications, that this paper seeks to resolve.

The Hipparcos Catalogue provides parallaxes for all stars in the observing programme, of sufficient (milliarcsec) accuracy not only to assign membership probabilities on the basis of the distances alone, but to resolve the depth of the cluster. The availability of annual proper motions with standard errors of order  $1 \text{ mas yr}^{-1}$  for all stars, leads to an opportunity to re-discuss membership on the basis of convergent point analysis, to probe the kinematical assumptions implicit in such analyses, and to examine, in combination with the parallaxes, the cluster membership and dynamics independently of any assumed dynamical model.

### 3. Observational material

#### 3.1. Data from the Hipparcos Catalogue

This study makes use of the final data contained in the Hipparcos Catalogue, which provides barycentric coordinates, inertially-referenced proper motions, and absolute trigonometric parallaxes for nearly 120 000 stars (ESA 1997). It is based on the 240 candidate Hyades members specifically included in the Hipparcos Input Catalogue, supplemented by the astrometric and photometric data for all Hipparcos Catalogue objects within the range  $2^{\text{h}} 15^{\text{m}} < \alpha < 6^{\text{h}} 5^{\text{m}}$  and  $-2^{\circ} < \delta < +35^{\circ}$  for independent membership studies of objects not considered as

candidate members in the past (this region includes all previous candidate cluster members).

We stress from the outset that the Hipparcos Input Catalogue, on which the final Hipparcos Catalogue contents are based, is not complete to the observability limit of the Hipparcos observations, although specific attention was given during its construction to the inclusion of potentially observable candidate Hyades cluster members. Thus, although membership analysis can be conducted on previously unsuspected cluster members contained in the Hipparcos Catalogue, this catalogue will not contain members fainter than the satellite observability limit, of around  $V \sim 12$  mag, nor objects omitted from the Hipparcos Input Catalogue for other reasons. Clearly, an incomplete survey will most likely result in a preferential selection of stars according to distance, and a biased value of the mean cluster distance – although it will not affect the discussion of the main sequence modelling when using individual distance estimates for each object.

The choice of Hipparcos targets in a given field of the sky was subject to many operational constraints which were, in some cases, in conflict with scientific requirements. Fig. 2 illustrates the sample of Hyades stars contained in the Hipparcos Catalogue with respect to the global content of Hyades candidate members contained in the data base for stars in open clusters ('Base des Amas', or BDA, Mermilliod 1995), on the basis of the photometric data,  $V$  and  $B - V$ , contained in the BDA. Stars from the BDA contained in the Hipparcos Catalogue are displayed as filled circles (190 stars). Stars not contained in the Hipparcos Catalogue, but appearing in a second major product of the Hipparcos mission, the Tycho Catalogue (ESA 1997), are displayed as open triangles (27 stars). The remaining 174 stars contained only in the BDA are displayed as open squares. The figure shows, as expected, the progressive incompleteness of the Hipparcos sample with increasing magnitude (and is also a useful demonstration of the completeness of the Tycho Catalogue down to about  $V = 10.5$  mag).

Up to 114 of the 'BDA only' stars lie within 5 pc of the cluster centre, assuming that all lie at the mean distance of the cluster centre. Any possible kinematical bias due to the present sample selection has not been studied in the present paper, as the distance, proper motion and radial velocity data for stars other than those contained in the Hipparcos Catalogue are either insufficiently accurate, incomplete, or very inhomogeneous.

For objects contained in the Hipparcos Catalogue, those considered to be members or candidate members by one or more previous workers are listed in Table 2. Column a gives the Hipparcos Catalogue identifier, while columns b–m give the designation and membership status according to a number of previous workers. These are not the only papers where membership of particular objects have been discussed (see, for example, references in Griffin et al. 1988) although they represent the most substantial developments of the cluster membership studies. The membership status listed in columns b–m do not necessarily reflect fully the membership assignment in the original papers: in some cases the authors give probabilities for membership or include some indication of 'doubtful member-

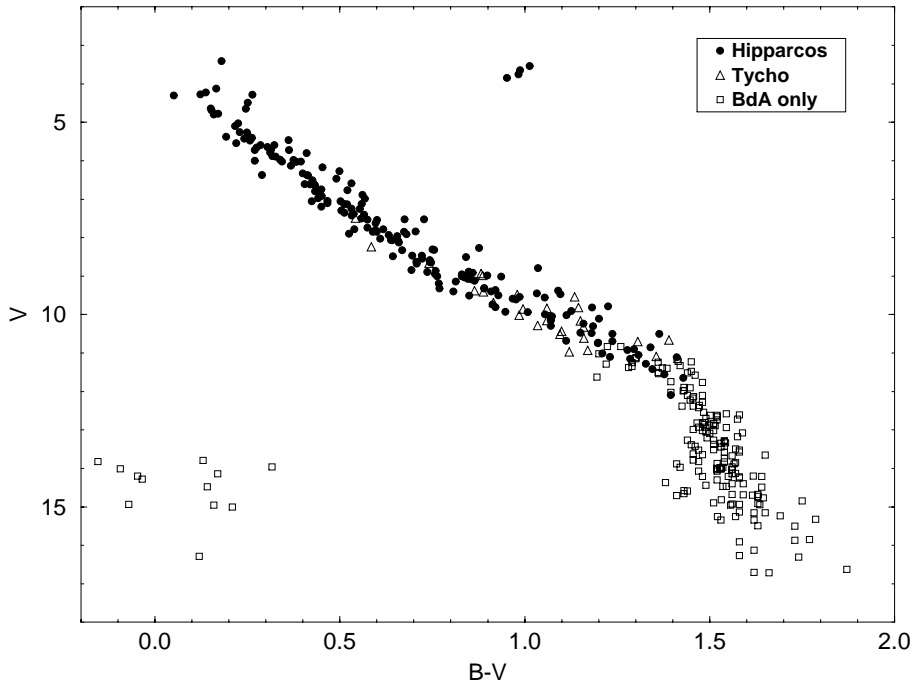


**Fig. 2.** Hyades stars from the ‘Base des Amas’ (BDA). Stars contained in the Hipparcos Catalogue are displayed as filled circles (190 stars). Stars not contained in the Hipparcos Catalogue, but appearing in the Tycho Catalogue, are displayed as open triangles (27 stars). The remaining 174 stars contained only in the BDA are displayed as open squares.

ship’, which we have converted (sometimes subjectively) into a 1 or 0. Table 2 thus reflects our own understanding of previous membership studies converted to a yes/no status. For full details we refer to the original papers. Entries in Table 2 with ‘–’ in columns b–m inclusive are new candidates arising from the present study, selected as described in subsequent sections (we considered it desirable to list all candidates sequentially in one table, independently of their history, and will distinguish their historical status by referring to these as ‘previous’ and ‘new’ members, where appropriate).

The previous candidates compiled in Table 2 form the basic list of objects for our initial studies. It is noted that this list contains objects already considered as non-members by some or even all previous workers (and which we will go on to confirm as non-members), while it does not include those objects which are considered as possible or secure Hyades members which are not contained within the Hipparcos Catalogue (as described above). Later in the paper, having determined the general spatial and kinematical properties of the cluster on the basis of the general properties of the previous members, we will provide our own assignment of membership to this basic list (this final result is given in the last column of Table 2). We will also supplement the previous candidates by additional candidates selected from the Hipparcos Catalogue having spatial and kinematical properties in common with the general cluster (also included in Table 2).

The Hipparcos Catalogue (ESA 1997) itself describes the details of the catalogue construction and contents, while recent summaries may be found in the literature related to the construction of the intermediate catalogue (Kovalevsky et al. 1995), and to the determination of the trigonometric parallaxes and associated errors (Perryman et al. 1995).

The Hipparcos and Tycho Catalogues have been constructed such that the Hipparcos reference frame coincides, to within

limits set by observational uncertainties, with the International Celestial Reference System (ICRS), as recommended by the IAU Working Group on Reference Frames (Ma et al. 1997, see also Lindgren & Kovalevsky 1995). The latter system is practically defined by the adopted positions of several hundred extragalactic radio sources. It supersedes, although it is consistent with, the optical reference frame defined by the FK5 catalogue, which was formally based on the mean equator and dynamical equinox of J2000. The resulting deviation from inertial, about all three axes, is considered to be less than approximately  $0.25 \text{ mas yr}^{-1}$ . For a discussion of the comparison of ground-based positions and proper motions with those of Hipparcos, see Lindgren et al. (1995). The Hipparcos Catalogue (ESA 1997, Volume 1, Sect. 1.5.7) details the relationship between the ICRS(Hipparcos) and J2000(FK5) frames. The epoch of the Hipparcos Catalogues is J1991.25, although the provision of the full covariance matrix of the astrometric solution for each star permits the positions, and corresponding standard errors, to be propagated to any epoch within the same reference system.

The Hipparcos trigonometric parallaxes are absolute, and are considered to be free from systematic (global) errors at a level of some 0.1 mas or smaller (Arenou et al. 1995). Studies so far suggest that the true external parallax and proper motion errors are unlikely to be underestimated, as compared with the formal standard errors, by more than about 10–20 per cent. We will demonstrate that the present results provide further evidence for the reliability of the quoted astrometric standard errors, and provide independent evidence for the absence of significant systematic errors in the parallaxes and proper motions. Columns (n–o) of Table 2 provide the Hipparcos parallax and standard errors (in mas). These values, as well as the remaining astrometric parameters (and correlations), are as published in the Hipparcos Catalogue.

The Hipparcos Catalogue also contains detailed photometric data, including broad-band, high-precision, multi-epoch photometry in the calibrated Hipparcos-specific photometric system  $H_p$ . These are homogeneous magnitudes derived exclusively from the satellite observations, providing the basis for detailed photometric variability analyses which are summarised, star-by-star, in the published catalogue (the  $H_p$  magnitudes were not used in the construction of the HR diagrams in Sect. 9 in view of the absence of appropriate bolometric corrections). In addition, the catalogue includes  $V$  magnitudes, and  $B - V$  and  $V - I$  colour indices derived on the basis of satellite and/or ground-based observations.

### 3.2. Binary information and radial velocity data

Information on the binary nature of the stars in the Hyades is important for a variety of reasons: in addition to the astrophysical relevance, the confidence which can be placed on the kinematic or dynamical interpretation of the radial velocities and proper motions (and hence the space motions) is affected by the (known or unknown) binary nature of the object. We have therefore attempted to compile the best available radial velocity and binary information for each object, and their inter-relationship.

Columns p–r of Table 2 provide the radial velocity, standard error, and source of radial velocity, respectively. These columns represent the result of our literature search, and are supplemented by Coravel radial velocity results specifically acquired in the context of this study by one of us (JCM, column r = 24). The Coravel velocities include the ‘standard’ zero-point correction of  $0.4 \text{ km s}^{-1}$  (Scarfe et al. 1990). The Griffin et al. radial velocities given in Table 2 are the ‘uncorrected’ values given in their paper: for use in our subsequent kinematical studies they have been corrected as described in Eq. (12) of Gunn et al. (1988), but accounting for a sign error which is present in their equation (and confirmed by the authors): in their notation, we have added a correction of  $-q(V) - 0.5 \text{ km s}^{-1}$  for stars fainter than  $V = 6 \text{ mag}$ , and a correction of  $-0.5 \text{ km s}^{-1}$  for brighter stars. In the assignment of errors from the compilation of Griffin et al. (1988) we adopted the ‘internal error’ quoted in their Table IV for stars with 3 measurements or less.

Column s indicates whether the object has been classified as a spectroscopic binary (SB), or as (possibly) variable in measured radial velocity and therefore indicative of a possible spectroscopic binary (RV), according to the given source. Radial velocities are systemic ( $\gamma$ ) velocities where available. If the radial velocity has been noted as variable, or if no  $\gamma$  velocity is available, a ‘#’ precedes the radial velocity error, indicating that it should be viewed with caution for dynamical studies of the cluster. Of the previous candidates in Table 2, 71 are classified as spectroscopic binaries, 37 of which have a  $\gamma$  velocity determined; these are mostly from the work of Griffin et al. (1988, and references therein), some are from refs. 10–11 accompanying Table 2, with others as referenced individually in the key to Table 2. [To assist cross-referencing to the results of Griffin et al., column j of Table 2 uses the sequential number of the object in Table IV of Griffin et al.; this sequential numbering

takes account of two ‘blocks’ containing 6 objects (rather than the usual 5) in their Table IV].

Columns t–u provide information on the (possible) binary nature of the star taken from the Hipparcos Catalogue. Each entry in the Hipparcos Catalogue includes duplicity/multiplicity information derived from the observations: very broadly, systems are resolved if their separations are larger than approximately  $0.1 \text{ arcsec}$  and their magnitude differences smaller than about 3 mag. For such systems the catalogue provides detailed information on the components in Part C of the Double and Multiple Systems Annex. Additional information, such as suspected duplicity inferred from the astrometric residuals, or observed photocentric acceleration implying the presence of short-period orbital systems, has been derived from the observations, and relevant catalogue entries are flagged accordingly and assigned to distinct parts of the Double and Multiple Systems Annex.

Column t is taken from Field H56 of the Hipparcos Catalogue and indicates that a CCDM identifier, denoting entries in the ‘Catalogue of Components of Double and Multiple Stars’ (Dommanget & Nys 1994), has been assigned to the catalogue entry: H indicates that the system was determined as double or multiple by Hipparcos (previously unknown); I that the system was identified as double in the Hipparcos Input Catalogue; and M that the system had been previously identified as double, but not recorded as such in the Hipparcos Input Catalogue. Column u is taken from Field H59 of Hipparcos Catalogue, and indicates which part of the Double and Multiple Systems Annex the entry has been assigned to: ‘C’ indicates components are resolved, ‘G’ indicates that a non-linear motion of the photocentre has been detected, ‘O’ that the entry is classified as an orbital system, ‘V’ that the entry is inferred to be double from a correlation between photocentric motion and photometric variability, and ‘X’ that the entry is likely to be an unclassified (close) double or multiple system. ‘S’ in this column is taken from Field H61 of the Hipparcos Catalogue and indicates, somewhat independently, that the entry is a suspected binary. Information in column t may overlap with that given in column u, i.e. it may simply indicate that detailed information on components is given in Part C of the Double and Multiple Systems Annex, but it may also indicate that the star is a component of a visual or wide binary (and not included in Part C).

In summary, ‘C’ in column u indicates that components of a double or multiple system have been resolved by the Hipparcos observations, while ‘G’, ‘O’, ‘V’, ‘X’, or ‘S’ indicates that the star is, or may be, a close binary system. The implications for the measured radial velocities will be taken into account in the discussions of membership and dynamics of the cluster.

## 4. Proper motions and the convergent point

Before developing the analysis of the 6-dimensional (position and velocity) data set provided by the Hipparcos proper motions and parallaxes in combination with the ground-based radial velocities, it is instructive to refer to the most recent determinations of the convergent point based upon the best-available ground-based data, and to examine the sensitivity of the resulting analy-

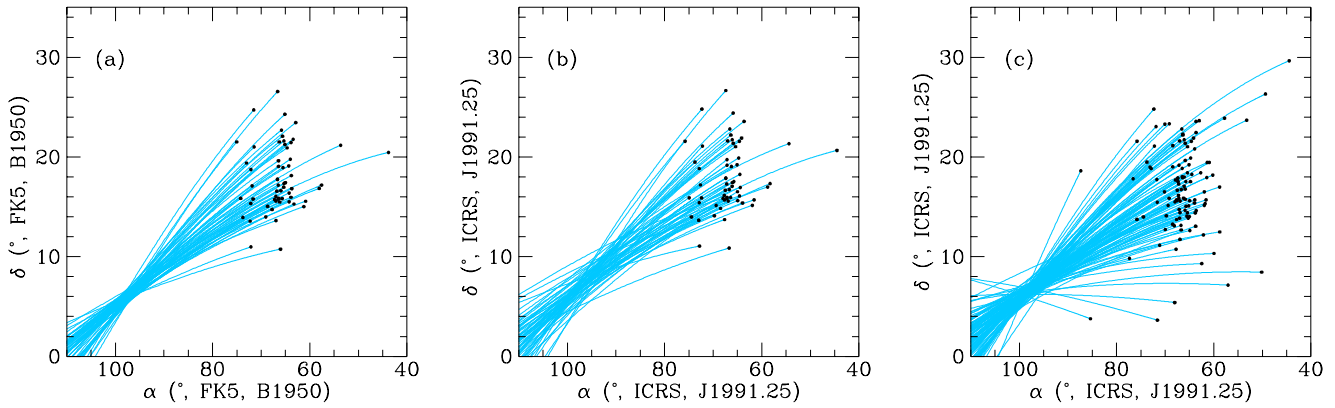


**Fig. 3.** **a** The set of stars selected by Schwan (1991) for his convergent point analysis, and according to his adopted membership criteria, showing the positions (solid circles) and motions of the selected stars on their great circles (lines) – including the region of the resulting convergent point (intersection of the lines) – based on Schwan’s data; **b** shows the Hipparcos Catalogue data for precisely the same selection of stars (note the difference in reference systems and epochs); **c** shows the stars selected from the Hipparcos Catalogue data according to Jones’ (1971) method. Notice the much ‘tighter’ distribution of stellar motions compared with **b**.

sis to the accuracy of the available proper motion data. We have not investigated all numerical implementations of the convergent point method using the Hipparcos data – the objective in this section is merely to gain insight into the performance and consistency of the classical convergent point methods.

Figs. 3a and b assemble the set of stars selected by Schwan (1991) for his convergent point analysis, and show the motions of the selected stars – including the region of the resulting convergent point – based on Schwan’s data (a), and for the Hipparcos Catalogue data for the *same* selection of stars (b). Note that Schwan’s data are referred to B1950(FK5).

Inspection of the less well-defined convergent point apparent in Fig. 3b compared with that of Fig. 3a could lead to the erroneous conclusion that the Hipparcos proper motions are of a degraded accuracy compared with those used by Schwan (1991). The correct explanation is, rather, that for any given set of proper motions and associated errors, the convergent point analysis selects as candidate cluster members those having a minimum dispersion about the selected convergent point. Evidently, for a given set of candidate members which have been selected according to a given, but erroneous, distribution of proper motions, an improvement in the corresponding proper motion accuracies will not necessarily result in a ‘tightening’ of the previously-determined convergent point for the same selection of candidate members. That the Hipparcos Catalogue data result in an increase in the scatter for the same selection of stars is a direct consequence of retaining a sub-optimum sample of stars on the basis of their (imprecise) proper motions. A revised analysis, as we will demonstrate, leads to a different convergent point, and a correspondingly different selection of stars. The consequences for the determination of the individual parallaxes of the candidate cluster members, and the resulting mean cluster distance, then follow directly from Eqs. (1) and (2).

Our implementation of the convergent point method applied to the Hipparcos proper motions used the maximum-likelihood technique described by Jones (1971), which has the merit of

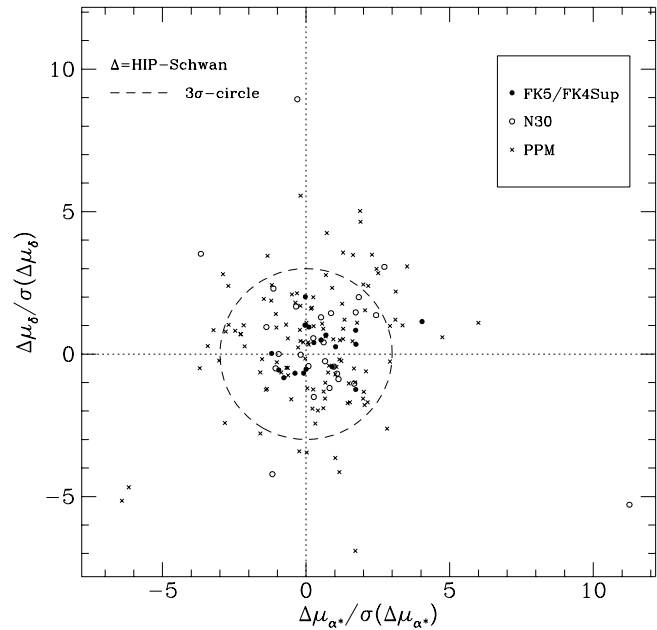


**Fig. 4.** The differences in the proper motions components (HIP – FK5 etc.) for the membership candidates selected by Schwan (1991), normalised to the combined standard errors in each component. Proper motion components given by Schwan (1991) in B1950(FK5) coordinates have been transformed to J2000(FK5) for comparison with the ICRS(Hipparcos) data. The good agreement between the FK5 and Hipparcos proper motions, with degraded accuracies from Schwan’s candidates with proper motions only from N30 or PPM, is evident.

locating the convergent point and, simultaneously, the corresponding cluster members. In essence, members are searched for amongst the set of stars showing the clearest converging motions. Applying it to the Hipparcos proper motions of the previous candidate members listed in Table 2 (those with entries in columns b–m which, we recall, is our basic starting point containing a large proportion of possible cluster members) resulted

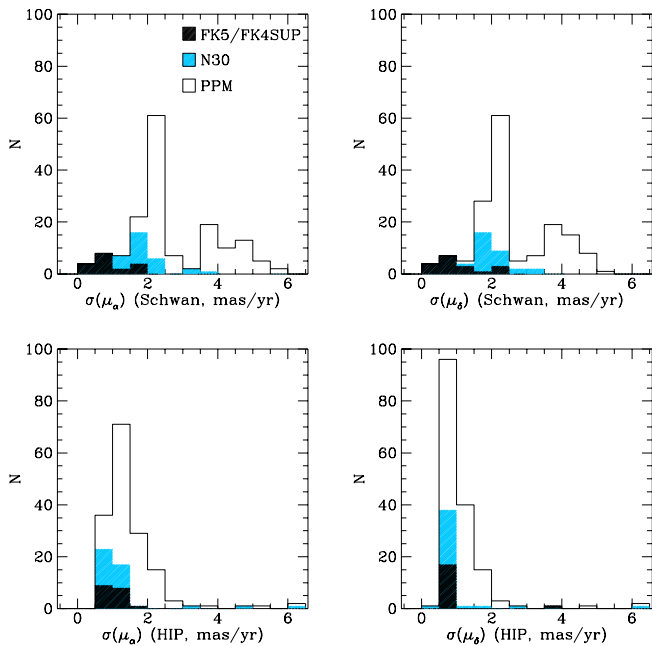


**Fig. 5.** The distribution of standard errors in the proper motion components for the membership candidates selected by Schwan (1991). Top: as used by Schwan (1991), derived from FK5, N30, and PPM. Bottom: the distribution of standard errors for the same objects from the Hipparcos Catalogue, according to their appearance in the previous source catalogues. The slightly better Hipparcos proper motion accuracies for the subsets of the FK5 and N30 objects reflects their generally brighter apparent magnitudes.

in about one half of the stars (113) being selected as cluster members in the first iteration. Two further applications of the same method to those stars not selected in the first iteration provided 17 and 18 additional candidate members in the second and third steps respectively. As shown in Fig. 3c the convergence of stars selected in the first step is now much tighter than seen in Fig. 3b, although the successively selected groups have different convergent points: at  $(\alpha, \delta) = (98^\circ 6, 6^\circ 4), (95^\circ 1, 8^\circ 3), (96^\circ 6, 5^\circ 8)$ , respectively (ICRS, epoch J1991.25).

The explanation for the absence of a unique convergent point is that the methods of Jones and Schwan for selecting members of the cluster (and convergent point methods in general) rely on finding stars which show the least deviations of the position angle of their proper motion,  $\theta$ , with respect to the direction from the stellar position to the convergent point,  $\theta_c$ . In reality each star has its own ‘convergent point’, given by the direction of its space motion, and the difference  $\Delta\theta = \theta - \theta_c$  will be small if the stellar convergent point is close to the great circle connecting the cluster centre to the cluster convergent point. As a result, the convergent point method tends to select stars with space motions that lie in the plane defined by the great circle passing through the cluster centre and the convergent point.

If there is a significant velocity dispersion in the cluster the convergent point membership selection will lead to an artificial flattening of the distribution of candidate members in velocity space, which may in turn lead, for example, to spurious infer-

ences of rotation. Conversely if there is significant systematic structure in the internal velocities of a cluster, the convergent point method may lead to a spatial bias in the selection of candidates. This would happen if the cluster possessed a significant component of rotation with the extreme internal velocities located primarily in a plane perpendicular to the great circle connecting the cluster centre and convergent point.

Schwan’s proper motions were from mixed sources, drawn from the FK5/FK4Sup, N30, and PPM catalogues. That the differences in membership selection resulting from Schwan’s values and the present Hipparcos values are arising from the different quality of the available proper motions is evident from Fig. 4, which illustrates the differences in the proper motion components (HIP–FK5 etc) for the membership candidates selected by Schwan (1991), normalised to the combined standard errors in each component. The corresponding distributions of the standard errors are shown in Fig. 5. The generally very good agreement between the FK5 and Hipparcos proper motions, with degraded accuracies for Schwan’s candidates with proper motions only from N30 or PPM, is evident. It should be borne in mind that the differences between, for example, FK5 and Hipparcos proper motions may partially reflect true differences in the measured proper motions of astrometric binaries where the FK5 proper motions reflect the long-term photocentric motion, with the Hipparcos measurements made over a period of only 3.5 years carrying information on orbital perturbations over these time scales. Indeed, there is some evidence that the proper motion differences between Hipparcos and FK5 exceed their combined standard errors, at least in a statistical sense (Wielen 1997).

We have identified that heterogeneous ground-based proper motions will affect the determination of the convergent point, the membership determination, and hence the cluster distance modulus. Although, alone, a systematic error of approximately  $1 \text{ mas yr}^{-1}$  in the proper motion system would be needed (Eq. 2) to account for distance errors of 1 per cent, the  $\sin \lambda$  term in Eq. (2) results in a greater sensitivity of the distance estimate to a combination of the proper motions and adopted convergent point. We will return to a discussion of the convergent point based on the Hipparcos data, and the consistency between the distances inferred from the convergent point (derived from the ground-based and Hipparcos proper motions) and the Hipparcos-based trigonometric parallaxes, in Sect. 6.1.

## 5. Membership determination and mean cluster distance

### 5.1. Determination of positions and space motions

The discussions of Sect. 4 also illustrate the point acutely evident to previous workers that membership selection based on proper motion data alone, however accurate, may also lead to erroneous inferences about cluster membership if significant departures from strictly parallel motion exist within the cluster.

With the availability of the full 6-dimensional position-velocity data, based on the 5 astrometric parameters provided by Hipparcos supplemented by the stellar radial velocity when

available, we are in a position to examine membership based on stricter spatial and kinematic criteria than has been possible hitherto.

We first assemble the equations used for the transformation between equatorial and Galactic coordinates, and for the determination of space velocities based on the observed proper motions, parallaxes and radial velocities. The transformation between the equatorial and Galactic systems is given by:

$$[\mathbf{x}_G \ \mathbf{y}_G \ \mathbf{z}_G] = [\mathbf{x} \ \mathbf{y} \ \mathbf{z}] \mathbf{A}_G \quad (3)$$

where  $[\mathbf{x} \ \mathbf{y} \ \mathbf{z}]$  and  $[\mathbf{x}_G \ \mathbf{y}_G \ \mathbf{z}_G]$  are the basis vectors in the equatorial and Galactic systems respectively ( $\mathbf{x}$  is the unit vector towards  $(\alpha, \delta) = (0, 0)$ ,  $\mathbf{y}$  is the unit vector towards  $(+90^\circ, 0)$ , and  $\mathbf{z}$  the unit vector towards  $\delta = +90^\circ$ ), and where the matrix  $\mathbf{A}_G$  relates to the definition of the Galactic pole and centre in the ICRS system. Currently no definition of this relation has been sanctioned by the IAU, and we adopt the following definition proposed by the Hipparcos project (ESA 1997, Volume 1, Sect. 1.5.3), using as celestial coordinates of the north Galactic pole in the ICRS system:

$$\begin{aligned} \alpha_G &= 192^\circ 859\ 48 \\ \delta_G &= +27^\circ 128\ 25 \end{aligned} \quad (4)$$

with the origin of Galactic longitude defined by the Galactic longitude of the ascending node of the Galactic plane on the equator of ICRS, taken to be:

$$l_\Omega = 32^\circ 931\ 92 \quad (5)$$

Eqs (4) and (5) preserve consistency with the previous B1950 definition of Galactic coordinates (Blaauw et al. 1960) to a level set by the quality of optical reference frames prior to Hipparcos, accounting for both the transformation to the J2000(FK5) system (cf. Eq. (33) of Murray 1989) and then to the ICRS(Hipparcos) system by application of the orientation difference between the Hipparcos and FK5 Catalogues.

These values of the angles  $\alpha_G$ ,  $\delta_G$  and  $l_\Omega$  are to be regarded as exact quantities. From them, the transformation matrix  $\mathbf{A}_G$  may be computed to any desired accuracy. To 8 decimals the result is:

$$\mathbf{A}_G = \begin{pmatrix} -0.054\ 875\ 56 & +0.494\ 109\ 43 & -0.867\ 666\ 15 \\ -0.873\ 437\ 09 & -0.444\ 829\ 63 & -0.198\ 076\ 37 \\ -0.483\ 835\ 02 & +0.746\ 982\ 24 & +0.455\ 983\ 78 \end{pmatrix} \quad (6)$$

If  $\mathbf{b}$  denotes the barycentric position of the star, measured in parsec, and  $\mathbf{v}$  its barycentric space velocity, measured in  $\text{km s}^{-1}$ , then:

$$\mathbf{b} = A_p \mathbf{u} / \pi \quad (7)$$

and:

$$\mathbf{v} = (\mathbf{p}\mu_{\alpha^*}A_v/\pi + \mathbf{q}\mu_{\delta}A_v/\pi + \mathbf{r}V_R)k \quad (8)$$

where  $\mathbf{u}$  is the unit vector in the barycentric direction,  $[\mathbf{p} \ \mathbf{q} \ \mathbf{r}]$  is the normal triad defined below, and  $A_p = 1000 \text{ mas pc}$  and  $A_v =$

$4.74047\dots \text{ km yr s}^{-1}$  designate the astronomical unit expressed in the appropriate form;  $\pi$  is the parallax expressed in mas, and  $\mu_{\alpha^*} = \mu_{\alpha} \cos \delta$  and  $\mu_{\delta}$  are the proper motion components expressed in  $\text{mas yr}^{-1}$ . The Doppler factor,  $k = (1 - V_R/c)^{-1}$ , is required to account rigorously for light-time effects in the calculation of the space velocity in terms of the observed proper motion and radial velocity.

In the equatorial system the components of the normal triad  $[\mathbf{p}, \mathbf{q}, \mathbf{r}]$  are given by the matrix:

$$\begin{aligned} \mathbf{R} &= \begin{pmatrix} p_x & q_x & r_x \\ p_y & q_y & r_y \\ p_z & q_z & r_z \end{pmatrix} \\ &= \begin{pmatrix} -\sin \alpha & -\sin \delta \cos \alpha & \cos \delta \cos \alpha \\ \cos \alpha & -\sin \delta \sin \alpha & \cos \delta \sin \alpha \\ 0 & \cos \delta & \sin \delta \end{pmatrix} \end{aligned} \quad (9)$$

The equatorial components of  $\mathbf{b}$  and  $\mathbf{v}$  may thus be written:

$$\begin{pmatrix} b_x \\ b_y \\ b_z \end{pmatrix} = \mathbf{R} \begin{pmatrix} 0 \\ 0 \\ A_p/\pi \end{pmatrix} \quad (10)$$

and:

$$\begin{pmatrix} v_x \\ v_y \\ v_z \end{pmatrix} = \mathbf{R} \begin{pmatrix} k\mu_{\alpha^*}A_v/\pi \\ k\mu_{\delta}A_v/\pi \\ kV_R \end{pmatrix} \quad (11)$$

The Galactic components of  $\mathbf{b}$  and  $\mathbf{v}$  are obtained through pre-multiplication by  $\mathbf{A}'_G$ . In the following we ignore the Doppler correction factor, and set  $k = 1$ .

## 5.2. Preliminary membership selection

At this point, our notion of cluster ‘membership’ is intentionally vague, based only on some general preconceptions about the uniformity of the space velocities in the central region. As we shall see, realistic  $N$ -body simulations predict, or reflect, dynamical properties such as mass segregation and cluster evaporation as members diffuse beyond the cluster tidal radius, or are ejected in dynamical interactions closer to the cluster core. Thus we might expect an increasing dispersion of the space velocities with increasing distance from the cluster centre.

Our approach will therefore involve the following steps: (i) assign preliminary membership based on rather non-rigorous spatial and kinematical criteria; (ii) estimate a preliminary centre of mass and centre of mass motion; (iii) examine the displacements and velocity residuals of each candidate member with respect to these preliminary reference values; and finally (iv) refine the membership criteria accordingly, once the preliminary spatial and velocity structure becomes more evident. Unlike previous implementations of the moving cluster method, we need not assume anything about the degree to which the cluster members participate in uniform parallel motion in space; rather, we will be able to examine directly the assumptions on which these methods have been invoked and, in particular, whether there is evidence for cluster rotation, expansion, or shear.

Our starting list of possible candidate members is given in Table 2, which includes all objects in the Hipparcos Catalogue which have, in the past, been considered as (possible) Hyades members or assigned a reference number in the quoted sources. Preliminary membership was assigned to a subset of these previous candidate members based on approximate limits placed on the parallax, the radial velocity, the object's position in the proper motion vector point diagram, and distributions of the Galactic components of  $\mathbf{b}$  and  $\mathbf{v}$ . This resulted in the elimination of the most obvious non-members and a list of 188 preliminary members. The subsequent stages of the membership selection are insensitive to this preliminary membership, so neither the details of this selection process, nor the list of preliminary members, are provided.

### 5.3. Preliminary determination of the centre of mass

The preliminary members show a projected spatial distribution extending over 10–20 pc in each coordinate on the sky; thus for a distance of  $\simeq 45$  pc, and for median Hipparcos parallax errors of  $\sigma_\pi \simeq 1$  mas ( $\simeq 1.5$  pc at this distance), the depth of the cluster is clearly resolved by the Hipparcos parallaxes. Our next step is to determine an approximate centre of mass for the cluster, not with the ultimate goal of determining a mean cluster distance, but rather in order to establish a well-defined cluster reference point and mean space motion to which more careful membership assignment may be referred.

In order to determine the centre of mass of the cluster, masses of single stars have been determined using a reference isochrone from the models of Schaller et al. (1992). The point on the isochrone nearest to the observed values of  $M_V$  and  $B - V$  was determined for each star, and a mass assigned corresponding to that point on the isochrone. The masses of spectroscopic binaries were taken from the literature or, if no published mass was available, an estimate of the minimum mass was made based on the luminosity of the primary. For resolved binaries, masses of the secondary were assigned according to the mass-luminosity calibration given by Henry & McCarthy (1993). For components of binaries with separations larger than about 20 arcsec, the number density criterion given in Brosche et al. (1992) was used to infer whether they are physically associated with the primary or not. Optical companions cross-referenced in the Hipparcos Input Catalogue through their CCDM identifier (see Sect. 3.2), mostly at separations of more than 100 arcsec, were not considered to be members of the Hyades, and were not included in the determination of the mass of the system – although the proper motions of these components may be listed in the Hipparcos Input Catalogue as identical to those of the ‘primary’, it is more probable that most of these are background objects. For an estimation of the errors on the position of the centre of mass, and for the dynamical investigations in Sect. 8, associated standard errors were arbitrarily assigned to be  $0.1 M_\odot$  for single stars and  $0.5 M_\odot$  for double stars.

The centre of mass was then determined as  $\Sigma m_i \mathbf{b}_i / \Sigma m_i$ . To avoid outliers in the space positions affecting the centre of mass, stars located in the central regions of the cluster, defined

(in parsecs and Galactic coordinates) by:

$$\begin{aligned} -50 &\leq b_x \leq -30 \\ -10 &\leq b_y \leq +10 \\ -25 &\leq b_z \leq -10 \end{aligned} \quad (12)$$

were selected for the determination of the centre of mass. Of the 188 preliminary members 142 lie in this central region. The resulting (preliminary) centre of mass in Galactic coordinates (in pc) is shown in the first line of Table 3.

The same 142 stars (of which 141 have a measured radial velocity) were used to derive the centre of mass motion. The derived velocity components in Galactic coordinates, and total space motion, are also given in the first line of Table 3. Assigning the binaries half the weight of single stars, to account for the larger uncertainties in their space motions, or using the inverse of the standard errors as weights, results in coordinates of the centre of mass which differ by no more than 0.3 pc in each component from the unweighted results, and in a mean velocity within a few tenths of  $\text{km s}^{-1}$ . We conclude that these results are rather insensitive to the weighting scheme adopted.

### 5.4. Final membership selection

The space velocity derived in the previous subsection can now be used to refine the membership criteria, and to determine additional candidate Hyades members (not previously considered as members according to columns b–m of Table 2) from the field around the cluster according to kinematic criteria. As stated in Sect. 2 the expected intrinsic velocity dispersion around the mean cluster motion is less than  $1 \text{ km s}^{-1}$ ; a dispersion of around  $0.2 \text{ km s}^{-1}$  would be expected for a Plummer potential with a core radius of  $4^\circ$  (Gunn et al. 1988 derived a corresponding core radius of 3.15 pc) and a mass of about  $400 M_\odot$ . For more realistic, simple stellar systems, a larger dispersion, of order  $0.4 \text{ km s}^{-1}$  for a half-mass radius of 5 pc (see Sect. 8) may apply (Binney & Tremaine 1987, Eq. 4–80b). In selecting cluster members, at least this intrinsic dispersion must be considered. But numerous other effects may be responsible for a dispersion of the velocities around the mean cluster motion. In addition to observational errors, including the contribution of different zero points for different radial velocity sources, the presence of (undetected) binaries will inflate the intrinsic velocity dispersion due to their orbital motion, affecting both the observed proper motion and radial velocity distribution.

The combined effects are clearly observed in the velocity distributions of the preliminary members. For the 142 candidate members located in the central region of the cluster (of which 141 have a measured radial velocity compiled in Table 2), the standard deviation in the Galactic components of  $\mathbf{v}$  are 2.3, 1.9 and  $2.1 \text{ km s}^{-1}$ . The median errors in the three components are 0.59, 1.04, and  $0.84 \text{ km s}^{-1}$ , suggesting that the internal dispersion is resolved. However, taking only the 51 single stars that have a radial velocity measured by Griffin et al. 1988 (essentially providing a single source of radial velocities with a carefully defined origin) the standard deviations are found to

be 0.4, 0.8, and 1.0 km s<sup>-1</sup> (in this case we have chosen half the inter-quartile range, which provides a more robust estimator for small samples of data), with median errors of 0.48, 1.29, and 0.92 km s<sup>-1</sup>. Thus the internal velocity dispersion is not resolved significantly in any of the components of  $\mathbf{v}$ .

Hence we assume at this stage that all cluster members move with the same velocity vector even though, due to the use of different radial velocity sources and the presence of binaries, the velocity data do show considerable dispersion. This has been accounted for by assigning an uncertainty to the relative velocity of each star with respect to the mean cluster space motion, which is the sum of the standard errors and covariances in the centre of mass motion and the observed standard errors and covariances in the individual data. We stress that this uncertainty does not reflect the physical internal dispersion of the velocities in the Hyades, but rather the quality of the data presently available.

The membership selection then proceeds as follows. For each star we can calculate, from Eq. (11), the expected values of the transverse and radial velocities for a star moving with the common cluster motion:

$$\begin{pmatrix} V_{\alpha*} \\ V_{\delta} \\ V_R \end{pmatrix}_0 = \mathbf{R}' \begin{pmatrix} v_x \\ v_y \\ v_z \end{pmatrix}_C \quad (13)$$

where  $V_{\alpha*} = \mu_{\alpha*} A_v / \pi$ ,  $V_{\delta} = \mu_{\delta} A_v / \pi$ , and  $V_R$  are the velocity components in equatorial coordinates, and the subscript C refers to the centre of mass motion. Similarly, from the observed values of  $\pi$ ,  $\mu_{\alpha*}$ ,  $\mu_{\delta}$ , and  $V_R$  we can calculate the values of the observed transverse and radial motions ( $V_{\alpha*}$ ,  $V_{\delta}$ ,  $V_R$ ).

A comparison between the expected and observed velocities requires an evaluation of the associated covariance matrices. If the covariance matrix associated with vector  $\mathbf{x}$  is  $\mathbf{C}_x$ , then the covariance matrix of  $\mathbf{y} = \mathbf{F}(\mathbf{x})$  is given by  $\mathbf{C}_y = \mathbf{J}\mathbf{C}_x\mathbf{J}'$  where  $\mathbf{J}$  is the Jacobian matrix associated with the transformation from  $\mathbf{x}$  to  $\mathbf{y}$ . The Jacobian matrices for the transformations from  $\mathbf{v}_C$  to  $(V_{\alpha*}, V_{\delta}, V_R)_0$ , and from  $(\pi, \mu_{\alpha*}, \mu_{\delta}, V_R)$  to  $(V_{\alpha*}, V_{\delta}, V_R)$  are:

$$\mathbf{J}_0 = \mathbf{R}' \quad (14)$$

and:

$$\mathbf{J} = \begin{pmatrix} -\mu_{\alpha*} A_v / \pi^2 & A_v / \pi & 0 & 0 \\ -\mu_{\delta} A_v / \pi^2 & 0 & A_v / \pi & 0 \\ 0 & 0 & 0 & 1 \end{pmatrix} \quad (15)$$

respectively. We will then consider a star to be a candidate Hyades member based on these kinematic criteria if the difference between the expected and observed velocities lies within a certain combined confidence region of the two calculated vectors. Assuming the two are statistically independent, the combined confidence region is described by the sum of the two covariance matrices,  $\Sigma$ , as:

$$c = \mathbf{z}' \Sigma^{-1} \mathbf{z} \quad (16)$$

where  $\mathbf{z}$  is the difference vector, and  $c$  is dimensionless. In order to account more easily for objects for which the radial velocity was unavailable, the membership selection was carried out in

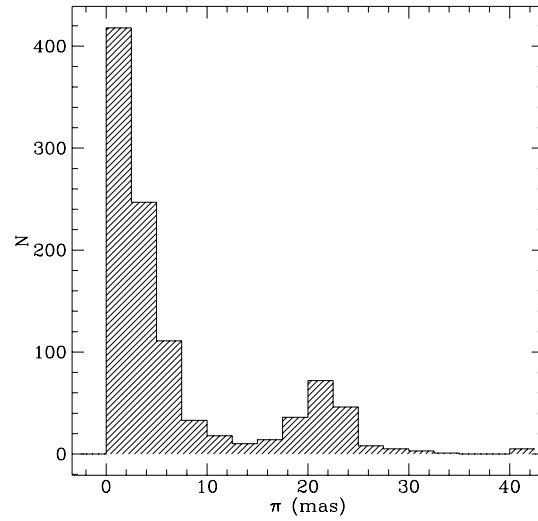


**Fig. 6.** The distribution of  $\pi$  for the 1027 stars described in the text. A subsequent membership selection criterion of  $\pi \geq 10$  mas was applied to these candidates.

equatorial coordinates, with  $\mathbf{v}_C = (-6.22, 44.97, 5.36)$  km s<sup>-1</sup>, this value corresponding to the velocity in Galactic coordinates given in the first line of Table 3. The uncertainty in the centre of mass motion corresponding to the 142 candidate members derived in Sect. 5.2 is:

$$\begin{pmatrix} +2.40 & -0.18 & +0.04 \\ -0.18 & +2.45 & +0.17 \\ +0.04 & +0.17 & +1.26 \end{pmatrix} \quad (17)$$

where the diagonal elements are the standard errors in km s<sup>-1</sup> and the off-diagonal elements are the associated correlation coefficients. For stars with unknown radial velocity the same procedure, excluding the component  $V_R$ , can be applied. In this case, we use information restricted to the tangential velocity components, using only the  $2 \times 3$  sub-matrix of Eq. (15). The quantity  $c$  is distributed according to a  $\chi^2$  distribution with 2 or 3 degrees of freedom, depending on the dimensions of  $\mathbf{z}$ . An adopted 99.73 per cent confidence region (corresponding, somewhat arbitrarily, to  $\pm 3\sigma$  for a one-dimensional Gaussian) corresponds to a value of  $c = 14.16$  for the full 3-dimensional difference vector ( $P = 0.9973$  for  $\chi^2 = 14.16$  and  $\nu = 3$ ), or to  $c = 11.83$  for the 2-dimensional difference vector if the radial velocity is unknown ( $P = 0.9973$  for  $\chi^2 = 11.83$  and  $\nu = 2$ ). We note that the uncertainties on the mean cluster motion are correlated, and return to this point in our discussion of the velocity distribution of the cluster members.

Applying the selection procedure to the 5499 stars in the Hipparcos Catalogue located in the area of sky noted in Sect. 3, and using  $V_R$  from Table 2 when available, or from the Hipparcos Input Catalogue compilation, when available, results in a list of 1027 candidate members. Fig. 6 shows the distribution of  $\pi$  for these stars – the Hyades cluster corresponds to the peak in the parallax distribution between 15 and 27 mas. Most of the ‘new candidates’ from this list of 1027 stars have small parallaxes with relatively large  $\sigma_\pi / \pi$ , and small expected

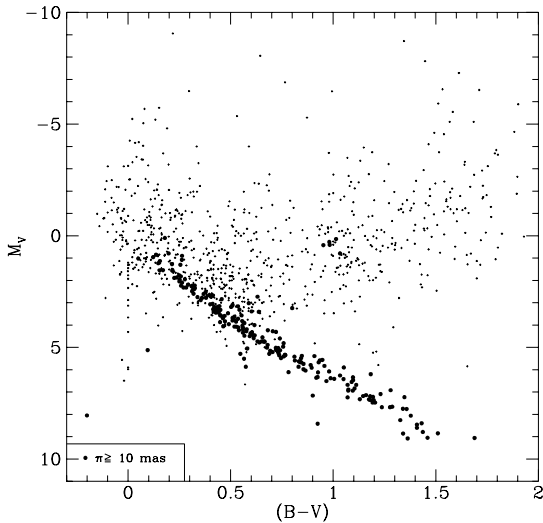


**Fig. 7.** The HR diagram represented by the 1027 stars selected according to the kinematical criteria (all points), and those retained according to the additional criterion  $\pi \geq 10$  mas ( $\bullet$ ).

proper motions, due to a combination of their large distances and/or their location close to the cluster’s convergent point. Radial velocity information is largely absent for these additional objects, which are generally likely to be unassociated with the Hyades cluster, and identified here as ‘possible’ candidates (at least we cannot exclude them on the basis of our data) simply due to the large uncertainties in the observational material.

The distribution of  $\pi$  offers no unambiguous criteria for further constraining possible membership. In the following we simply exclude objects with  $\pi < 10$  mas from further consideration, leaving a list of 218 candidate Hyades members; adopting a membership threshold of  $\pi \geq 8$  mas would result in 246 candidate members. Of the 218, 179 are in the list of previous candidate members from Table 2, with the 39 ‘new’ candidates also listed in Table 2 (‘–’ in all of columns b–m). The remaining 64 out of the 282 objects in Table 2 are considered now as non-members.

In compiling the list of new candidates in Table 2 we have already made use of additional radial velocities acquired by one of us (JCM) using Coravel, which were valuable in excluding some of the stars located at large distances as members – while Griffin et al. (1988) estimated a 1 per cent probability that a field star will exhibit a radial velocity indistinguishable from that of a cluster member, the combination of radial velocity and proper motion data provides an almost unambiguous membership criterion for objects participating in the same overall space motion. These new radial velocities have already been introduced into Table 2, as indicated in the notes to the table. New velocities acquired during late 1996 were already used to suppress intermediate candidates: this is the case for HIP 10920, 11815, 15288, 15406, 19757, 22802, 22809, 23810, 25419, while a further 23 stars with  $\pi < 10$  mas could also be excluded as candidate members based on the new radial velocities. The final status is that all of the previous 179 candidate members in Table 2 now

have a known radial velocity, while 18 of the 39 ‘new’ candidates in Table 2 have a known radial velocity. More definitive membership assignment would clearly benefit from the acquisition of radial velocities for those candidates for which the full 3-d space motion is presently unknown.

The process of recalculating the centre of mass after each membership selection step, and further refining it once new radial velocities were acquired and putative members rejected, leads to velocity changes by only  $\sim 0.1$  km s $^{-1}$  or so in each component. The resulting sensitivity of membership selection to changes in the resulting systemic space motion is also small: varying all three velocity components by  $\pm 0.5$  km s $^{-1}$  (over a  $3 \times 3 \times 3$  grid), the number of selected stars in the inner 10 pc only changes by 3 or 4 at most (out of 134). Taking steps of 1 km s $^{-1}$  the number of stars changes by  $\pm 5$ . So we may be confident that the precise value of the adopted space motion will not significantly affect the determination of members.

After membership selection a redetermination of the centre of mass could be made for the stars within, say,  $r < 10$  pc (roughly corresponding to the tidal radius of the cluster) or  $r < 20$  pc of the Hyades centre. Starting from the preliminary centre of mass only two iterations were needed to converge to corresponding determinations of the centre of mass and mass motion, and these are very robust in terms of the initial estimate. The results are given in the second and third lines of Table 3. We adopt a reference distance of  $46.34 \pm 0.27$  pc, corresponding to a distance modulus  $m - M = 3.33 \pm 0.01$  mag, for the objects contained in the Hipparcos Catalogue within 10 pc of the cluster centre (roughly corresponding to the tidal radius).

The resulting value of the space velocity in equatorial coordinates (ICRS) is  $(-6.28, +45.19, +5.31)$  km s $^{-1}$  with a corresponding convergent point of  $(\alpha, \delta) = (97^\circ 91, 6^\circ 66)$  for the inner 10 pc (134 stars), and  $(-6.32, +45.24, +5.30)$  km s $^{-1}$  with a corresponding convergent point of  $(\alpha, \delta) = (97^\circ 96, 6^\circ 61)$  for the inner 20 pc (180 stars). The resulting motion of the Hyades with respect to the LSR is derived from a solar motion of 16.5 km s $^{-1}$  in the direction  $(\ell, b) = (53^\circ, 25^\circ)$  (Binney & Tremaine 1987), and is approximately  $(-32.7, -7.3, +5.9)$  km s $^{-1}$  in Galactic coordinates.

Although the results for the  $r < 10$  pc and  $r < 20$  pc samples are reasonably consistent, it should be evident that we are not in a position to provide an unambiguous value for the ‘mean distance’ of the Hyades, since the centre of mass is sensitive to the subset of stars used to calculate it, which in turn depends on the selection of stars contained in the Hipparcos Catalogue, as well as on the contribution of faint stars, white dwarfs, and secondary components of unresolved double systems.

In principle the consistency of the results can be improved by using the redetermined centre of mass to carry out a new iteration of the membership selection. This process should ultimately lead to a consistent set of members and centre of mass. We used the centre of mass velocity for the stars in the inner 10 pc and a redetermination of the matrix in Eq. (17) from their space velocities, to carry out a second iteration of the membership selection. The result is that ten objects listed as (possible) members in Table 2 drop out as non-members. All these are

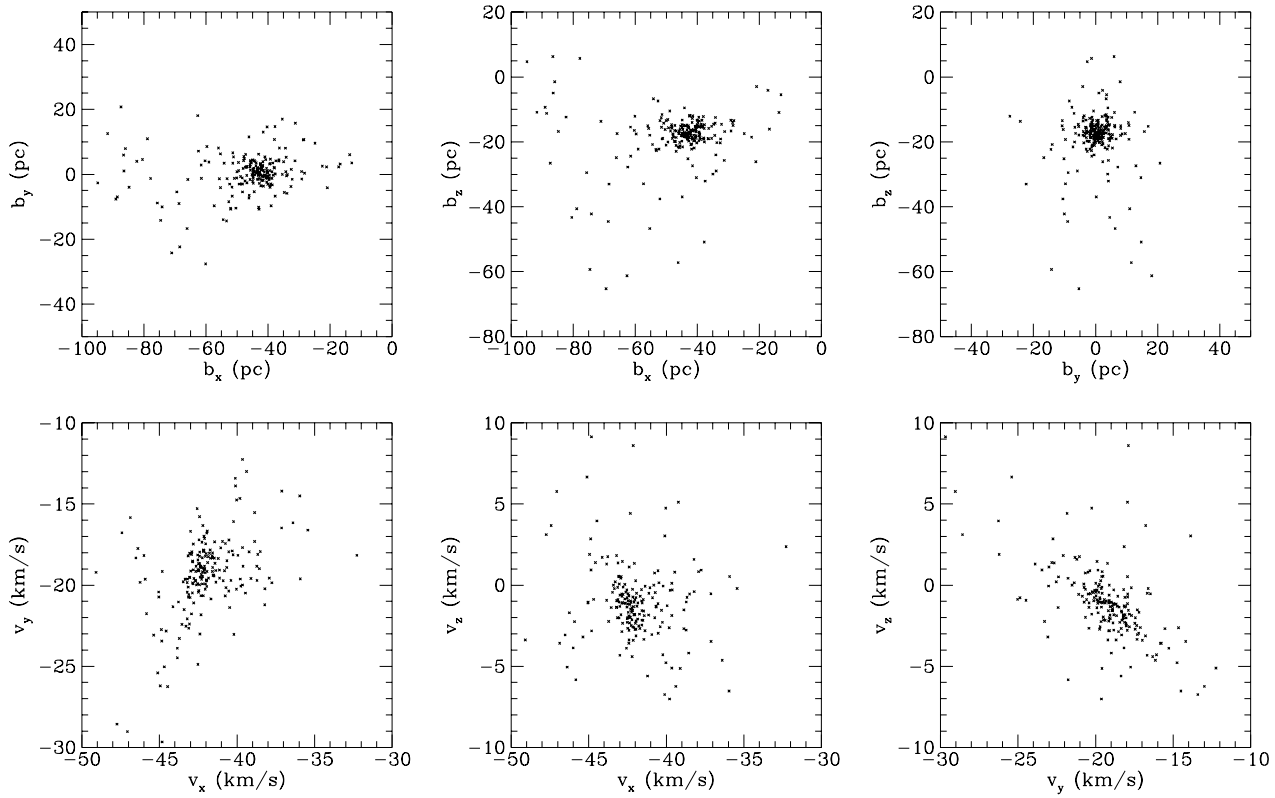


**Fig. 8.** **a** Projected positions for the 218 candidate members, in Galactic coordinates (top); **b** projected velocity distributions, in Galactic coordinates (bottom).

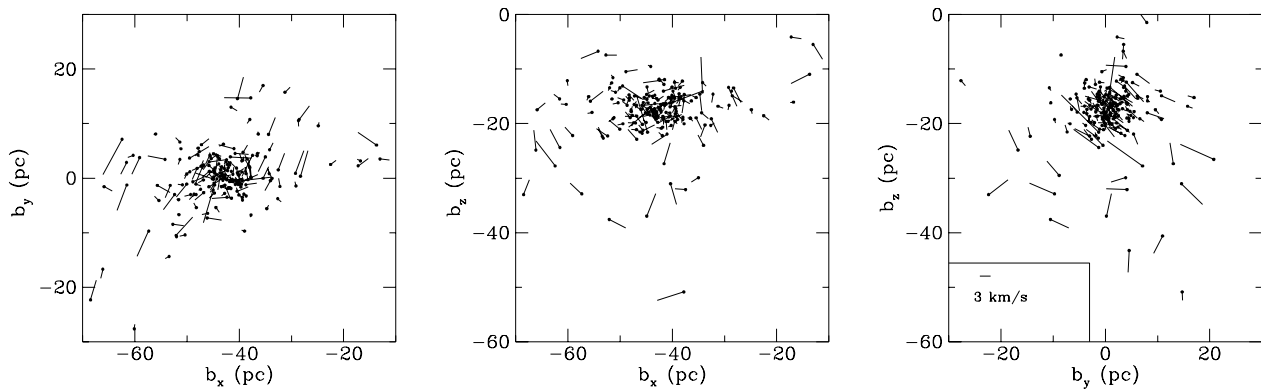


**Fig. 9.** Projected velocities as a function of position for the 197 candidate members with available radial velocities. The residuals are given with respect to the velocity of the cluster centre in Galactic coordinates. HIP 13117 is omitted due to large errors in its space velocity.

**Table 3.** Distance and velocity of the inferred centre of mass of the Hyades, as described in the text. The first line corresponds to the preliminary determination based on 142 stars in the central region. The last two lines correspond to the ‘final’ determination for the 134 stars within  $r = 10$  pc of the cluster centre, and for the 180 stars within  $r = 20$  pc of the cluster centre, respectively.

Selection	$N$	$\mathbf{b}_c$ (pc)			$\mathbf{v}_c$ (km s $^{-1}$ )			$D$ (pc)	$V$ (km s $^{-1}$ )
		$x$	$y$	$z$	$u$	$v$	$w$		
Preliminary	142	$-42.23 \pm 0.24$	$+0.15 \pm 0.06$	$-17.09 \pm 0.10$	$-41.53 \pm 0.16$	$-19.07 \pm 0.11$	$-1.06 \pm 0.11$	$45.56 \pm 0.27$	$45.72 \pm 0.22$
$r < 10$ pc	134	$-43.08 \pm 0.25$	$+0.33 \pm 0.06$	$-17.09 \pm 0.11$	$-41.70 \pm 0.16$	$-19.23 \pm 0.11$	$-1.08 \pm 0.11$	$46.34 \pm 0.27$	$45.93 \pm 0.23$
$r < 20$ pc	180	$-43.37 \pm 0.26$	$+0.40 \pm 0.09$	$-17.46 \pm 0.13$	$-41.73 \pm 0.14$	$-19.29 \pm 0.11$	$-1.06 \pm 0.10$	$46.75 \pm 0.31$	$45.98 \pm 0.20$

located beyond 10 pc from the cluster centre listed in line 3 of Table 3. Hence, a redetermination of the centre of mass would lead to the same result for the stars in the inner 10 pc and to convergence of the membership selection process. This illustrates the robustness of our membership selection procedure.

The positions of the resulting candidates in the Hertzsprung-Russell diagram are shown in Fig. 7. Those candidates retained according to the additional criterion  $\pi \geq 10$  mas are indicated separately. Fig. 8a shows the positions of the 218 candidate members in Galactic coordinates. Fig. 8b shows the projected velocity distributions. Fig. 9 shows the projected velocities as a function of position for the 197 candidate members with available radial velocity. We return to a discussion of these distributions in Sect. 7.

In the final three columns of Table 2, we provide the distance,  $d$  (in pc), of each object with respect to the adopted cluster centre defined by 134 stars within  $r < 10$  pc (see Table 3) (column v); the statistic  $\mathbf{z}'\Sigma^{-1}\mathbf{z}$ , constructed with respect to the velocity of the preliminary centre of mass (column w); and the assignments '0', '1', or '?' (column x) as our final membership indicator. A '1' is assigned on the basis of the  $\mathbf{z}'\Sigma^{-1}\mathbf{z}$  statistic alone (with the limits of  $c = 14.16$ , or  $c = 11.83$  if the radial velocity is unknown, corresponding to the  $3\sigma$  confidence interval defined previously), and independent of distance from the cluster centre; '?' is assigned in column w to objects with appropriate values of the  $\mathbf{z}'\Sigma^{-1}\mathbf{z}$  statistic but for which we have no radial velocity, and are thus unable to rule on the overall stellar space motion for that object. Future assignments can be made on the basis of new or improved radial velocities, or  $\gamma$  velocities as new binary orbits are determined. In interpreting Table 2 it should be noted that objects with column x = 0 but without known radial velocity are unlikely to be members, irrespective of their radial velocity. Objects with apparently 'reasonable' values of  $\pi$  and  $V_{\text{rad}}$ , but with large values of  $c$  (and hence column x = 0) will have discrepant proper motions (not evident from the table).

## 6. Discussion of the Hipparcos parallaxes

### 6.1. Parallaxes determined from the convergent point

In Sect. 4 we demonstrated that the proper motions used by Schwan (1991) result in a different convergent point from that derived from the Hipparcos proper motion data, and that the Hipparcos proper motion data themselves do not lead to a unique convergent point, but to a successive selection of objects at each iteration of the convergent point method occupying a different location in velocity space (a closer study of the stars listed in Table 2 and our final list of members reveals that no corresponding spatial bias is introduced).

Before proceeding with a discussion of the resulting space and velocity distributions of the candidate members, we will now examine to what extent the distances inferred from the convergent point analysis using ground-based and Hipparcos proper motions respectively, are consistent with the Hipparcos trigonometric parallaxes. In principle, this should give addi-

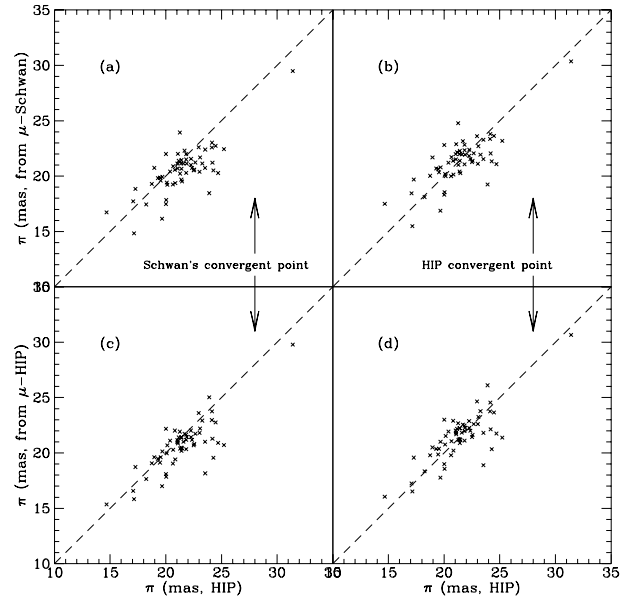


**Fig. 10a–d.** This figure shows, for the stars used by Schwan (1991), the parallaxes inferred from the convergent point, the space motion and the proper motions, versus the Hipparcos parallax. The two left panels show the parallaxes inferred from Schwan's convergent point and space motion, using Schwan's proper motions (top) and the Hipparcos proper motions (bottom). The two right panels show the same, but now the space motion derived in Sect. 5.3 is used to calculate the parallaxes from the respective proper motions.

tional confidence in the quality of the Hipparcos parallaxes and proper motions, and an insight into whether our explanations for the distance discrepancies resulting from previous ground-based proper motion investigations are correct.

Fig. 10a shows the parallaxes inferred by Schwan (1991) from his proper motion analysis (and based on his published convergent point) compared with the Hipparcos trigonometric parallaxes for the same stars. Fig. 10b is again constructed using Schwan's proper motions, but using the space motion derived in Sect. 5.3 to calculate the parallaxes from his values of the proper motions. The lower panels show corresponding results but now based entirely on the Hipparcos proper motions, using the convergent point determined by Schwan (c), and finally the space motion from Sect. 5.3 (d). The important feature of these diagrams is that Schwan's inferred parallaxes are systematically smaller than the Hipparcos trigonometric values, a trend which is visible in Fig. 10b, and still not completely eliminated in Fig. 10c, i.e. when the individual Hipparcos proper motions are used but taken in combination with Schwan's convergent point. In contrast, as seen in Fig. 10d, there is no systematic difference between the parallaxes derived from the Hipparcos proper motions and our present determination of the convergent point on the one hand, and the Hipparcos trigonometric parallaxes on the other.

Fig. 11 shows the parallaxes inferred from the Hipparcos proper motions and the present determination of the space motion of the cluster centre of mass (ordinate) versus the Hipparcos

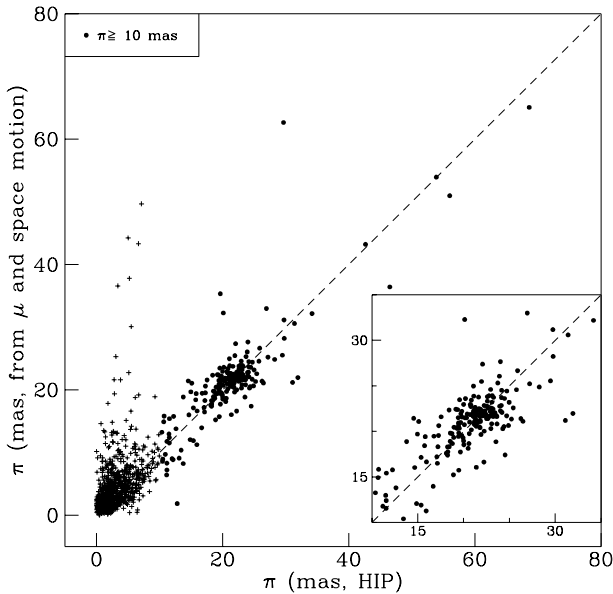


**Fig. 11.** The parallax inferred from the Hipparcos proper motions and the present determination of the space motion of the cluster centre of mass versus the Hipparcos parallaxes, for all the kinematically selected members discussed in Sect. 5.4. The outliers are stars with large errors in their astrometry, objects located close to the convergent point, or objects located at almost the same declination as the convergent point with  $\mu_{\alpha*} \gg \mu_{\delta}$  (two other outliers fall off the top of the plot). The inset shows the relevant cluster region in more detail.

parallaxes (abscissa) for all the kinematically selected members discussed in Sect. 5.4. For the subset of  $\pi \geq 10$  mas objects, the excellent correlation between the two quantities indicates that the space motion and the trigonometric parallaxes are fully consistent. The outliers include stars with large errors in their astrometry, objects located close to the convergent point, or objects located at almost the same declination as the convergent point with  $\mu_{\alpha*} \gg \mu_{\delta}$  (which will lead to a greater probability of erroneously accepting the object as a member). From Fig. 4 the proper motions from Hipparcos appear systematically larger than those used by Schwan in both right ascension and declination. Applying a sign-test to the observed differences shows that this trend is statistically significant at the 95 per cent confidence level.

We can reconcile these results as follows. The discrepancy between our reference distance modulus of  $m - M = 3.33$ , and that derived by Schwan (1991) of  $m - M = 3.40$ , corresponds to 0.07 mag in distance modulus, or a ratio of  $47.9/46.34 = 1.034$  in distance. From Eq. (2),  $d_S/d_H = |\mu_H|/|\mu_S| \times |V_S|/|V_H| \times \sin(\lambda_S)/\sin(\lambda_H)$ , where H and S refer to parameters from Hipparcos and Schwan (1991) respectively. Using  $|V_S|/|V_H| = 46.60/45.72 = 1.02$ , where  $V_H$  corresponds to the velocity of the 142 stars used for the membership selection (Table 3); and median values of  $\sin(\lambda_S)/\sin(\lambda_H) = 1.003$  and  $|\mu_H|/|\mu_S| = 1.007$  corresponding to the objects in common between the two determinations (and after transforming Schwan's data from B1950 to J2000) also leads to a combined difference of 3 per cent.

**Table 4.** Parallaxes for the objects in common between the Hipparcos Catalogue and Upgren et al. (1990).

HIP No.	van Altena No.	$\pi_{\text{abs}}$ (HIP) (mas)	$\pi_{\text{abs}}$ (U 90) (mas)
20485	276	$21.08 \pm 2.69$	$17.4 \pm 3.8$
20527	294	$22.57 \pm 2.78$	$18.5 \pm 4.8$
20563	310	$19.35 \pm 1.79$	$24.2 \pm 3.2$
20679	363	$20.79 \pm 1.83$	$23.4 \pm 4.4$
20827	459	$17.29 \pm 2.23$	$22.4 \pm 5.6$
20850	472	$21.29 \pm 1.91$	$29.5 \pm 5.2$
20978	560	$24.71 \pm 1.27$	$29.0 \pm 5.8$
21138	645	$15.11 \pm 4.75$	$22.0 \pm 5.0$

While the median differences between the two sets of proper motions are below 1 per cent, the derived cluster distance is also sensitive to the cluster's space velocity – Schwan's larger radial velocity at the cluster centre ( $39.1 \text{ km s}^{-1}$  compared to  $38.6 \text{ km s}^{-1}$ ), and larger angular distance from cluster centre to the convergent point, both lead to a larger space velocity, and to larger values of  $\sin(\lambda)$  for all stars.

## 6.2. Comparison with previous parallax determinations

In demonstrating that the Hipparcos parallaxes and proper motions together provide a consistent picture of the Hyades structure, space velocity, and dynamics, our results provide independent evidence (in addition to that provided by the catalogue construction) that the trigonometric parallaxes and their standard errors may be taken at face value. Since recent ground-based determinations of trigonometric parallaxes for candidate Hyades members have reached formal standard errors of a few milliarcsec, a comparison between these and the Hipparcos Catalogue values should therefore permit further insight into discrepancies between parallaxes (and resulting cluster distance modulus) determined by different ground-based observatories. In this section we undertake a first examination of these differences. It is important to recall that the Hipparcos parallaxes are to be considered as absolute, while ground-based determinations require corrections to convert the measurements to absolute values, taking into account the parallax distribution of the reference stars.

Eight of the 23 Hyades parallax stars observed by Upgren et al. (1990), three of the stars from the list of Ianna et al. (1990), six of the 10 Hyades parallax stars observed by Patterson & Ianna (1991), the spectroscopic interferometric binary 51 Tauri observed by Gatewood et al. (1992) and Torres et al. (1997a), and the spectroscopic interferometric binaries 70 Tauri and 78 Tau observed by Torres et al. (1997b,c), are also contained in the Hipparcos Catalogue. In addition, 60 of our candidate members are contained in the Fourth Edition of the General Catalogue of Trigonometric Parallaxes (van Altena et al. 1995).

Mean magnitudes of ground-based parallax stars are typically about  $V = 11$  mag, significantly fainter than the median of the Hipparcos programme, which leads to relatively large values of  $\sigma_{\pi, \text{HIP}} \sim 2 - 4$  mas for these comparison objects compared

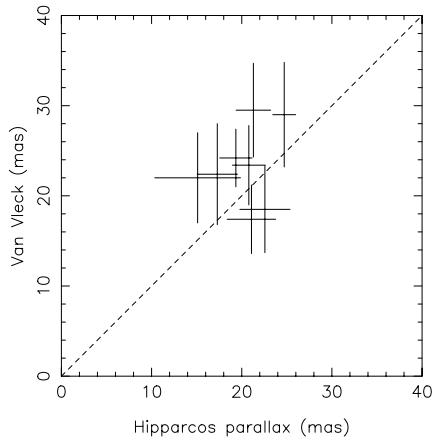


**Fig. 12.** The differences between the Hipparcos parallaxes, and  $\pi_{\text{abs}}$  determined by Uppgren et al. (1990) from observations made at the Van Vleck Observatory for the eight stars in common between the two programmes.

with the median value, of  $\sigma_{\pi, \text{HIP}} \sim 1$  mas, for the Hipparcos Catalogue as a whole.

Fig. 12 shows the relationship between the Hipparcos parallaxes and the determinations derived from the Van Vleck observations by Uppgren et al. (these are listed in Table 4, which also gives the correspondence between the HIP number and the van Altena number used by Uppgren et al.). We have eliminated HIP 20605 (vA 334) from the comparisons because of its inaccurate Hipparcos parallax, largely as a result of its faint magnitude ( $V = 11.7$  mag). Uppgren et al. used the corrections from relative to absolute parallaxes according to the precepts of van Altena et al. (1991). The ground-based and Hipparcos parallaxes are in reasonable overall agreement, with  $\langle \pi_{\text{HIP}} - \pi_{\text{U90}} \rangle = -2.5 \pm 4.6$  mas, to be compared with the average correction from relative to absolute parallaxes, applied by Uppgren et al., of 2.6 mas.

Three Hyades objects observed by Ianna et al. (1990), and referred to there by their Johnson number (Johnson et al. 1962), were also observed by Hipparcos, and these yield  $\pi_{\text{HIP}} = 19.17 \pm 1.93$  mas and  $\pi_{190} = 18.9 \pm 4.7$  mas for HIP 20419 (HY 259);  $\pi_{\text{HIP}} = 21.10 \pm 2.22$  mas and  $\pi_{190} = 11.4 \pm 4.8$  mas for HIP 21946 (HY 318); and  $\pi_{\text{HIP}} = 18.44 \pm 1.66$  mas and  $\pi_{190} = 35.7 \pm 5.3$  mas for HIP 23498 (HY 351, more commonly called vB187); the significant discrepancy for the latter may be partly attributable to the acceleration of the photocentric motion observed by Hipparcos.

Fig. 13 shows the relationship between the Hipparcos parallaxes and the determinations derived from the McCormick and Stromlo observations by Patterson & Ianna,  $\pi_{\text{abs, GCTP}}$  (these are listed in Table 5; note that their Tables 1 and 3 refer to van Bueren numbers for the first four stars, and Johnson numbers for the last six stars). The comparison uses their reductions from relative to absolute parallaxes based on the statistical corrections determined from the General Catalogue of Trigonometric Parallaxes (van Altena et al. 1991), with an average correction of 2.8 mas. The corrections to absolute derived by Patterson

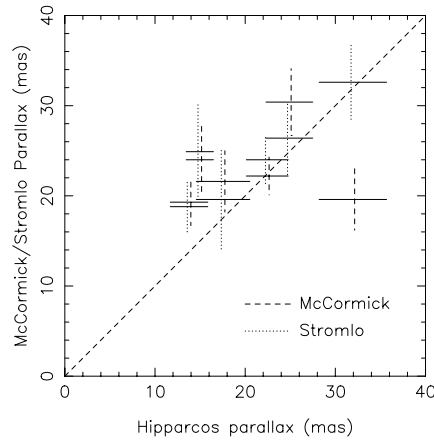


**Fig. 13.** The differences between the Hipparcos parallaxes, and  $\pi_{\text{abs, GCTP}}$  determined by Patterson & Ianna (1991) from observations made at the McCormick and Stromlo Observatories for the six stars in common between the two programmes. To avoid overlap of the error bars, the Hipparcos values have been shifted by +0.2 mas for the McCormick comparisons, and by  $-0.2$  mas for the Stromlo comparisons.

& Ianna (1991) on the basis of spectroscopic parallaxes of field stars were slightly larger and result in an increasing discrepancy with the Hipparcos values for all but the McCormick observations of HIP 19834. On the basis of this small number of stars, the ground-based trigonometric parallaxes (and especially those from the Stromlo observations) are seen to be reasonably consistent with those from Hipparcos, with reliable estimates of the standard errors, and  $\langle \pi_{\text{HIP}} - \pi_{\text{P91}} \rangle = -3.5 \pm 3.5$  mas for the GCTP-corrected Stromlo values.

Gatewood et al. (1992) have used the Multichannel Astrometric Photometer at the Allegheny Observatory to determine the parallax of the spectroscopic-interferometric binary 51 Tauri (HIP 20087, vB24) of  $19.4 \pm 1.1$  mas (employing a correction from relative to absolute parallaxes of 1.7 mas), compared with  $\pi_{\text{HIP}} = 18.25 \pm 0.82$  mas. A more recent orbital parallax for the same object has been derived by Torres et al. (1997a),  $\pi_{\text{orb}} = 17.9 \pm 0.6$  mas, a value which puts these two fundamental distance determinations of this object in excellent agreement. Determinations for the binary 70 Tau (HIP 20661, vB57) by Hipparcos,  $\pi_{\text{HIP}} = 21.47 \pm 0.97$  mas, and by Torres et al. (1997b),  $\pi_{\text{orb}} = 21.44 \pm 0.67$  mas, as well as for the binary 78 Tau (HIP 20894, vB72,  $\theta^2$  Tau) by Hipparcos,  $\pi_{\text{HIP}} = 21.89 \pm 0.83$  mas, and by Torres et al. (1997c),  $\pi_{\text{orb}} = 21.22 \pm 0.76$  mas, are also in particularly good agreement, and may be taken as further evidence for the reliability of these separate distance determinations, as well as for the robustness of the Hipparcos parallax determinations for binary systems.

It is noted that the subsequent determinations of the mean cluster distance by Torres et al. (1997a,b,c), based on these three specific objects, is sensitive to the proper motions adopted for the individual cluster members. While they derive a resulting distance modulus of  $3.40 \pm 0.07$  based on 51 Tau, of  $3.38 \pm 0.11$  based on 70 Tau, and of  $3.39 \pm 0.08$  based on 78 Tau, we can in-

**Table 5.** Parallaxes from the Hipparcos Catalogue and from Patterson & Ianna (1991).

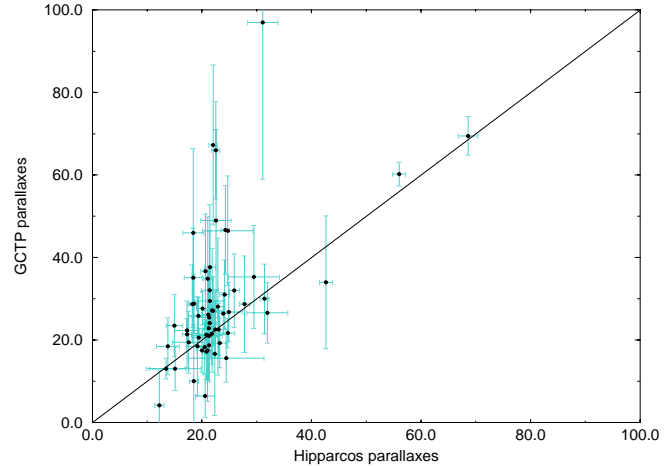
HIP No.	van Bueren No.	Johnson No.	$\pi_{\text{abs}}$ (HIP)	$\pi_{\text{abs}}$ (PI 91)		$\pi_{\text{abs, GCTP}}$ (PI 91)	
			(mas)	McCor. (mas)	Stromlo (mas)	McCor. (mas)	Stromlo (mas)
19316	–	233	24.90±2.59	31.6±3.7	27.6±4.1	30.4±3.7	26.4±4.1
19834	–	245	31.94±3.74	20.0±3.4	33.0±4.4	19.6±3.4	32.6±4.4
20601	140	–	14.97±1.51	24.5±3.7	25.4±5.2	24.0±3.7	24.9±5.2
21179	–	288	17.55±2.97	23.2±3.4	21.1±5.5	21.6±3.4	19.6±5.5
22177	–	326	22.45±2.32	22.7±2.1	24.5±2.8	22.2±2.1	24.0±2.8
23701	151	–	13.78±2.08	20.7±2.6	20.2±2.8	19.3±2.6	18.8±2.8

fer that any revised estimate of the mean cluster distance based on the use of the inertially referenced Hipparcos proper motions would yield essentially the same distance modulus as that presented here. For example, using the Hipparcos parallax for 51 Tau, our convergent point for the inner 20 pc region, and the Hipparcos proper motions, we find a mean cluster distance of 46.14 pc for the 53 stars used by Torres et al. (1997a), a value very close to our centre of mass value. The formula used by Torres et al. to derive distances ( $d_i = d_0(\mu_0/\mu_i)(\sin(\lambda_i)/\sin(\lambda_0))$ , where the subscript zero refers to the reference object), utilises the PPM proper motion for 51 Tau (about 5 per cent larger than the Hipparcos value), and the PPM proper motions of the additional cluster stars, which are almost all smaller than those of Hipparcos (as discussed in Sect. 6.1). These effects together cause the systematically larger distances derived by Torres et al. for the cluster.

McClure (1982) derived a dynamical parallax for the Hyades binary HD 27130 (vB 22, HIP 20019) leading to a distance modulus of  $3.47 \pm 0.05$  mag, considerably larger than most astrometric determinations. The Hipparcos parallax,  $\pi_{\text{HIP}} = 21.40 \pm 1.24$  mas (distance modulus  $3.35 \pm 0.12$  mag) suggests that the distance modulus inferred by McClure was overestimated. The resulting M-L relationship for binaries (including vB 22) has been discussed by Torres et al. (1997a).

As discussed by van Altena et al. (1993, 1994), and in the Introduction to the Fourth Edition of the General Catalogue of Trigonometric Stellar Parallaxes (van Altena et al. 1995), the heterogeneous nature of ground-based parallaxes makes any comparisons between them and the corresponding Hipparcos parallaxes difficult to interpret in any unified manner. Thus, in establishing the system of the Fourth Edition of the GCTSP (van Altena et al. 1995) three distinctly different problems were addressed: (1) the correction from relative parallax to absolute parallax; (2) the relative accuracy of parallaxes determined at different observatories; and (3) systematic differences, or zero-point differences between observatories. Whether the present results, and in particular Figs. 12 and 13, suggest that the corrections from relative to absolute parallaxes, or the relative parallaxes themselves, have typically been slightly overestimated from ground-based observations, remains to be understood.

A comparison for the 60 candidate Hyades members contained in the Fourth Edition of the GCTSP is shown in Fig. 14. Determination of the distance modulus based on 104 Hyades members from the GCTSP yielded  $m - M = 3.32 \pm 0.06$  mag

**Fig. 14.** A comparison between the GCTSP parallax (van Altena et al. 1995) and the Hipparcos parallax (both in mas) for the 60 candidate members in common between the two catalogues.

(van Altena et al. 1997b), in good agreement with our present determination, suggesting that the GCTSP and Hipparcos systems are indistinguishable to within the limits set by the ground-based parallax accuracies, at least for the Hyades region.

The are significant differences between the Hipparcos parallaxes (and proper motion components) and the individual Hubble Space Telescope Fine Guidance Sensor observations reported by van Altena et al. (1997a). For the three brightest stars out of the four in common between the two sets of observations (HIP 20563/vA310, HIP 20850/vA472, HIP 21123/vA627) the Hipparcos parallaxes are between 26–42 per cent larger than the corresponding HST values. Discrepancies between the proper motion components reach  $10\text{--}20$  mas yr $^{-1}$ . We offer no convincing explanation for these differences but, given the consistency of the Hipparcos measurements presented elsewhere in this paper, presently favour the Hipparcos values. Additional investigations will be required in order to substantiate these claims.

### 6.3. Lutz-Kelker corrections, and other effects

Problems with the use of trigonometric parallaxes have long been recognised (Eddington 1913, Lutz & Kelker 1973, Smith

& Eichhorn 1996). One particular difficulty of interpretation arises because the distance estimate  $d = 1/\pi$  is biased, with the error distribution of this estimate obtained by multiplying the probability density function of  $\pi$  by the Jacobian of the transformation from  $\pi$  to  $d$  (Luri & Arenou 1997). As a consequence, with  $d = 1/\pi$  used to estimate distances, an *a posteriori* correction is required – this statistical correction is applicable when determined for and applied to a particular sample population. ‘Lutz-Kelker’ type luminosity corrections arise correspondingly, and may be understood qualitatively as arising from the fact that the error volume beyond the distance corresponding to the measured parallax is larger than the associated error volume at smaller distances; accounting for this effect makes all derived luminosities brighter by an amount depending on the relative parallax error,  $\sigma_\pi/\pi$ . Applicable corrections are not the same for a uniform space distribution of stars compared with a sample drawn from a concentrated population.

The bias on the distance estimates for individual objects in the Hyades cluster based on the Hipparcos parallaxes can be calculated analytically (Smith & Eichhorn 1996), depending on the relative error in the parallax, which is less than 0.1 for 78 per cent of the Hyades members (94 per cent have  $\sigma_\pi/\pi \leq 0.2$ ). Hence for most of the members the expectation value of the bias in the distance will be less than 1 per cent. Since the same bias enters in the tangential velocities  $V_{\alpha*}$  and  $V_\delta$ , the process of selecting members based on kinematics should not be affected. However, for individual objects the bias in  $v_x$  and  $v_z$  (derived from  $V_{\alpha*}$ ,  $V_\delta$  and  $V_R$ ) can be quite large (up to 20 per cent overestimate for  $v_x$  and 8 per cent underestimate for  $v_z$ ). Thus particular care must be taken when interpreting space velocities for individual objects with a large relative error on the parallax.

Smith & Eichhorn (1996) demonstrated that although one can calculate analytically the bias in the distance derived from the parallax of an individual star, the variance in the expectation value for the distance is infinite, so that a correction of the measured distance is not possible. However, if the distribution of true parallaxes were known, the parallax of each individual object could be corrected, in a statistical sense, *a posteriori*. Given the observed parallax and the associated error, the most likely value of the true parallax, and hence the true distance, could be estimated. In principle one could deconvolve the distribution of measured parallaxes (e.g. Lindegren 1995) to derive the error-free distribution of parallaxes. However, this necessarily assumes that the observed sample of stars is statistically representative of the underlying parent sample. In reality, the parallaxes are measured for a sample of stars subject to specific selection effects.

In the case of Hipparcos the selection effects are complicated, and the parent sample of stars is known with only limited accuracy. In view of the uncertainties in the knowledge of both the parent sample of stars and the selection effects, and given that for the relevant values of  $\sigma_\pi/\pi < 0.1$  individual magnitudes are likely to be biased at levels at or below about 0.01 mag (cf. Smith & Eichhorn, Fig. 6) no statistical corrections of the individual parallaxes have been attempted in the present work. Any resulting effect on the HR diagram, including the slope of

the main sequence (the fainter stars, having larger errors, will have a larger bias) is expected to be small, and has not been considered further in this work.

However, an assessment of the possible resulting bias in the *mean* Hyades distance and velocity, corresponding to a realistic space distribution of Hyades member stars, has been investigated by Monte Carlo simulation based on: (i) a synthetic cluster at the position of the Hyades, generated with an (albeit simplified) Plummer density distribution with a core radius of 2.85 pc (see Sect. 8.1); (ii) the luminosity function for the Hyades derived by Reid (1993); (iii) a crude approximation to the Hipparcos selection of stars as a function of magnitude; (iv) errors on the parallax which increase with the apparent magnitude of the star.

For 1000 realizations of the cluster, 220 stars were generated and realistic errors reflecting the Hipparcos observations (with a median increasing with apparent magnitude) were added to the parallaxes. For each star the corresponding (ICRS) values of  $b_x$ ,  $b_y$  and  $b_z$  were calculated, and the space velocity components were calculated from the true proper motions and radial velocities combined with the parallax. From these quantities the mean values of the components of  $\mathbf{b}$  and  $\mathbf{v}$  were calculated, as well as the distance and velocity of the cluster.

These results suggest that our mean distance to the cluster and overall velocity are each overestimated by about 0.09 per cent. The coordinate transformations imply that the components of  $\mathbf{b}$  are then overestimated by 0.2, 0.06 and 0.03 per cent respectively, while the velocity component  $v_x$  is overestimated by 0.8 per cent,  $v_y$  by 0.06 per cent and  $v_z$  is underestimated by 0.29 per cent. These biases are typically small in comparison with the errors quoted for these quantities in Table 3.

To these problems of working with trigonometric parallaxes, we note finally one effect resulting from the specific observational configuration of Hipparcos, which results in a correlation length of  $1-2^\circ$  over which some small residual correlations will probably exist in the derived astrometric parameters (Lindegren 1989). Such an effect results in the error in the mean decreasing not as  $n^{0.5}$  but probably more as  $n^{0.35}$ , leading to a small underestimate in the final error on the estimated distance of the centre of mass.

## 7. Structure and kinematics of the Hyades cluster

### 7.1. Spatial distribution

Fig. 8 shows clear evidence for a centrally concentrated group, possibly extended in  $b_x$  (in the direction of the Galactic centre), with an evident correlation between the velocities in the Galactic coordinate directions  $y$  and  $z$ . Fig. 9 indicates velocity residuals which increase with distance from the cluster centre, and which may be suggestive of systematic motions. In this section we compare these results with the expected space and velocity distributions predicted from  $N$ -body simulations, and address the question of whether the cluster members display velocity residuals consistent with a co-moving system with constant space velocity, or whether there is evidence for systematic expansion

(or contraction), rotation, or shearing motion due, for example, to the effects of the Galactic tidal field or passing interstellar clouds, or to the shearing effect of differential Galactic rotation. These effects, as well as the evaporation of stars through relaxation by stellar encounters, are considered to represent primary mechanisms responsible for the disruption of open clusters.

Realistic  $N$ -body simulations of the dynamical evolution of open clusters have been made by Terlevich (1987), de la Fuente Marcos (1995), Kroupa (1995) and others, aiming to reproduce features such as the observed distribution of cluster ages, mass density, binary distribution, and mass loss. Comparison with the models of Terlevich prove to be of particular interest since her  $N$ -body interactions not only took into account specific forms for the initial mass function and mass loss due to stellar evolution, but were also supplemented by the effects of the Galactic tidal field and transient tidal shocks produced by passing interstellar clouds. Since it is known that the age distribution of Galactic open clusters barely extends beyond about 1 Gyr, and that disruptive encounters are likely to be responsible for cluster break-up, we may hope to investigate whether the space and velocity distribution of objects beyond the tidal radius provides evidence for such a disruptive encounter. For example, Terlevich finds that a cluster loses 90 per cent of its stars in 100 million years after a collision with a giant molecular cloud, in which the stars would acquire rather high velocities.

Kroupa (1995) starts with a very large proportion of primordial binaries, and traces the stellar luminosity function as a result of mass segregation, evaporation, and changing proportion of binary systems, assuming models with  $\langle M \rangle = 0.32$  and  $M_C = 128 M_\odot$ , near to the peak of the mass function of Galactic clusters. He takes the disintegration time to be the time taken for the number density to reach  $0.1 \text{ stars pc}^{-3}$ , characteristic of the Galactic disc in the proximity of the Sun and, finding that these disintegration times are significantly longer than the lifetimes of real clusters (Battinelli & Capuzzo-Dolcetta 1991), suggests that mechanisms other than internal dynamical evolution must be responsible for cluster disintegration, such as impacts with giant molecular clouds. These encounters have been further modelled by Theuns (1992a, b), and confirm the systematic velocity signatures in the outer cluster regions, depending on the nature of the encounter, predicted previously (e.g. Binney & Tremaine 1987, Sect. 7.2).

The equipotential cluster surface becomes open, due to the effects of the Galactic tidal potential, at distances from the cluster centre referred to as the tidal radius  $r_t$  (King 1962, Wielen 1974). These openings provide an escape route for stars to evaporate from the system. In the case of the Hyades, we find  $r_t \simeq 10 \text{ pc}$  (see Sect. 8.3). The existence of an extended halo formed by stars outside this tidal radius, but sharing the proper motion characteristics of the rest of the cluster members was originally noted by Pels et al. (1975), and has since been reported for other clusters.

A striking feature of Fig. 8 is that, although the tidal radius is of the order of 10 pc, about 45 stars are nevertheless found between 10–20 pc, a result consistent with the simulations by Terlevich (1987) – these demonstrated that since the openings

of the equipotential surface are on the  $x$ -axis, stars can spend some considerable time within the cluster before they find the windows on the surface to escape through. Such  $N$ -body simulation models consistently show a halo formed by 50–80 stars in the region between 1–2 tidal radii – some of these stars, despite having energies larger than that corresponding to the Jacobi limit, are still linked to the cluster after 300–400 Myr.<sup>1</sup>

These results appear to be weakly dependent on the slope of the IMF: Terlevich used  $\alpha = 2.75$ , although de la Fuente Marcos (1995) has argued that for systems with large numbers of members the different models have very similar behaviour for the escape rate. [In any detailed interpretation of the spatial distribution of our candidate members in Fig. 8, it should be noted that certain selection effects operate in restricting the region of these diagrams which may be populated, due to the restricted region of  $\alpha$ ,  $\delta$  used for the study (Sect. 3) combined with the projection of the equatorial coordinates into Galactic coordinates.]

It would seem natural to identify escaping stars, evident both from numerical simulations and from our observations, with the extended Hyades stellar group. The existence of such a system – stars having the same average motion as the cluster but a very much larger space and velocity distribution – was first suggested by Hertzsprung (1909), and followed up by Strömberg (1922, 1923), Eggen (1960, 1982 and references therein) and others. Recent models have been discussed by Casertano et al. (1993). This group is characterised by proper motions coinciding in direction with that of the Hyades, but considerably smaller in size. We will examine the relationship between this group and the central cluster in Sect. 7.2.

A possible flattening of the Hyades cluster has long been debated. Flattening of the equipotential surfaces, perpendicular to and directed toward the Galactic plane, was predicted by Wielen (1967) and in the  $N$ -body models of Aarseth (1973). Van Bueren (1952) noted that the cluster appeared to be flattened along the Galactic plane. Although this was not evident in the observational studies of Pels et al. (1975), the suggestion re-emerged with a fairly clear indication of flattening in the outer region noted by Oort (1979), and subsequently by Schwan (1991). The effect is clearly evident in the  $N$ -body simulations by Terlevich (1987, Fig. 8).

A principal components analysis of the distribution of space positions for our Hyades members within 20 pc from the cluster centre shows that the cluster has a prolate shape. The major axis lies almost along  $b_x$  in Galactic coordinates, making an angle of  $\sim 16^\circ$  with the positive  $x$ -axis. The intermediate axis lies almost along  $b_y$ , making an angle of  $\sim 16^\circ$  with the positive  $y$ -axis. The short axis lies along  $b_z$ . The axis ratios are 1.6 : 1.2 : 1, where these values have been derived from the standard deviations in position along the three axes, corrected for the median error in position along the corresponding axes (similar axis ratios of 1.5 : 1.2 : 1 are derived by multiplying the quartiles of the

<sup>1</sup> Another mechanism which can allow a cluster to hold on to stars that are beyond the tidal limit is binding by an angular-momentum-like non-classical integral, cf. Hénon 1970, Innanen et al. 1983.

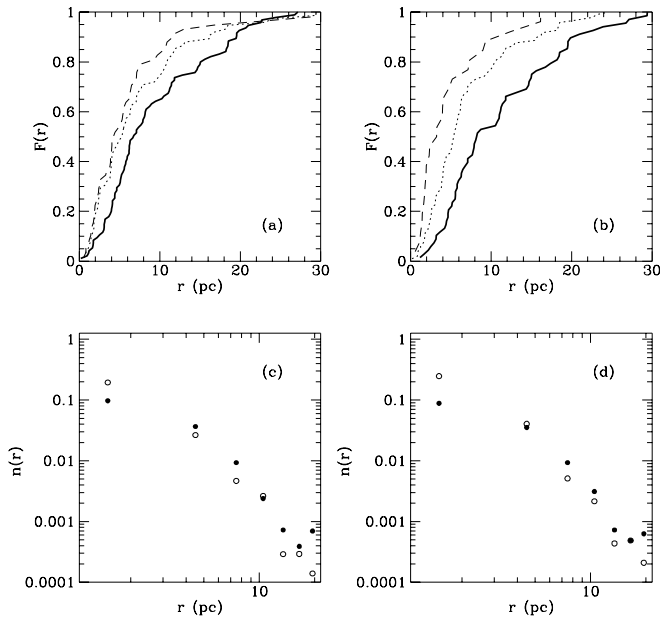


**Fig. 15a–d.** In **a** cumulative distributions versus distance from the cluster centre are shown for single stars (solid line, 95 objects); binaries (resolved or spectroscopic; dotted line, 75 objects); and spectroscopic binaries only (dashed line, 58 objects). In **b** cumulative distributions are shown for  $M \leq 1M_{\odot}$  (solid line 68 objects);  $1 \leq M \leq 2M_{\odot}$  (dotted line, 97 objects); and  $M > 2M_{\odot}$  (dashed line, 26 objects). In **c** the corresponding number densities are shown for single stars (●, 89 objects) or binaries (○, 71 objects). In **d** corresponding number densities are shown for  $M \leq 1.2M_{\odot}$  (●, 90 objects and  $M > 1.2M_{\odot}$  (○, 91 objects).

distribution by the factor converting the quartile to the standard deviation for a normal distribution). The inner 10 pc region of the Hyades is more nearly spherical. The fact that the shape of the outer parts of the cluster is prolate suggests that it is primarily extended in  $b_x$ , although it is possibly also slightly compressed in  $b_z$ , as shown in Sect. 8.2. This is consistent with the extension being caused by stars slowly escaping through the Lagrangian points on the  $x$ -axis.

Fig. 15 shows the cumulative distributions and number densities versus distance from the adopted cluster centre, for single stars and binaries for various mass groups. In the central 2 pc region, only stars more massive than about  $1 M_{\odot}$  are found (right-hand figures), and most of these are binaries (left-hand figures). This general effect was already noted by van Bueren (1952) and Pels et al. (1975), and is precisely as found in the simulations by Terlevich (1987). We note in passing that the division between ‘hard’ and ‘soft’ binaries, taken as the separation at which the (circular) orbital velocity ( $v = \sqrt{GM/r}$ ) is equal to the rms random motion is, for a system mass of  $1 M_{\odot}$  and  $v = 0.25 \text{ km s}^{-1}$  (see Sect. 7.2) is about 0.07 pc, or  $\sim 5$  arcmin at the distance of the Hyades. Numerical and statistical theories of star clusters predict the formation of a halo where the density falls as  $r^{-q}$ , with  $q$  between 3 and 3.5 (King 1966, Spitzer 1975). Although for clusters with low central concentration such a power-law density distribution over the whole cluster is an inadequate rep-

resentation, from Fig. 15 we find  $q \simeq 3.3$  for single stars in the range  $r = 4 - 10$  pc,  $q \simeq 2.9$  for  $M < 1.2M_{\odot}$  and  $q \simeq 3.5$  for  $M > 1.2M_{\odot}$ . Thus less massive stars are more spatially extended than the more massive ones, with a lower density than for the high mass stars in the central regions, consistent with results from numerical simulations. Binaries follow the radial distribution according to their mass, implying that mass is the predominant segregation factor, rather than whether the system is binary or not.

This mass segregation in turn implies that cluster luminosity functions derived from the central regions of the cluster will include an artificial flattening due to such mass segregation. The overabundance of bright stars is well established observationally, with Reid (1993) attributing this to mass segregation and stellar evaporation, while Eggen (1993) also shows that the luminosity function is depleted at the faint end compared with the observed field-star luminosity function.

In the numerical models, massive stars sink to the central region, forming binaries, which become harder through the interaction with lighter stars, which in turn acquire enough energy to reach the outer parts of the cluster. There is a strong preference for energetic binaries to be formed among the heaviest members, which tend to segregate towards the dense central part of the cluster. Binaries themselves may not play a significant role in the evolution of the cluster, unless there is a significant population of primordial binaries (e.g. as concluded by Kroupa 1995). Griffin et al. (1988) estimate that 30 per cent of the cluster members with  $2.6 < M_V < 10.6$  are radial velocity binaries. For systems brighter than  $M_V \simeq 13$  Eggen (1993) finds a photometric binary proportion of 0.4. Kroupa interprets his own simulation results as suggesting that the total proportion of systems in the central 2 pc sphere that are binary stars may be as high as 65 per cent. Such models have been extrapolated by Kroupa (1995), Reid (1993), Weidemann et al. (1992) and others to derive a mass of around  $1300 M_{\odot}$  (and around 3000 stars in total) at birth.

Counting the stars with an SB or RV indication in column s of Table 2 and those with an indication C, G, O, V, X, or S in column u as *bona fide* binaries, we find in our sample of members a binary fraction of 40 per cent. This fraction increases to 61 per cent for the stars located within 2 pc from the cluster centre, with almost all binaries in the central region being spectroscopic.

## 7.2. Velocity distribution

We now turn to an examination of the velocity distribution within the cluster. As stated in Sect. 5.2 the internal velocity dispersion in the centre of the cluster is not resolved with the accuracy of our present velocity data. The intrinsic dispersion expected for a cluster like the Hyades, in dynamical equilibrium, is  $\sim 0.2 \text{ km s}^{-1}$  (van Bueren 1952, Gunn et al. 1988), below the upper limit of the observed dispersion.

Investigation of the possible systematic effects due to rotation of the cluster was investigated by Wayman et al. (1965), while Wayman (1967) estimated a limit on the contraction of

$K = -0.013 \pm 0.015 \text{ km s}^{-1} \text{ pc}^{-1}$ . Hanson (1975) considered the possibility of expansion, contraction, or rotation contributing significantly to the star's space velocities, and inferred that the convergent point solution was sufficiently insensitive to rotation that observable effects would be seen before impacting on the convergent point distance. Hanson also discounted significant shear due to differential Galactic rotation. Gunn et al. devoted particular attention to the assessment of the velocity dispersion and the possible rotational flattening of the system.

The residual velocities shown in Fig. 9 suggest that a number of stars in the outer regions of the Hyades show very substantial deviations from the mean cluster motion. These deviations are, by definition, within '3 $\sigma$ ' of our mean cluster motion, but a systematic pattern suggestive of a rotation or shearing motion in the cluster does seem to exist, although it is noted that the interpretation of a projection into two-dimensions of systematic structures in three dimensions is not necessarily clearly evident to the eye. Although other interpretations have been considered (see below), the correlations between the residual velocities in Fig. 8 turn out to be fully consistent with the observational errors, as we shall demonstrate.

In deriving space velocities for the cluster stars we make use of the observed vector  $(\pi, \mu_{\alpha*}, \mu_{\delta}, V_R)$ . This vector is transformed to a space velocity, implicitly invoking a transformation to  $(V_{\alpha*}, V_{\delta}, V_R)$ . On the assumption that the astrometric errors are uncorrelated the transformation of the observables to the vector  $(\pi, V_{\alpha*}, V_{\delta}, V_R)$  yields the covariance matrix:

$$\begin{pmatrix} & & & 0 \\ & \mathbf{S} & & 0 \\ & & & 0 \\ 0 & 0 & 0 & \sigma_{V_R}^2 \end{pmatrix} \quad (18)$$

With  $a = A_v/\pi^2$ ,  $\mathbf{S}$  is given by:

$$\begin{pmatrix} \sigma_{\pi}^2 & -\mu_{\alpha*} a \sigma_{\pi}^2 & -\mu_{\delta} a \sigma_{\pi}^2 \\ -\mu_{\alpha*} a \sigma_{\pi}^2 & a^2 \mu_{\alpha*}^2 \sigma_{\pi}^2 + A_v a \sigma_{\mu_{\alpha*}}^2 & a^2 \mu_{\alpha*} \mu_{\delta} \sigma_{\pi}^2 \\ -\mu_{\delta} a \sigma_{\pi}^2 & a^2 \mu_{\alpha*} \mu_{\delta} \sigma_{\pi}^2 & a^2 \mu_{\delta}^2 \sigma_{\pi}^2 + A_v a \sigma_{\mu_{\delta}}^2 \end{pmatrix}$$

Hence, even in the absence of correlations between astrometric errors, the parallaxes and velocity components  $V_{\alpha*}$  and  $V_{\delta}$  will in general be correlated. Moreover, because of the position of the convergent point of the system with respect to the cluster centre,  $\mu_{\alpha*}$  is positive and  $\mu_{\delta}$  is negative for most cluster members, and hence the product  $\mu_{\alpha*} \mu_{\delta}$  is negative. Thus for most stars the uncertainties in  $\pi$  and  $V_{\alpha*}$  are anti-correlated, the uncertainties in  $\pi$  and  $V_{\delta}$  are correlated, and the uncertainties in  $V_{\alpha*}$  and  $V_{\delta}$  are anti-correlated, which will lead to systematic behaviour of the uncertainties in the sample as a whole. These systematics will be transferred to the space velocities.

To confirm the prediction of correlations in the velocity residuals we proceed as follows. If we assume that the motions of the cluster members are only due to the mean motion of the cluster, then the observations of the velocities of the cluster members will all have the same expectation value. We can then average all measured velocities to obtain a mean motion, with the uncertainty in the mean given by the mean of the covariance

matrices of the individual members. This mean covariance matrix can then be used to construct the confidence region within which all residual velocities should lie. This is illustrated in Fig. 16 for all the Hyades members with a known radial velocity. The contours delineate the confidence region at confidence levels 68.3%, 95.4%, 99.73%, and 99.99%. From an eigenvector analysis of the mean covariance matrix, the minor axis of the distribution of velocity residuals is found to point in the direction  $\ell = 105^\circ$ ,  $b = 46^\circ$ , which explains the flattened appearance of the distribution of residuals in Fig. 8b (rightmost diagram).

An examination of Fig. 9 reveals a correlation between the velocity residuals (magnitude and direction) and the distances (parallaxes) of the stars. This effect, especially evident in the leftmost diagram, can be understood as follows. The difference between the observed and true stellar parallaxes ( $\Delta\pi = \pi_{\text{obs}} - \pi_{\text{true}}$ ) is not correlated with the true parallaxes. However, adding  $\Delta\pi$  to  $\pi_{\text{true}}$  implies that, on average, the stars with the largest observed parallaxes will have a positive  $\Delta\pi$  (and vice versa for the stars with the smallest observed parallaxes). So the sign of the parallax error is correlated with the observed parallax. The correlation between  $\Delta\pi$  and  $V_{\alpha*}$  and  $V_{\delta}$ , discussed above, will then lead to a correlation between the observed distances of the stars and the velocity residuals. Thus both the overall distribution of the velocity residuals, as well as the correlation of the direction of the residuals with spatial position, can be attributed to observational errors.

Nevertheless, a large number of stars (32 out of 197) are located outside the '3 $\sigma$ ' contour. About half of these lie beyond 10 pc from the centre of the cluster, with around one half of the 32 stars being binaries. This indicates that many of these stars may have suspect velocities. But even for the 165 stars inside the '3 $\sigma$ ' contour,  $\mathbf{z}'\Sigma^{-1}\mathbf{z}$  is not distributed according to the expected  $\chi^2$  distribution with 3 degrees of freedom. A large fraction of the stars shows larger deviations from the mean motion, suggesting that the model 'mean motion plus error in the mean' is insufficient to fully describe the residual velocities.

To investigate the distribution of  $\mathbf{z}'\Sigma^{-1}\mathbf{z}$  further we restrict our attention to a 'high-precision subset' of the cluster members: stars without any indications of multiplicity, with a radial velocity determined by Griffin et al. (1988), and with standard errors on the Hipparcos parallax and proper motions of less than 2 mas and 2 mas yr $^{-1}$  respectively. This selection results in a subset of 40 stars from which HIP 18962 is suppressed because it is located at a very large distance from the cluster centre (45 pc), and HIP 21788 is suppressed because of its large residual  $v_x$  (5 km s $^{-1}$ ). Fig. 17 shows the cumulative distribution of  $\mathbf{z}'\Sigma^{-1}\mathbf{z}$  for these stars (lower solid line), where we have used the appropriate mean velocity of this subset  $\mathbf{v}_C = (-42.31, -19.08, -1.43)$  km s $^{-1}$  (in Galactic coordinates) to characterise the mean cluster motion. The dotted line shows the expected distribution in the absence of any intrinsic dispersion in the velocities, from which it is clear that there is an extra dispersion unaccounted for in our model, or present in our observational errors.

This extra dispersion may originate from underestimates of the standard errors in the radial velocities, from the Hipparcos astrometry, from the presence of undetected binaries (Mathieu

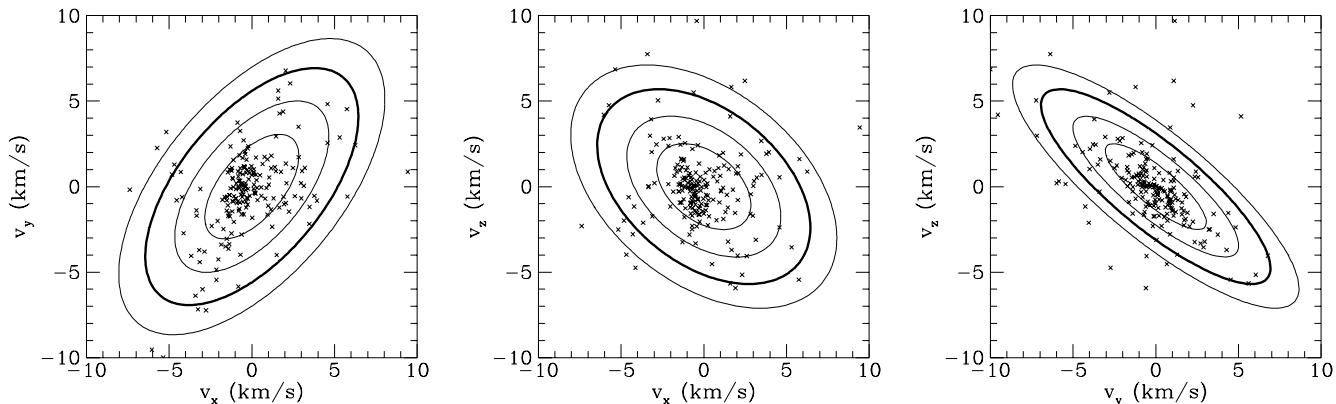


**Fig. 16.** Contour diagrams delineating the (projected) confidence regions corresponding to the mean covariance matrix of the space velocities for all candidate members with available radial velocities (cf. Fig. 8b). The confidence regions indicate the expected distributions of residual velocities in the absence of intrinsic dispersion. The contours correspond to the 68.3%, 95.4%, 99.73%, and 99.99% confidence levels. The thick line, at 99.73%, is the  $c = 14.16$  contour (see Eq. 16). The crosses correspond to the residuals between the observed space motions, and the mean (centre of mass) cluster motion.

1985), from systematic motions (e.g. rotation), or simply from the intrinsic velocity dispersion of the cluster. If the cause of the extra dispersion is attributed solely to the quoted standard errors being underestimates of the true external errors, then the standard errors in the astrometry would have to be increased by 50 per cent (factor 1.5), the errors on the radial velocities would have to be increased by a factor of 3, or both would have to be increased by 40 per cent. We consider such explanations unlikely.

Given the fact that the observed binary fraction provides a firm lower limit on the actual binary population, and that many workers consider that the true binary fraction may approach unity, the cumulative distribution of  $\mathbf{z}'\Sigma^{-1}\mathbf{z}$  has been constructed as before, but with a standard error of  $0.3 \text{ km s}^{-1}$  added quadratically to each of the components  $v_x$ ,  $v_y$ , and  $v_z$  (shown by the thick solid line in Fig. 17). The resulting agreement is now excellent. For a cluster mass of  $\simeq 460 M_{\odot}$ , an estimated core radius of  $\sim 2.5\text{--}3 \text{ pc}$ , and a half-mass radius of roughly  $4\text{--}5 \text{ pc}$ , the expected mean cluster velocity dispersion is  $0.2\text{--}0.4 \text{ km s}^{-1}$ . Our ‘high-precision subset’ contains mainly stars in the central region of the cluster where the velocity dispersion will be higher than the mean. Thus we postulate that the  $0.3 \text{ km s}^{-1}$  added to the standard errors of the space velocity components can be ascribed to a combination of the internal motion of the cluster, possibly supplemented by the presence of undetected binaries in the high-precision sample which would contribute further to the observed dispersion. This is in good agreement with a recent estimate of the internal cluster velocity dispersion of  $0.25 \pm 0.04 \text{ km s}^{-1}$  derived by Dravins et al. (1997) on the basis of a maximum-likelihood determination of the cluster’s astrometric radial velocities.

In principle the errors in the space velocities originating only from the radial velocities can be decoupled from those in the (more homogeneous) proper motions by selecting objects in a thin ‘parallax slice’ in order to assess whether the cluster dispersion can be resolved exclusively in the proper motions.

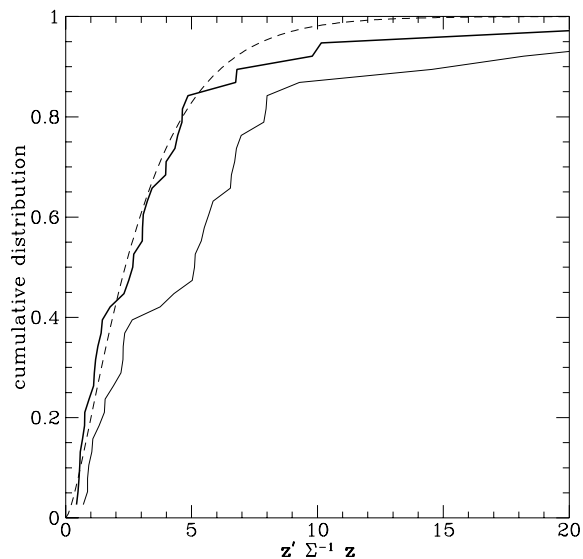


**Fig. 17.** The cumulative distribution of  $\mathbf{z}'\Sigma^{-1}\mathbf{z}$  for the high-precision subset of objects described in the text (lower solid line) compared to the expected distribution in the absence of intrinsic dispersion given by the  $\chi^2$  distribution with 3 degrees of freedom (dashed line). The thick solid line has been constructed by adding a standard deviation of  $0.3 \text{ km s}^{-1}$  to each of the components  $v_x$ ,  $v_y$ , and  $v_z$ .

Restricting the data set to the parallax slice 21–21.5 mas, and using only single stars within 5 pc from the cluster centre, each proper motion is transformed into a component parallel to the direction of the convergent point (which can be corrected for the angular size of the cluster), and a perpendicular component which should reflect only observational or intrinsic dispersions (the classical  $v$  and  $\tau$  components, e.g. Smart 1938). In the perpendicular direction the spread in the proper motions as measured by the inter-quartile range is smaller than the median error. Although the spread in the parallel component is about twice as large as the median error, the parallel motion is very

large (about  $110 \text{ mas yr}^{-1}$ ) so that even the 2 per cent spread in distance caused by the narrow parallax range selected leads to a considerable artificial spread in the proper motions, of the order of  $1\text{--}2 \text{ mas yr}^{-1}$ . As a result, the intrinsic dispersion in the proper motions remains unresolved.

Although our observations therefore appear fully consistent with uniform space motion, we also examined four possible causes of systematic structure in the space velocities in an attempt to obtain a better fit to the residuals seen in Fig. 9 without resorting to the assumption of an unmodelled internal velocity dispersion:

(i) systematic errors in the Hipparcos parallaxes or proper motions, or in the ground-based radial velocities, will affect the inferred velocity field. Geometrical considerations demonstrate that a spatially extended system participating in uniform space motion does not yield constant space velocities if the radial velocities, or  $\mu_\alpha$  and/or  $\mu_\delta$ , are subjected to offsets of the type expected for our particular observational quantities. For example, a constant offset in the radial velocity zero-point does not transform to a constant displacement in the space velocity because of the angular extension of the cluster on the sky. Similarly, a non-inertial ‘spin’ in the Hipparcos proper motion system (an effect whose elimination was the subject of considerable effort during the finalisation of the Hipparcos Catalogue) would lead to proper motion displacements of the form:

$$\begin{aligned} \Delta\mu_\alpha \cos \delta &= -\omega_x \sin \delta \cos \alpha - \omega_y \sin \delta \sin \alpha + \omega_z \cos \delta \\ \Delta\mu_\delta &= +\omega_x \sin \alpha - \omega_y \cos \alpha \end{aligned} \quad (19)$$

where  $(\omega_x, \omega_y, \omega_z)$  represents the non-inertial spin components of the proper motion system, and  $\Delta\mu_\alpha \cos \delta$  and  $\Delta\mu_\delta$  are the resulting offsets in the individual proper motions. We were not able to model both the magnitude and structure of the residuals as due to a combination of these zero-point errors, and large radial velocity offsets alone would lead to a very different structure in the residual velocities from that seen in Fig. 9. Taking only the magnitude of the residuals into account  $|\boldsymbol{\omega}|$  would have to be of the order of  $10 \text{ mas yr}^{-1}$ , more than an order of magnitude above the limits on the non-inertial spin-components of the Hipparcos proper motions noted in Sect. 3.1;

(ii) objects beyond the cluster tidal radius will be subjected to systematic velocity perturbations from the Galactic tidal field, which will lead to a systematic pattern of residual velocities with increasing distance from the cluster centre, and periodic with time. The effects can be calculated on the basis of the epicyclic approximation (Binney & Tremaine 1987, Sect. 3.2). It is therefore expected that the velocity residuals in the regions of the cluster beyond the tidal radius will deviate from a pattern of uniform space motion. However, the resulting velocity perturbations depend on the escape velocity and the time of escape, making it difficult to model them on the basis of only a few escaping members;

(iii) the velocity residuals increase with distance from the centre, and superficially appear consistent with a gradient of  $\Delta v \simeq 0.3 \text{ km s}^{-1} \text{ pc}^{-1}$  out to distances of about 10 pc, a gradient necessary to explain the largest velocity residuals in Fig. 9.

**Table 6.** Stars from Eggen’s (1982) list of Hyades group stars, classified according to distance from our adopted cluster centre,  $d$ ,  $\Delta v$ , and  $\mathbf{z}'\boldsymbol{\Sigma}^{-1}\mathbf{z}$ .

HIP	$d$ (pc)	$\Delta v$ ( $\text{km s}^{-1}$ )	$\mathbf{z}'\boldsymbol{\Sigma}^{-1}\mathbf{z}$
12184	21.2	13.0	22.09
12189	21.1	15.8	33.05
12828	25.7	7.3	18.25
16813	49.4	19.4	51.11
18692	45.9	6.3	13.67
18975	12.7	5.5	14.75
22697	63.4	5.4	3.32
26382	16.2	3.0	2.07

Such a high value would exclude rotation as the source of the largest velocity deviations seen in Fig. 9, since this would require a mass orders of magnitude larger than the observed mass if the cluster is not to be disrupted on a short time scale. A lower rotation within the central 5 pc region is not required to explain the velocity residuals which, we re-iterate, are consistent with a non-rotating system and our observational errors;

(iv) we have examined the possibility that the cluster recently experienced an encounter with a massive object causing a tidal shear in the outer regions of the cluster. The magnitude of space motion of the Hyades with respect to the LSR is rather large ( $34 \text{ km s}^{-1}$ ), and since most known massive objects in the vicinity of the Hyades are molecular or atomic interstellar clouds having a much smaller motion with respect to the LSR, the consequent large relative velocity between the Hyades and any object encountered make the interacting system well suited to treatment using the impulsive approximation (e.g. Binney & Tremaine 1987, Chapter 7, Theuns 1992a, b). In this approximation the relative velocity of the two colliding objects is perpendicular to the velocity disturbances generated in the less massive system. We can use the direction of the minimum velocity dispersion given by the results of the eigenvector analysis noted above to derive the direction of the relative velocity of a postulated encounter. Since the space motion of the Hyades is known, we can infer the minimum velocity with which the perturbing object moves with respect to the LSR. This turns out to be about  $30 \text{ km s}^{-1}$ , thus tending to exclude the possibility of a recent high-speed encounter with a nearby giant molecular cloud. Moreover, since the velocity increments imparted to the perturbing object scale as  $2GM/b^2V$ , where  $M$  is the mass of the perturbing object,  $V$  the relative impact velocity, and  $b$  the impact parameter, for any plausible values of  $b$  and  $V$  a very high mass, of the order of  $10^6 M_\odot$ , is required for the perturbing cloud, uncomfortably large compared with estimates for nearby giant molecular clouds (e.g., Dame et al. 1987).

We conclude that systematic effects in our data, or external perturbations of the velocity field, are not evident in our results, for which the parallaxes, proper motions, and radial velocities are all consistent with uniform space motion. In contrast, our results do not permit an unambiguous or definitive assignment of cluster membership, at least beyond the cluster tidal radius, or

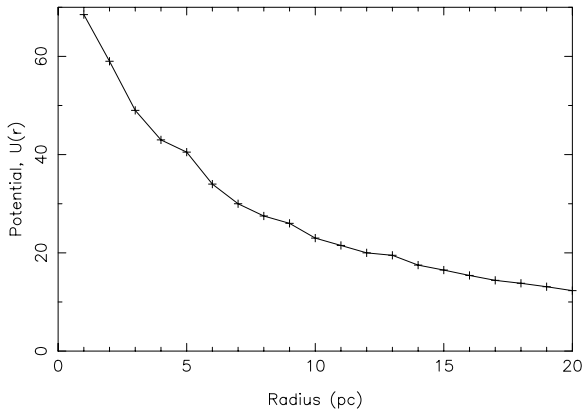


**Fig. 18.** The gravitational potential as a function of radial distance,  $\Psi(r)$ , for the objects within 20 pc of the cluster centre, constructed as described in the text.

as the velocity discrepancies between the individual 3-d space velocity and the mean cluster motion increase.

Table 2 includes objects with low values of  $\mathbf{z}'\Sigma^{-1}\mathbf{z}$ , but with large distances (small parallaxes) for which the distance from the cluster centre is large. Candidate ‘escapers’ can also be identified, on the basis of their small  $d$ , but discrepant motions. Of the list of 97 Hyades group stars listed by Eggen (1982) 92 are contained in the Hipparcos Catalogue and, of these, 8 are in the region of sky covered by the present study. Table 6 lists these objects, together with their distance from the cluster centre, the velocity deviation, and the value of  $\mathbf{z}'\Sigma^{-1}\mathbf{z}$ .

HIP 18692 and 26382 are among the 218 members already contained in Table 2. HIP 22697 has a velocity consistent with membership, but with a parallax (9.27 mas) just below our adopted threshold, while HIP 18975 is only just outside our  $3\sigma$  membership limit. All of the stars in Table 6 are located beyond the tidal radius of 10 pc; HIP 18975 may be especially interesting in this context since it appears to be an example of an object emerging from the Hyades, still close to the tidal radius. HIP 21788 (vB 110), rejected from our high-precision subset, may fall into the same category – while still within our  $3\sigma$  kinematical contour, it evidently has a somewhat discrepant motion, and was rejected as a plausible member on the basis of its radial velocity by Griffin et al. (1988).

Breger (1968) used Strömgren photometry to classify false members of Eggen’s Hyades-group list on the basis of their discrepant metallicity indices. Breger modelled the metallicity distribution of the moving group as a 50:50 mixture of Hyades stars with field stars of lower metallicity. Breger’s list contains five of the stars in our area of study, and two of these (HIP 13834 and 18692) are considered by us as members. The former does not occur in the later Eggen lists, although it has the appropriate metallicity for membership according to Breger, and is well matched to the cluster kinematics despite its relatively large distance from the cluster centre (20.5 pc). The latter object also occurs in Table 6, is far from the cluster centre, and is only just contained within our kinematical selection limit. With a

low metallicity according to Breger, further studies may well confirm it as a non-member.

While our present membership analysis is based only on kinematical arguments, metallicity determinations clearly contribute important additional information to the membership, especially farther from the cluster centre. Meanwhile, our findings underline a plausible connection between the Hyades stars and escaping Hyades members.

We summarise the various kinematical populations evident from this study as consisting of the core, the corona (extending out to the tidal radius  $r_t$ , Kholopov 1969), the halo (with  $r > r_t$  but still dynamically bound to the cluster), and the moving group population (with  $r \gtrsim 2r_t$ , and with similar kinematics signifying remnants of past membership).

## 8. Dynamical properties of the cluster

### 8.1. Potential and density

In the previous sections we have demonstrated confidence in the spatial distributions derived for the cluster members, and our objective now is to derive a description of the smoothed mass distribution within the cluster, in order to assess its dynamical behaviour, and its interaction with the Galactic potential.

The form of the cluster potential determines the distances at which it behaves dynamically as a spherical system or point mass. The potential at a position  $\mathbf{r}$  is given by:

$$\Psi = \sum_{k=1}^N \frac{m_k}{|\mathbf{r} - \mathbf{r}_k|} \quad (20)$$

where the potential is expressed in units such that the gravitational constant is equal to 1, masses are expressed in solar masses, and distances are expressed in pc. Potentials were computed on a regular mesh of points within a 20 pc radius sphere, centred at the centre of the cluster. To avoid local irregularities due to stars too close to one of the points where  $\Psi$  was computed, the effect of a star was ignored if it was within 0.1 pc of that point (introducing a softening parameter to model the potential at smaller separations has a negligible effect on the conclusions). The values on the mesh were interpolated to obtain the coordinates of points with specific rounded values of the potential. Finally, equipotential surfaces were determined by a least-squares fitting of an ellipsoid through points with the same potential.

Other than close to the centre of the cluster ( $r < 1.5$  pc), the ellipsoids could be approximated by spheres to better than 2 per cent indicating that, dynamically, the cluster has a high degree of spherical symmetry. Fig. 18 shows the value of the potential as a function of distance  $r$  from the centre. For  $r > 9$  pc,  $\Psi(r)$  is well represented numerically by:

$$\Psi(r) = \frac{240}{r} \quad (21)$$

where  $\Psi$  is expressed in  $M_\odot \text{ pc}^{-1}$ , assuming  $GM = 1$  for the Sun. Beyond 9 pc from its centre the cluster can therefore be

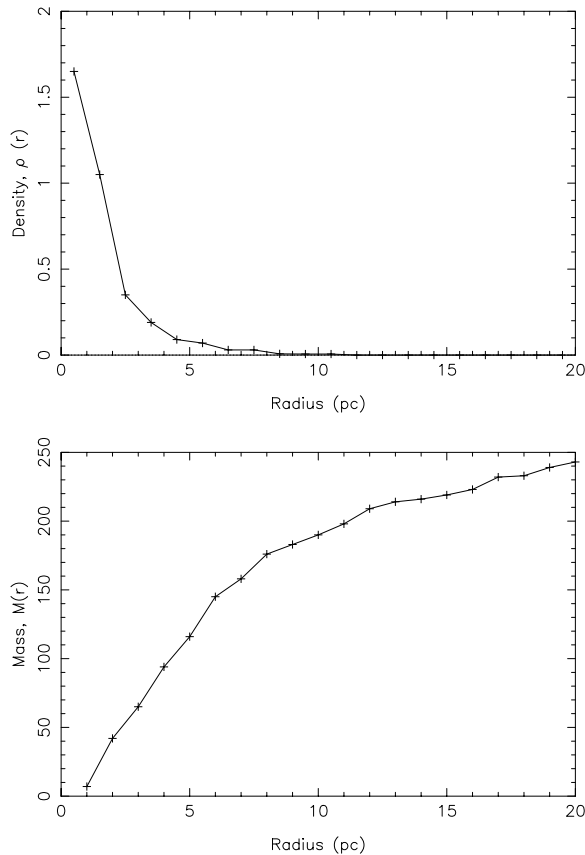


**Fig. 19.** **a** The mean density distribution within the cluster,  $\rho(r)$ , in  $M_{\odot} \text{pc}^{-3}$ ; and **b** the mass within the sphere of radius  $r$ , in  $M_{\odot}$ , constructed as described in the text.

approximated dynamically by a point mass, with a mass (corresponding to all of the Hipparcos stars considered here) of  $m_0 = 240 M_{\odot}$ . This result is a consequence of the low space density of the stars farther out from the cluster centre.

The results presented in Fig. 18 and Eq. (21) are representative only of the 180 stars selected within the 20 pc radius sphere. If we make the assumption that the Hyades stars not contained in the Hipparcos Catalogue have the same distribution, and that the total mass within this sphere is  $M_0$ , the ordinates of Fig. 18, and the coefficient of Eq. (21), would have to be multiplied by  $M_0/m_0$  – the total mass of the cluster has been variously estimated at between  $300 M_{\odot}$  (Pels et al. 1975, Oort 1979),  $400 M_{\odot}$  (Gunn et al. 1988), and  $460 M_{\odot}$  (Reid 1992), according to the corrections made for duplicity, faint stars, and white dwarfs.

To represent the mean density of the cluster, each star of mass  $m$  was replaced by a sphere with the same mass, but with a spatially extended and continuous density distribution. The adopted model is of a constant density within a sphere of radius  $s/2$ , linearly decreasing up to  $s$ , with  $s = 6$  pc. Several density distributions were tested, all giving similar results provided that the radius of the sphere  $s$  is not significantly different from this value. The same procedure as for the potential was then followed to determine equidensity surfaces. In practice, these were very close to spheres, confirming the spherical structure

**Table 7.** Moments of inertia (in  $M_{\odot} \text{pc}^2$ ) with respect to the three coordinate planes (Galactic coordinates).  $r$  is the radius of the sphere (pc) and  $N$  the number of stars included.

$r$	$N$	$xy$	$\sigma$	$xz$	$\sigma$	$yz$	$\sigma$
6	98	490	60	590	10	810	170
8	123	870	70	1110	20	1420	250
10	133	1110	80	1420	30	2020	300
12	151	1360	100	2080	40	3430	410
14	155	1430	210	2450	110	4010	450
16	163	1880	220	2660	120	4970	500
18	169	2970	270	3310	130	5900	560
20	180	3490	330	4720	150	7560	710

of the cluster out to a radial distance of about 7–8 pc. Beyond this radius, the density is too small for the method to yield significant results. The resulting density distribution  $\rho(r)$  (in  $M_{\odot} \text{pc}^{-3}$ ) and the cumulative mass distribution (in  $M_{\odot}$ ) are shown in Figs. 19(a,b). As for the potential, the results scale as  $M_0/m_0$  in order to take account of missing stars. From the values of the potential, the escape velocity of the star can in principle be determined although, as demonstrated in Sect. 7.2, in most cases the velocity errors are too large for individual conclusions to be drawn.

The resulting density distribution has been compared to both a Plummer model and a King model. For the former the best fit values of the core radius and central density are 2.9 pc and  $1.8 M_{\odot} \text{pc}^{-3}$ , corresponding to a central velocity dispersion of  $0.21 \text{ km s}^{-1}$ . In the case of the King model, the best fit model has a core radius of 2.6 pc, a central density of  $1.8 M_{\odot} \text{pc}^{-3}$  and a value of  $\Psi(0)/\sigma^2 = 2.6$ , where  $\Psi(0)$  is the central potential (Binney & Tremaine 1987, Sect. 4.4). This corresponds to a true central velocity dispersion of  $0.24 \text{ km s}^{-1}$ .

For both models the central velocity dispersion is in good agreement with the value derived in Sect. 7.2. However, results inferred from these particular models should be viewed with some caution. The masses in both models fall short of the total mass observed in the Hyades. This is in part due to the fact that we are missing the faint end of the luminosity function in the sample under study. Adding fainter members of the Hyades may change the overall density distribution, while significant mass may also be present in the outer regions of the cluster. This is supported by the fact that the observed half-mass radius ( $\sim 5.7$  pc) is larger than the half mass radius for the models above (3.7 and 3.0 pc, respectively).

## 8.2. Dynamical shape of the outer region

The previous results concern primarily the central part of the cluster. The star density in the outer region is rather low, and these stars do not significantly modify the local potential, as demonstrated by the  $1/r$  form of the potential in the outer regions. The dynamical approach to the study of the large-scale structure is through the computation of the moments and products of inertia of the cluster. Table 7 gives the value of the moments of inertia with respect to the three principal coordinate

planes, in Galactic coordinates, computed within spheres with increasing radii  $r$ .

The evolution of the moments of inertia within 6 pc is rather chaotic, although demonstrating a tendency for a spherical dynamical shape. Beyond  $r = 8$  pc, the moments of inertia with respect to the  $y$  and  $z$  axes become prominent, confirming the extension of the star distribution essentially along the  $x$  axis. The determination of the principal moments of inertia confirms this: the principal axis is very close to the  $x$  axis (within  $10^\circ$ ), while stars lie both in the direction of the Galactic centre and anticentre.

The moment of inertia with respect to the  $xy$  plane is systematically smaller than that with respect to the  $xz$  plane, indicating that the elongated part of the cluster is slightly flattened, and that the spread is slightly smaller in the direction perpendicular to the Galactic plane, as found by Oort (1979) and confirmed by Terlevich (1987).

The angular momentum of the cluster, derived from the individual space velocities, is small and insignificant in the central region, but grows as more distant stars are taken into account, with a major axis tending towards the direction  $\ell = 125^\circ$ ,  $b = 50^\circ$ . That the observed angular momentum is negligible for the main dynamical core of the cluster lends further support to the conclusions of Sect. 7, that the velocity residuals are a consequence of the observational errors, and further studies would be required to demonstrate the existence or absence of significant angular momentum or rotation.

### 8.3. The effect of the Galactic potential

The cluster is immersed in the potential of the Galaxy, so that the equipotential surfaces, unlike the spherical surfaces for isolated clusters, are distorted and eventually become open.

In the disk, the location of these Lagrangian points in an open cluster can be calculated from the Oort constants:

$$x_L = \left( \frac{GM_c}{4A(A-B)} \right)^{1/3} \quad (22)$$

where  $M_c$  is the total mass of the cluster (King 1962, Eq. 24) and  $A$  and  $B$  are Oort's constants. This distance is referred to as the tidal radius of the cluster,  $r_t$  (although the volume defined by the equipotential surface is not spherical). Adopting  $A = 14.8 \text{ km s}^{-1} \text{ kpc}^{-1}$  and  $B = -12.4 \text{ km s}^{-1} \text{ kpc}^{-1}$  (Feast & Whitelock 1997) and using  $M_c = 400 M_\odot$  gives  $r_t = 10.3$  pc. Since this distance is beyond the limit where the cluster potential has the form of Eq. (21), we can conclude that the tidal radius is of order  $r_t = 10$  pc, the precise value depending on the value of  $M_c$ . This is consistent with the consequences of the asymmetry in the evolution of the moments of inertia with  $r$ : beyond this distance the stars behave like companions of the cluster but under the predominant forces of the Galactic gravitational field.

## 9. The Hyades Hertzsprung-Russell Diagram

We have established well-defined spatial and velocity criteria for the assignment of cluster membership, at least within the cen-

tral 10–20 pc region, and we now use these members to refine the Hertzsprung-Russell diagram with the objective of presenting a consistent picture of the observational (i.e. colour versus absolute magnitude) and theoretical (i.e. bolometric magnitude versus effective temperature) relationships. Clusters provide an important environment for testing associated stellar evolutionary theories, representing a number of stars which are considered, as a first approximation at least, to be at the same distance, co-eval, and of a constant metallicity. The Hyades, as the nearest moderately rich cluster, has been studied in detail for these reasons.

While stellar models have been highly successful in matching the overall features of cluster colour-magnitude diagrams, unambiguous detailed model fitting has proved more elusive. The major problems compounding these studies in the specific case of the Hyades have been the uncertain distance modulus of the cluster, and its associated depth, both conspiring to make the transformation to absolute magnitudes uncertain; the uncertainty in the mean metal content and in particular the discrepancies between photometric and spectroscopic determinations (e.g. Cayrel de Strobel 1982, 1990) leaving open the initial conditions for the stellar evolutionary models; the contribution to both coordinates of the observational HR diagram due to the contribution of (undetected) binary systems; and additional complications associated with all such models such as the transformation from theoretical to observational quantities (requiring accurate bolometric corrections and colour conversions) and remaining theoretical uncertainties, primarily those associated with the theory of convection, including the value of the mixing-length parameter and the possibility of significant convective overshooting (e.g. Maeder & Mermilliod 1980, Vandenberg & Bridges 1984).

Although the distance modulus of the cluster as a whole may have been assigned a small standard error in any given study, the depth of the cluster is such that the contribution to the intrinsic scatter of the observational main sequence from significantly different distances of the individual members may be substantial (see, e.g., Cayrel de Strobel 1982). The direct result of this depth effect is a spread in individual distance moduli of member stars leading to a main-sequence population in the  $(V, B - V)$  plane less sharply defined than those of more distant clusters (cf. Figs. 2 and 21). The consequence of this observational scatter is that it has been difficult to make a reliable estimate of the helium abundance of the cluster members on the basis of model fitting which has, in turn, precluded unambiguous matching of evolutionary models to features such as the cluster turn-off.

With the trigonometric parallaxes from Hipparcos, we are in a position to construct the observational HR diagram with an accuracy of about 0.1 mag on individual values of  $M_V$  or  $M_{\text{bol}}$  (these errors are still dominated by the standard error of the parallaxes; in comparison, the error on  $V$  is typically 0.01 mag or smaller, and may be neglected). Our goals in this section are to derive an optimally constructed observational HR diagram for the cluster, and to use these observations in isochrone fitting to determine the cluster age.

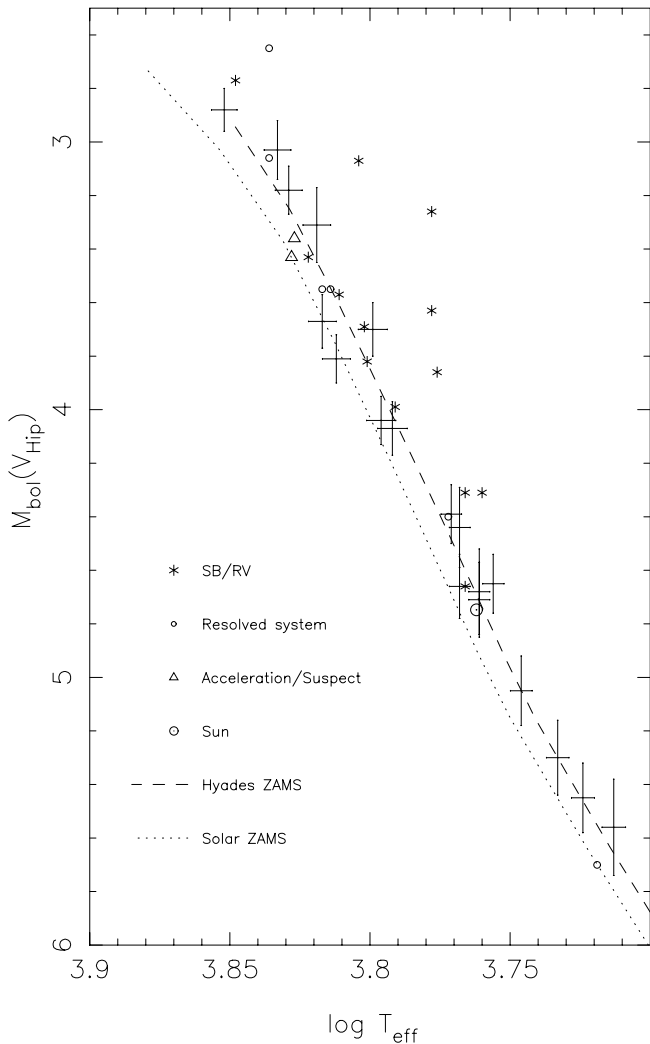


**Fig. 20.** Hertzsprung-Russell diagram ( $M_{\text{bol}}$ ,  $\log T_{\text{eff}}$ ) for the 40 dwarfs listed in Table 8. The symbols follow the multiplicity flags given in Table 2: objects which are spectroscopic binaries or radial velocity variable are indicated “\*”; objects which are resolved by Hipparcos or known to be double systems are shown as circles; one object (HIP 18658) with detected photocentric acceleration, and one object (HIP 19504) possibly resolved in photometry, are shown by triangles. For the remaining objects, error bars correspond to  $\pm 50$  K in  $T_{\text{eff}}$  for  $\log T_{\text{eff}} \leq 3.78$  and to  $\pm 75$  K for  $\log T_{\text{eff}} > 3.78$ , and to  $\sigma_{\pi}$  in  $M_{\text{bol}}$ . ZAMS loci as a function of mass were constructed as described in the text, and are given for the Hyades (dashed line) and solar (dotted line) metallicities given in Table 10. The location of the Sun is also shown.

These goals are achieved in two successive steps: (i) using stellar evolutionary model fits to a carefully constructed  $M_{\text{bol}}$  versus  $T_{\text{eff}}$  diagram for the lower part of the main sequence, we will define the locus of the Hyades zero-age main sequence (ZAMS) and hence, through modelling, an estimate of the cluster’s helium content; (ii) the observations over the complete part of the HR diagram in combination with theoretical isochrones will be used to determine the cluster age, using models with and without convective overshooting in the core. In both cases, it is important to suppress known binary systems from the observa-

tional diagram, and to take into account the possible remaining biases in both coordinates caused by unrecognised duplicity. The influence of interstellar reddening effects has been considered to be negligible for the Hyades stars (Crawford 1975, Taylor 1980) and is neglected in the following discussions.

### 9.1. The Hyades ZAMS and He abundance

The physical parameters (effective temperature, spectroscopic gravity, and metallicity) of a significant number of stars in the cluster have been derived over the last 25 years, and with advances provided by recent solid-state detectors, excellent spectroscopic data are now available. We have selected 40 stars, with bolometric magnitudes in the range 3–6 mag, for which high-resolution, high S/N spectra are available (Cayrel de Strobel 1980, Branch et al. 1980, Cayrel et al. 1984, Cayrel et al. 1985, Boesgaard 1989, Boesgaard & Friel 1990). From these studies, the metal content and effective temperature are known with high accuracy for each star, with  $T_{\text{eff}}$  determined to typically 50 K, or even better for some objects. Further details of the determination of the  $[\text{Fe}/\text{H}]$  is given by Cayrel et al. (in preparation).

The relevant data are listed in Table 8. Bolometric magnitudes were calculated from the  $V$  magnitude given in the Hipparcos Catalogue, the Hipparcos parallax, and applying the appropriate bolometric corrections of Bessel et al. (1997). The error in  $M_v$ , and therefore  $M_{\text{bol}}$ , is still dominated by the error on the trigonometric parallax, rather than by the apparent magnitude (which can be seen from an inspection of the standard errors on the mean magnitudes for these objects given in the Hipparcos Catalogue). Lutz-Kelker-type corrections have been ignored in view of the small values of  $\sigma_{\pi}/\pi$  (see Sect. 6.3). Fig. 20 shows the resulting positions in the ( $M_{\text{bol}}$ ,  $\log T_{\text{eff}}$ ) diagram. For the subset of 20 stars for which no evidence of binarity is indicated in Table 2, error bars are given corresponding to the standard error on the trigonometric parallax contributing to the standard error in  $M_{\text{bol}}$ . The errors on  $T_{\text{eff}}$  are harder to quantify. Although the less massive stars were all observed, reduced, and analysed with the same methods (observations and modelling), the more massive stars were observed, reduced and analysed by different authors, with different model atmospheres and different effective temperature scales. We have assigned error bars corresponding to  $\pm 50$  K in  $T_{\text{eff}}$  for  $\log T_{\text{eff}} \leq 3.78$ , and to  $\pm 75$  K for  $\log T_{\text{eff}} > 3.78$ , the latter in part taking into account the effect of the higher rotational velocity.

Table 8 yields a metallicity for the Hyades of  $[\text{Fe}/\text{H}] = 0.14 \pm 0.05$ . The observational quantity,  $[\text{Fe}/\text{H}]$ , the logarithm of the number abundances of iron to hydrogen relative to the solar value, is related to the metallicity  $Z$ , in mass fraction, through  $[\text{Fe}/\text{H}] = \log(Z/\text{X}) - \log(Z/\text{X})_{\odot}$  for a solar mixture of heavy elements ( $X$  is the hydrogen abundance by mass). With the solar value  $(Z/\text{X})_{\odot} = 0.0245$  of Grevesse & Noels (1993a) and the adopted Hyades  $[\text{Fe}/\text{H}]$  we obtain  $Z/\text{X} = 0.034 \pm 0.007$  which is slightly, but significantly, higher than the solar value. This is the observational quantity to be used

**Table 8.** Data for the 40 stars for which high-resolution spectra provide accurate values for  $T_{\text{eff}}$  and  $M_{\text{bol}}$  for the metallicity determination of the main sequence. The columns are: (1) Hipparcos Catalogue number; (2) van Bueren number; (3)  $V$  magnitude from the Hipparcos Catalogue; (4) Hipparcos parallax; (5) parallax standard error; (6) absolute visual magnitude,  $M_v$ ; (7) error on  $M_v$  due only to the parallax error; (8) log of effective temperature; (9) bolometric correction from Bessel et al. (1997); (10) resulting absolute bolometric magnitude; (11) [Fe/H]; (12) reference for [Fe/H]: BLT = Branch, Lambert & Tomkin (1980); B = Boesgaard (1989); BB = Boesgaard & Budge (1988); BF = Boesgaard & Friel (1990); CCC = Cayrel, Cayrel de Strobel & Campbell (1985); CCS = Chaffee, Carbon & Strom (1971); F = Foy (1975).

HIP	vB	V	$\pi$	$\sigma_\pi$	$M_v$	$\sigma_{M_v}$	$\log T_{\text{eff}}$	BC	$M_{\text{bol}}$	[Fe/H]	Ref.
(1)	(2)	(mag)	(mas)	(mas)	(mag)	(mag)	(8)	(mag)	(mag)	(11)	(12)
15310	2	7.78	21.64	1.33	4.46	0.13	3.772	-0.057	4.40	0.22	BLT
18170	6	5.97	24.14	0.90	2.88	0.08	3.852	-0.007	2.88	0.30	BB
18658	8	6.35	25.42	1.05	3.38	0.09	3.827	-0.014	3.36	0.20	BB
19148	10	7.85	21.41	1.47	4.50	0.15	3.768	-0.062	4.44	0.12	CCS
19261	11	6.02	21.27	1.03	2.66	0.11	3.836	-0.011	2.65	0.10	BF
19504	13	6.61	23.22	0.92	3.44	0.09	3.828	-0.014	3.43	0.18	BF
19554	14	5.71	25.89	0.95	2.78	0.08	3.848	-0.008	2.77	0.08	BF
19781	17	8.45	21.91	1.27	5.15	0.13	3.746	-0.103	5.05	0.10	CCC
19786	18	8.05	22.19	1.45	4.78	0.14	3.761	-0.072	4.71	0.23	CCS
19793	15	8.05	21.69	1.14	4.73	0.11	3.756	-0.079	4.65	0.19	CCS
19796	19	7.11	21.08	0.97	3.73	0.10	3.799	-0.029	3.70	0.18	BF
19877	20	6.31	22.51	0.82	3.07	0.08	3.836	-0.011	3.06	0.27	BB
19934	21	9.14	19.48	1.17	5.59	0.13	3.724	-0.139	5.45	0.09	CCC
20215	29	6.85	23.27	1.14	3.68	0.11	3.778	-0.049	3.63	0.23	CCS
20357	37	6.60	19.46	1.02	3.05	0.11	3.833	-0.012	3.03	0.16	BF
20480	42	8.84	20.63	1.34	5.41	0.14	3.733	-0.108	5.30	0.10	CCC
20491	44	7.18	20.04	0.89	3.69	0.10	3.817	-0.018	3.67	0.13	B
20492	46	9.11	21.23	1.80	5.74	0.18	3.713	-0.186	5.56	0.07	CCC
20557	48	7.13	24.47	1.06	4.07	0.09	3.796	-0.032	4.04	0.11	BF
20567	51	6.96	18.74	1.17	3.32	0.14	3.819	-0.017	3.31	0.16	B
20577	52	7.79	20.73	1.29	4.37	0.14	3.766	-0.065	4.31	0.05	CCC
20661	57	6.44	21.47	0.97	3.10	0.10	3.804	-0.025	3.07	0.11	BF
20712	62	7.36	21.54	0.97	4.03	0.10	3.791	-0.035	3.99	0.14	BF
20719	63	8.04	21.76	1.46	4.73	0.15	3.766	-0.066	4.66	0.05	F
20741	64	8.10	21.42	1.54	4.75	0.16	3.761	-0.073	4.68	0.14	CCC
20815	65	7.41	21.83	1.01	4.11	0.10	3.792	-0.035	4.07	0.12	B
20899	73	7.83	21.09	1.08	4.45	0.11	3.771	-0.058	4.39	0.14	CCC
20935	77	7.02	23.25	1.04	3.85	0.10	3.801	-0.028	3.82	0.10	BB
20948	78	6.90	21.59	1.09	3.57	0.11	3.814	-0.020	3.55	0.12	BF
20951	79	8.95	24.19	1.76	5.87	0.16	3.719	-0.166	5.70	0.14	CCC
21008	81	7.09	19.94	0.93	3.59	0.10	3.811	-0.022	3.57	0.13	BF
21066	86	7.03	22.96	0.99	3.83	0.09	3.812	-0.021	3.81	0.12	BF
21152	90	6.37	23.13	0.92	3.19	0.09	3.829	-0.013	3.18	0.13	BB
21317	97	7.90	23.19	1.30	4.73	0.12	3.768	-0.063	4.66	0.10	CCC
21474	101	6.64	22.99	0.95	3.45	0.09	3.822	-0.016	3.43	0.19	BB
21543	102	7.53	23.54	1.29	4.39	0.12	3.760	-0.078	4.31	0.05	CCS
22496	119	7.10	22.96	1.17	3.90	0.11	3.776	-0.049	3.86	0.17	CCS
22524	121	7.29	19.30	0.95	3.72	0.11	3.802	-0.027	3.69	0.15	BF
22550	122	6.79	20.15	1.14	3.31	0.12	3.778	-0.049	3.26	0.16	CCS
23214	128	6.75	23.09	0.83	3.57	0.08	3.817	-0.018	3.55	0.13	BF

in the models. The error of 0.007 on ( $Z/X$ ) includes the error on the solar ( $Z/X$ ) of about 11 per cent (Anders & Grevesse 1989).

Earlier discrepancies in the determination of [Fe/H] for the Hyades, in particular the differences determined from photometric and spectroscopic observations, have been summarised by Cayrel de Strobel (1982, 1990). The present value is in reasonable agreement with (although is not independent

from) more recent determinations, e.g. Cayrel et al. (1985) ([Fe/H] =  $+0.12 \pm 0.03$ , or 0.14–0.15 accounting for the difference in activity between the Sun and the Hyades dwarfs); Vandenberg & Poll (1989) ([Fe/H] = +0.15). Note that vB52 was rejected as representative of the cluster mean by Cayrel et al. (1985) on the basis of its colour anomaly, possibly related to the strong emission of  $H\alpha$ .

The lower part of the Hyades main sequence relevant to this study is populated by low mass stars which are only slightly evolved, and therefore rather close to their ‘zero age’ position, the zero-age main sequence (ZAMS) defining the locus on the HR diagram where the stars become fully supported by core hydrogen burning. Being of intermediate or low temperature, their spectra do not show He-lines, and their photospheric He abundance cannot be determined spectroscopically. Theoretical computations of internal structure have shown that the ZAMS locus depends on the initial chemical composition, both in terms of metallicity and He content. Comparison with theoretical models is therefore used to estimate the He abundance.

In order to fit the data with improved theoretical calculations, new zero-age main sequence models have been calculated by one of us (YL) with the CESAM stellar evolutionary code (Morel 1993, 1997). Updated input physics, appropriate to the mass interval covered by this sample of Hyades stars (from about 0.8–1.6  $M_{\odot}$ ) has been used: updated OPAL opacities (Iglesias & Rogers 1996) complemented at low temperatures by the Alexander & Ferguson data (1994), nuclear reaction rates from Caughlan & Fowler (1988), a solar mixture of heavy elements from Grevesse & Noels (1993a) corresponding to the mixture used in opacity calculations and the CEFF equation of state (Christensen-Dalsgaard 1991).

The mixing-length parameter used for all models was  $\alpha = l/H_p = 1.64$  pressure scale-heights ( $l$  is the mixing-length and  $H_p$  the pressure scale-height), derived from the calibration in radius of the solar model with the same input physics (see below). The same value was applied to the Hyades following investigations of visual binary systems with known masses and metallicity (Fernandes et al., in preparation) resulting in similar values of  $\alpha$  for a wide range of ages and metallicities. A value of  $\alpha = 1.5$  was suggested by Vandenberg & Bridges (1984), although a somewhat higher value was also not ruled out. Models using standard mixing-length theory are very sensitive to the precise choice of  $\alpha$ , although the region of sensitivity is restricted. For a summary of the effects of the major uncertainties associated with the use of such models, including the physical terms such as the reaction rates, the opacities, the universality of the mixing-length parameter, and the relevance of overshooting, see Lebreton et al. (1995). In the sample of low mass stars considered here, stars are believed to be essentially homogeneous on the ZAMS so that modelling uncertainties associated with convective core overshooting are avoided.

As the models strongly depend on chemical composition (Y, Z in mass fraction), a first set of calculations was made with a wide range of chemical compositions yielding a grid of theoretical ZAMS with different helium and metal contents. Interpolation between these ZAMS then yielded the value of the helium abundance giving the best fit to the low-mass stars for the mean observational value of  $(Z/X)$  given in Table 9.

A final ZAMS (see Table 10) was computed for  $Y = 0.260$  and  $Z = 0.024$ , corresponding to the mean Hyades metallicity. As shown in Fig. 20 this ZAMS fits the observational data rather satisfactorily, with the larger scatter for  $\log T_{\text{eff}} > 3.78$  possibly originating from underestimated errors on the derived

effective temperatures for the more massive stars, as noted above. We provide for comparison, in Table 10 and Fig. 20, the corresponding results which, with the same physical assumptions, give a proper calibration of the observed luminosity ( $L_{\odot} = 3.846(1 \pm 0.005)10^{33}$  erg s $^{-1}$ ) and radius ( $R_{\odot} = 6.9599 10^{10}$  cm) of the Sun at an age of 4.75  $10^9$  years $^2$  using  $Z = 0.0175 \pm 0.0015$  (Grevesse & Noels 1993b).

The resulting ZAMS for the Hyades lies significantly above that of the Sun. Although the values of Y found for the Sun (0.2659) and the Hyades (0.260) are rather close, the higher metallicity of the Hyades implies that the relative helium to metal enrichment ratio is smaller than that obtained for the Sun (for the relevance of the assessment of this enrichment ratio, see Pagel 1995). The value of  $Y = 0.26$  is close to the value used by Vandenberg & Bridges (1984) and would appear to rule out the suspicions that the Hyades is helium deficient compared with field stars (Strömgren et al. 1982). A refined value of the He content of the Hyades will be presented in a forthcoming paper, combined with the analysis of a number of Hyades binaries, whose masses are very sensitive to the He content.

The uncertainty on our final estimate of Y has two sources. The observational uncertainty on  $[\text{Fe}/\text{H}]$  gives an error on Y of 0.02, as shown in Table 9. Additional uncertainties arise from the determinations of  $T_{\text{eff}}$  and  $M_{\text{bol}}$ . From three different ZAMS models computed with  $Z = 0.024$ , and with  $Y = 0.25, 0.26$ , and  $0.27$ , we infer that an error of 0.1 mag on  $M_{\text{bol}}$  leads to an error of about 0.025 on Y. For the lower part of the main sequence, and a given  $M_{\text{bol}}$ , an error of 50 K on  $T_{\text{eff}}$  leads to an error of about 0.025 on Y. Assuming that our individual errors on  $M_{\text{bol}}$  and  $T_{\text{eff}}$  are uncorrelated, we estimate that the observational scatter in the overall  $T_{\text{eff}}/M_{\text{bol}}$  diagram results in an error of only  $\pm 0.01$  in Y. Combined with the independent error arising from the uncertainty in Z, we infer that the final error in Y is dominated by the mean value of  $[\text{Fe}/\text{H}]$  used for the Hyades, and is  $Y = 0.26 \pm 0.02$ .

We note that the ‘single’ objects apparently located  $1 - 2\sigma$  above the resulting main sequence have a metallicity close to the mean value of the 40 stars. They may be undetected binaries, although their velocity residuals with respect to the mean cluster space motion (see Fig. 9) show no evidence for systematic departures which might be expected as a result of their perturbed radial velocity. Since these objects are not outliers in a colour-colour diagram, the  $T_{\text{eff}}$  values may also be slightly suspect.

## 9.2. Isochrone fitting to the Hyades and the cluster age

If the chemical composition of a cluster is known, the observational HR diagram in combination with theoretical isochrones allow the cluster age to be determined. Fig. 21 shows the HR diagram ( $M_V$  versus  $B - V$ ) for 131 stars where, in order to en-

<sup>2</sup> The age derived for the Sun by different authors ranges from 4.5 Gyr (Guenther 1989) to 4.75 Gyr (Christensen-Dalsgaard 1982). Guenther’s comparisons of two solar models with ages of 4.5 and 4.7 Gyr did not yield significant differences in the derived solar helium content nor in the mixing-length parameter.

**Table 9.** Correspondence between [Fe/H] and Y, Z and Z/X used for the theoretical models described in the text.

[Fe/H]	Y	Z	Z/X
0.14	0.26	0.024	0.034
0.09	0.24	0.020	0.027
0.19	0.28	0.028	0.041

**Table 10.**  $\log(L/L_{\odot})$  and  $\log T_{\text{eff}}$  as a function of mass for the Hyades ( $Y = 0.260, Z = 0.0240$ ) and solar ( $Y = 0.2659, Z = 0.0175$ ) zero-age main sequences derived from the CESAM code, as described in the text (see also Fig. 20).

M/M $_{\odot}$	Hyades ZAMS		Solar ZAMS	
	$\log(L/L_{\odot})$	$\log T_{\text{eff}}$	$\log(L/L_{\odot})$	$\log T_{\text{eff}}$
0.80	-0.695	3.6632	-0.598	3.6859
0.90	-0.461	3.6986	-0.362	3.7216
0.95	-0.354	3.7144	-0.255	3.7368
1.00	-0.254	3.7285	-0.161	3.7498
1.05	-0.164	3.7408	-0.065	3.7614
1.10	-0.073	3.7516	+0.032	3.7717
1.15	+0.018	3.7615	+0.138	3.7832
1.20	+0.121	3.7727	+0.231	3.7934
1.30	+0.301	3.7932	+0.400	3.8124
1.40	+0.458	3.8113	+0.551	3.8309
1.50	+0.598	3.8286	+0.687	3.8534
1.60	+0.725	3.8485	+0.810	3.8800

sure minimal contamination from non-cluster members, objects have been retained only if they satisfy our kinematical membership criteria, and are drawn from the objects lying within the  $r < 10$  pc radius of the cluster centre (Table 2). From this sample, we have eliminated a few with  $\sigma_{B-V} > 0.05$  mag. Error bars correspond to the standard error in  $M_V$ , estimated from the standard error in the parallax, and in  $B - V$ . The apparent magnitudes  $V$ , the  $B - V$  colours, and the standard errors in parallax and  $B - V$  were taken from the Hipparcos Catalogue. Among these stars 72, indicated as filled circles in Fig. 21, are not classified as (suspected) double or multiple (Table 2) nor variable (as compiled in the Hipparcos Catalogue). The open circles represent the double or multiple systems, spectroscopic binaries, and variable stars, and these will not be used in further discussions of the main sequence modelling. The main sequence has significantly reduced scatter in comparison with the  $V, B - V$  diagram of Fig. 2, and may be compared with recent determinations from ground-based observations, e.g. Schwan (1991).<sup>3</sup>

As expected, most of the stars falling significantly above the main sequence are double or multiple stars. There is no sub-

<sup>3</sup> Dravins et al. (1997) have been able to further reduce the scatter in the Hyades HR diagram by constraining the radial velocities and parallaxes of the members according to the hypothesis of uniform space motion of the cluster. Although a model-dependent approach, the reduced scatter in their HR diagram, especially towards the faint end, supports our conclusions about the absence of systematic velocity structure within the cluster, whilst confirming our estimate of the internal velocity dispersion, and providing further evidence that the majority of binaries, at least with a not too large  $\Delta m$ , have been identified.

**Table 11.** Stellar rotation,  $v \sin i$ , for stars in the turnoff region.

HIP	$M_V$	$B - V$	$v \sin i$ (km s $^{-1}$ )
20542	1.55	0.15	40
20635	0.85	0.14	75
21029	1.54	0.17	70
21683	1.23	0.15	115
23497	1.13	0.16	115

dwarf sequence, a fact already noted in previous work (Hanson & Vasilevskis 1983, Griffin et al. 1988). One star, HIP 17962, is located below the main sequence. This is V471 Tau (WD 0347+171), an eclipsing binary consisting of a K0V star and a white dwarf (Nelson & Young 1970). In the turnoff region ( $B - V < 0.2$  mag), there are five stars with no indications of duplicity or variability: HIP 20542 (vB47), 20635 (vB54), 21029 (vB82), 21683 (vB108) and 23497 (vB129). The star with the bluest colour index is HIP 20648 (vB56), a known blue straggler (Abt 1985, Eggen 1995).

After elimination of the identified binaries, the lower part of the main sequence has an increased scatter compared to that seen for the bluer stars, a fact partly attributable to the lower accuracy of the corresponding parallaxes (as illustrated by the error bars), but possibly partially related to chromospheric activity. Campbell (1984) has shown that many red Hyades dwarfs show colour anomalies which are found to correlate with various indicators of chromospheric activity. The four third-magnitude red giants  $\gamma$  (vB28, HIP 20205),  $\delta^1$  (vB41, HIP 20455),  $\epsilon$  (vB70, HIP 20889) and  $\theta^1$  (vB71, HIP 20885) Tau represent the cluster's giant branch. The stars vB41 and vB71 are known spectroscopic binaries. The star vB28 was reported to be double from the speckle result of Morgan et al. (1982), although this result was not confirmed in the speckle duplicity survey of the Hyades cluster of Mason et al. (1993), possibly because the star was observed when the seeing was approximately 2 arcsec.

After accounting for known binaries and variable stars, the diagram still appears to be possibly contaminated by unrecognised binaries. In particular, the stars HIP 20901 (vB74), 21670 (vB107) and 20614 (vB53) lie significantly above the cluster main sequence. HIP 20901 and 21670 are apparently Am type stars (Abt & Morrell 1995), amongst which the high frequency of spectroscopic binaries is well established (Abt 1961, Jaschek & Jaschek 1987); the possibility that these stars are binaries cannot therefore be ruled out. HIP 20614 is a fast rotator ( $v \sin i = 145$  km s $^{-1}$ ) (Abt & Morrell 1995), and photometry indicates a possible binary (Eggen 1992). These three stars have been omitted in the subsequent fitting of the main sequence.

Rotation affects the colours of the stars, the effect depending on the equatorial velocity and on the inclination of the rotational axis with respect to the line of sight, leading to shifts of a few hundredths in  $B - V$  and a few tenths in  $M_V$ , generally towards the red and to higher luminosities. Values of  $v \sin i$  taken from Abt & Morrell (1995) for the stars in the turnoff region are given in Table 11.

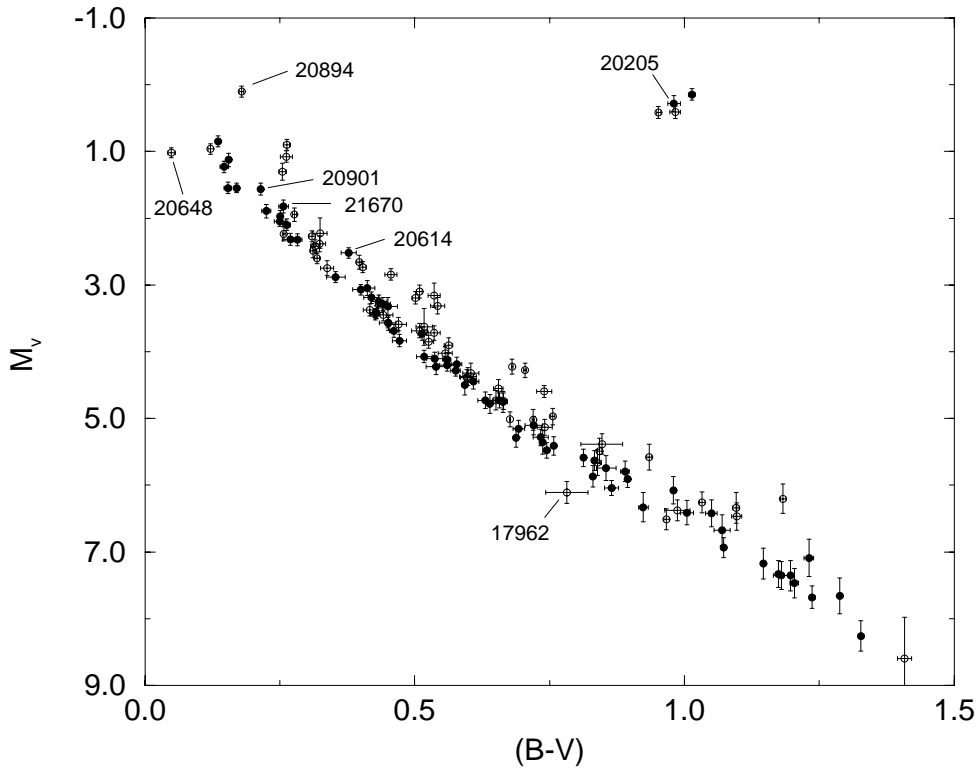


**Fig. 21.** Absolute magnitude,  $M_V$ , versus  $B - V$ , for the stars considered as reliable cluster members within  $r < 10$  pc. Filled circles indicate objects which are not classified as (suspected) double or variable. Error bars correspond to the standard error in the Hipparcos parallaxes and  $B - V$  colour indices. Specific objects indicated are discussed in the text.

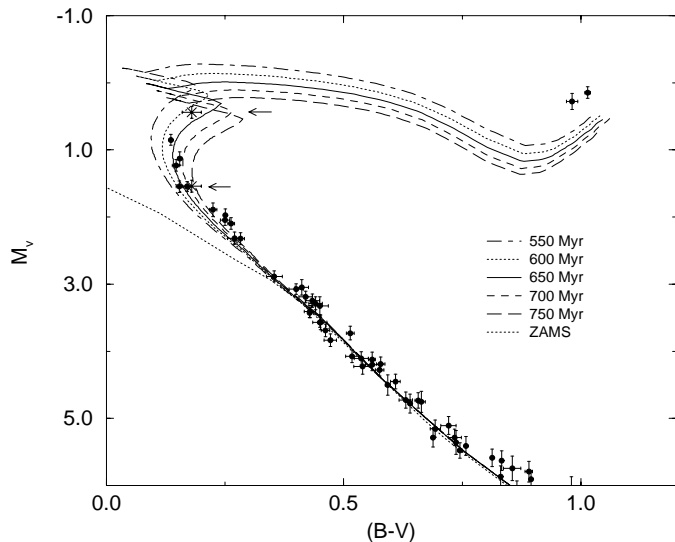
In order to compare the observational HR diagram with theoretical isochrones, evolutionary models were calculated using the same input physics as for the ZAMS models from which the initial helium abundance was estimated ( $Y = 0.26$ ,  $Z = 0.024$ ,  $\alpha = 1.64$ ). Sequences were determined for masses of 0.8, 1.0, 1.2, 1.4, 1.7, 2.0, 2.5, 3.0 and 4.0  $M_{\odot}$ , from the ZAMS to the beginning of the red-giant branch. For each mass, two evolutionary sequences were calculated: a standard sequence, and one taking into account an overshooting of the mixed convective core which extends the size of the convective core over a distance of 0.20 pressure scale-heights (the latter significantly modifying the shape of the resulting isochrones and hence the estimated ages – the reference value of 0.2 comes from Schaller et al. 1992). Representative evolutionary states for each mass were extracted, and the Geneva isochrone program used to obtain isochrones with ages in the range 500–750 Myr in steps of 50 Myr, with and without overshooting.

One of the main difficulties in the transformation of isochrones from the theoretical plane ( $M_{\text{bol}}$ ,  $\log T_{\text{eff}}$ ) to the observational plane ( $M_V$ ,  $B - V$ ) lies in the colour/temperature transformation. As a temperature indicator, the  $B - V$  index has the disadvantage of also being sensitive to metallicity. Moreover, since the stellar surface gravity varies along the position on the isochrone, the influence of gravity on the  $B - V$  index has to be taken into account. We adopted the calibration from Alonso et al. (1996) which allows derivation of the  $B - V$  colour as a function of  $T_{\text{eff}}$  and  $[\text{Fe}/\text{H}]$ . This calibration, valid in the range  $4000 \text{ K} < T_{\text{eff}} < 8000 \text{ K}$ , was extrapolated to higher  $T_{\text{eff}}$  according to the results of Haywood (1997, private communication). The adopted calibration yields, for the Sun ( $T_{\text{eff}} = 5780 \text{ K}$ ), a  $B - V$  index of 0.62, in good agreement with the recent estimation of

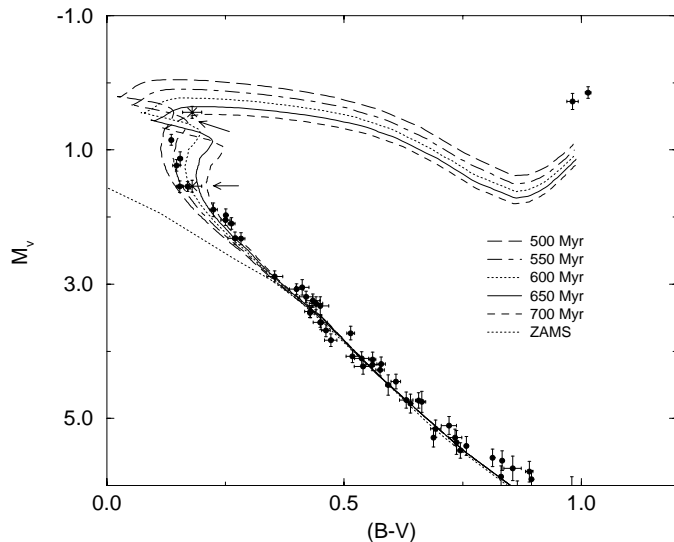
$0.628 \pm 0.009$  by Taylor (1997). The transformed  $B - V$  colours were then corrected for the influence of gravity according to the relationships given by Arribas & Martínez Roger (1988). Finally, in order to estimate  $M_V$  from  $M_{\text{bol}}$  the  $V$  bolometric corrections from Bessel et al. (1997) were adopted.

Fig. 22 shows the theoretical isochrones corresponding to 550, 600, 650, 700 and 750 Myr calculated with overshooting, superimposed on the observational HR diagram. Fig. 23 shows isochrones corresponding to 500, 550, 600, 650, 700 Myr calculated without overshooting. On both figures the zero-age main sequence is also indicated. Our present results show that the five stars located in the turn-off region, for which we have no evidence of duplicity, can be reasonably modelled either with an isochrone of 550 Myr without overshooting, or with an isochrone of about 650 Myr calculated with overshooting. As the turnoff region is sparsely populated, we have included in the HR diagram the star HIP 20894 ( $\theta^2$  Tau, vB72). This is the brightest star in Fig. 21, not counting those in the giant branch, and is the brighter component of a wide visual pair (with  $\theta^1$  Tau) and a well-known spectroscopic binary. A difference in  $V$  magnitude of  $1.10 \pm 0.01$  and in  $B - V$  colour of  $0.006 \pm 0.005$  between the components of the SB star were estimated by Peterson et al. (1993). We adopted these values in combination with the Hipparcos parallax to place these two stars in Figs. 22–23, where they are indicated as different symbols (arrowed).

Using this system as an additional constraint, it appears that the primary component of the system ( $\theta^2$  Tau A) does not lie on the isochrones between 500 and 600 Myr without overshooting, while an agreement with the isochrone grid including overshooting remains very satisfactory. Although not included in Fig. 22 to avoid crowding, we estimate that the theoretical isochrone



**Fig. 22.** The 69 single stars with the location of the ZAMS, and with isochrones corresponding to the range 550–750 Myr calculated with overshooting. The two objects indicated by different symbols (arrowed) are discussed in the text.



**Fig. 23.** The 69 single stars with the location of the ZAMS, and with isochrones corresponding to the range 500–700 Myr calculated without overshooting. The two objects indicated by different symbols (arrowed) are discussed in the text.

corresponding to 625 Myr, calculated with overshooting, provides an optimum fit to the present observational data.

For a given set of models (with or without overshooting) we estimate an age uncertainty of about 30 Myr coming from the visual fitting of an isochrone to the observations. However, the cluster age determination is model dependent, and an uncertainty of about 15 per cent arises from the uncertainty on the amount of overshooting adopted in the calculations. Another significant source of uncertainty comes from the relationship adopted in the transformation between  $T_{\text{eff}}$  and  $B - V$ , where the corresponding uncertainty in the age determination could reach some 20 per cent. The effect of rotation, relatively unimportant in the Hyades (as shown in Table 11), is unlikely to lead to an overestimation of the age by 50 Myr (Maeder 1971). From all of these considerations, and taking into account uncertainties coming from the adopted models, the transformation between  $T_{\text{eff}}$  and  $B - V$ , and the effect of undetected binaries, it is difficult to assign a very meaningful estimate of the uncertainty of our age determination, which may reach 100 Myr, although an uncertainty of about 50 Myr may be a more realistic estimate. In summary, our results suggest a cluster age of  $625 \pm 50$  Myr, with observational evidence for the presence of convective overshooting. Support for overshooting from cluster main sequence fitting was already presented by Maeder & Mermilliod (1980), who compared observational HR diagrams for 34 clusters in the age range spanning the Pleiades to the Hyades, and found that agreement could be obtained if the stellar convective cores are extended by a certain amount due to convective overshooting or other physical mechanisms.

Previous estimates of the age of the Hyades from isochrone fitting ranged between 500 and 900 Myr (Barry et al. 1981). Cayrel de Strobel (1990) gave 655 Myr from the mean value of different age determinations. Recently, Torres et al. (1997a)

found 600 Myr. Kroupa (1995) estimated a dynamical age of about 500 Myr. Direct comparison of our result with the isochrone-based ages quoted in the literature is complicated by differences in the models used. All of the previous estimates rely on models with solar composition, or interpolated from models having different metallicities. In this work, we have calculated models specifically for the Hyades abundance.

We stress that distances to star clusters based on main sequence fitting to the Hyades must be corrected for chemical composition differences: thus the fitted  $m - M$  value for a system with solar abundance should be reduced by roughly 0.13 mag to allow for the fact that  $[\text{Fe}/\text{H}]_{\text{Hyades}} = 0.14$ .

## 10. Conclusions

The Hipparcos parallaxes and proper motions together provide a consistent picture of the Hyades distance, structure and dynamics. They yield a cluster convergent point motion consistent with the individual trigonometric parallaxes, and together explain the larger distance modulus derived from the most recent ground-based proper motion investigations as originating from differences in the magnitude of the adopted cluster space motion, and small systematic effects in the ground-based proper motions. Conversely, the smaller distance modulus traditionally derived from a variety of ground-based trigonometric parallax programmes are attributed to errors in these ground-based parallaxes, a conclusion supported by the most recent distance modulus derived from consideration of the GCTSP parallaxes by van Altena (1997b), in good agreement with our present results. There is good agreement with determinations using high-precision radial velocities (Stefanik & Latham 1985, Gunn et al. 1988). Recent distance determinations to individual objects in the cluster, most notably the results of Torres et al. (1997a,b,c),

are in excellent agreement with the Hipparcos trigonometric parallaxes, although their extrapolation to a corresponding mean cluster distance is again affected by systematic effects in the ground-based proper motions used.

The combination of the Hipparcos astrometry with radial velocity measurements from ground-based programmes provides three-dimensional velocities allowing candidate membership selection to be based on positional and kinematical criteria. A number of new cluster members have been found within 20 pc of the cluster centre, and candidates can be classified as escaping members on the basis of their velocity residuals. No evidence for systematic internal velocity structure is found; rather, the results are fully consistent with a uniform cluster space motion with an internal velocity dispersion of about  $0.3 \text{ km s}^{-1}$ . Spatial distribution, mass segregation, and binary distributions are consistent with  $N$ -body simulations.

The cluster has a tidal radius of  $r_t \simeq 10 \text{ pc}$ . Outside this region, the stellar distribution is elongated along the direction of the Galactic centre and anti-centre, and is slightly flattened in the direction perpendicular to the Galactic plane. Inside this region, the cluster has spherical symmetry with a core radius of  $r_c \simeq 2.7 \text{ pc}$ , and a half-mass radius of  $5.7 \text{ pc}$ . The presence of objects closely linked kinematically with the cluster core, but well beyond the tidal radius, probably originates from stellar encounters and diffusion beyond the Lagrangian points.

The well-defined observational main sequence has been transformed into a theoretical  $M_{\text{bol}}$  versus  $T_{\text{eff}}$  diagram, from which fitting of the cluster zero-age main sequence yields a helium abundance of  $Y = 0.26 \pm 0.02$ . Theoretical isochrones matching the helium and metal content provide observational evidence for convective overshooting, and yield a cluster age of  $625 \pm 50 \text{ Myr}$ .

With the caveat that the primary importance of the Hipparcos results is to provide individual distances to cluster members, rather than an estimated distance to the cluster centre of mass (a concept meaningful only in the restricted context of the cluster members contained in the Hipparcos Catalogue), our estimated distance to the observed centre of mass for the objects within 10 pc of the cluster centre is  $46.34 \pm 0.27 \text{ pc}$ , corresponding to a distance modulus  $m - M = 3.33 \pm 0.01 \text{ mag}$ . This mean distance is, in practice, only marginally modified (formally by about 0.4 pc) for the derived centre of mass for Hipparcos objects within  $r < 20 \text{ pc}$  of the cluster centre.

*Acknowledgements.* We thank the members of the Hipparcos scientific consortia who participated in the creation of the Hipparcos Catalogue on which this study has been based. We thank E. Høg, L. Lindegren, R.S. Le Poole, and H. Schrijver for valuable comments and contributions. M. Mayor (Geneva) provided radial velocities from the Coravel systematic survey of Hipparcos stars in advance of publication, and S. van Eck (Brussels) kindly obtained measurements for about half of the newly-measured stars. We are grateful to W. van Altena for guidance in interpreting discrepancies between the Hipparcos and ground-based parallaxes. Our particular thanks are due to the referee, I.R. King, for his careful and critical reading of the manuscript, and for his numerous valuable and substantial suggestions for improvements of the paper.

## References

- Aarseth, S.J., 1973, *Vistas in Astr.*, 15, 13  
 Abt, H.A., 1961, *ApJSS*, 6, 37  
 Abt, H.A., 1985, *ApJ*, 294, L103  
 Abt, H.A., Morell, N.I., 1995, *ApJSS*, 99, 135  
 Alexander, D.R., Ferguson, J.W., 1994, *ApJ* 437, 879  
 Alonso, A., Arribas, S., Martínez Roger, C., 1996, *A&A*, 313, 873  
 van Altena, W.F., 1974, *PASP*, 86, 217  
 van Altena, W.F., Lee, J.T., Hoffleit, E.D., López, C.E., 1991, *General Catalogue of Trigonometric Parallaxes*, Yale Univ. Press  
 van Altena, W.F., Lee, J.T., Hoffleit, E.D., 1993, in ‘Workshop on Databases for Galactic Structure’, Davis Philip, A.G., Hauck, B., Uggren, A.R. (eds), L. Davis Press, 65  
 van Altena, W.F., Lee, J.T., Hoffleit, E.D., 1994, in ‘Galactic and Solar System Astronomy: Observation and Application’, Morrison, L.V., Gilmore, G.F., D. Reidel, Dordrecht, 50  
 van Altena, W.F., Lee, J.T., Hoffleit, E.D., 1995, *General Catalogue of Trigonometric Stellar Parallaxes*, Fourth Edition, Yale Univ. Obs.  
 van Altena, W.F., Lu, C.L., Lee, J.T., et al., 1997a, *ApJ Letters*, in press  
 van Altena, W.F., Lee, J.T., Hoffleit, E.D., 1997b, *Baltic Astron.*, 6(1), 27  
 Anders, E., Grevesse, N., 1989, *Geochim. Cosmochim. Acta*, 53, 197  
 Arenou, F., Lindegren, L., Fröschlé, M., Gómez, A.E., Turon, C., Perryman, M.A.C., Wielen, R., 1995, *A&A*, 304, 52  
 Arribas, S., Martínez Roger, C., 1988, *A&A*, 206, 63  
 Battinelli, P., Capuzzo-Dolcetta, R., 1991, In ‘The Formation and Evolution of Star Clusters’, Janes, K. (ed.), *ASP Conf. Ser.*, 13, 139  
 Barry, D.C., Cromwell, R.H., Hege, K., Schoolman, S.A., 1981, *ApJ*, 247, 210  
 Bessel, M., Castelli, F., Plez, B., 1997, *A&A*, in press  
 Binney, J., Tremaine, S., 1987, *Galactic Dynamics*, Princeton University Press  
 Blaauw, A., Gum, C.S., Pawsey, J.L., Westerhout, G., 1960, *MNRAS*, 121, 123  
 Boesgaard, A.M., 1989, *ApJ*, 336, 798  
 Boesgaard, A.M., Budge, K.G., 1988, *ApJ*, 332, 410  
 Boesgaard, A.M., Friel, E.D., 1990, *ApJ*, 351, 467  
 Boss, L., 1908, *AJ*, 26, 31  
 Branch, D., Lambert, D.L., Tomkin, J., 1980, *ApJ*, 241, L83  
 Breger, M., 1968, *PASP*, 80, 578  
 Brosche, P., Denis-Karafistan, A.I., Sinachopoulos, D., 1992, *A&A* 253, 113  
 Brown, A., 1950, *ApJ*, 112, 225  
 Buchholz, M., 1977, *A&A*, 58, 377  
 van Bueren, H.G., 1952, *Bull. Astron. Inst. Neth.*, XI, 385  
 Cameron, L.M., 1985, *A&A*, 152, 250  
 Campbell, B., 1984, *ApJ*, 283, 209  
 Casertano, S., Iben, I., Shiels, A., 1993, *ApJ*, 410, 90  
 Caughlan, G.R., Fowler, W.A., 1988, *Atomic Data Nuc. Data Tables*, 40, 284  
 Cayrel de Strobel, G., 1980, In ‘Star Clusters’, Hesser, J.E. (ed.), *IAU Symp.* 85, Reidel, 91  
 Cayrel de Strobel, G., 1982, In ‘The Scientific Aspects of the Hipparcos Space Astrometry Mission’, *ESA SP-177*, 173  
 Cayrel de Strobel, G., 1990, *Mem. Soc. Astron. Ital.*, 61, 613  
 Cayrel de Strobel, G., 1996, *A&A Rev.*, 7, 243  
 Cayrel, R., Cayrel de Strobel, G., Campbell, B., Däppen, W., 1984, *ApJ*, 283, 205  
 Cayrel, R., Cayrel de Strobel, G., Campbell, B., 1985, *A&A*, 146, 249  
 Chaffee, F.H., Carbon, D.F., Strom, S.E., 1971, *ApJ*, 166, 593

- Christensen-Dalsgaard, J., 1982, *MNRAS*, 199, 735
- Christensen-Dalsgaard J., 1991, in 'Challenges to Theories of the Structure of Moderate-Mass Stars', Gough D.O., Toomre J. (eds), Springer-Verlag, 11
- Corbin, T.E., Smith, D.L., Carpenter, M.S., 1975, *Bull. Am. Astron. Soc.*, 7, 337
- Crawford, D.L., 1975, *AJ*, 80, 955
- Dame, T.M., Ungerechts, H., Cohen, R.S., de Geus, E.J., Grenier, I.A., May, J., Murphy, D.C., Nyman, L.-Å., Thaddeus, P., 1987, *ApJ* 322, 706
- Detweiler, H.L., Yoss, K.M., Radick, R.R., Becker, S.A., 1984, *AJ*, 89, 1038
- Dommanget, J., Nys, O., 1994, *Comm. Obs. R. de Belg., Serie A*, No. 115
- Dravins, D., Lindegren, L., Madsen, S., Holmberg, J. 1997, in *HIPPARCOS Venice '97*, ESA SP-402, 733
- Eddington, A.S., 1913, *MNRAS*, 73, 359
- Eggen, O.J., 1960, *MNRAS*, 120, 540
- Eggen, O.J., 1967, *Ann. Rev. Astron. Ast.*, 5, 105
- Eggen, O.J., 1969, *ApJ*, 158, 1109
- Eggen, O.J., 1982, *ApJSS*, 50, 221
- Eggen, O.J., 1992, *AJ*, 104, 1482
- Eggen, O.J., 1993, *AJ*, 106, 1885
- Eggen, O.J., 1995, *AJ*, 110, 823
- ESA, 1997, *The Hipparcos and Tycho Catalogues*, ESA SP-1200
- Feast, M.W., Whitelock, P.A., 1997, *MNRAS*, in press
- Foy, R., 1975, In 'Abundance Effects in Classification', Hauck, B. Keenan, P.C. (eds), *IAU Symp.* 72, Reidel, 209
- Fuente Marcos, R. de la, 1995, *A&A*, 301, 407
- Gatewood, G., Castelaz, M., de Jonge, J.K., Persinger, T., Stein, J., Stephenson, B., 1992, *ApJ*, 392, 710
- Golay, M., 1972, In 'Problems of Calibration of Absolute Magnitudes and Temperatures of Stars', Hauck, B., Westerlund, B.E. (eds), *IAU Symp.* 54, Reidel, 27
- Grevesse N., Noels A., 1993a, in 'Origin and Evolution of the Elements', Prantzos, N., Vangioni-Flam E., Cassé, M. (eds), Cambridge University Press
- Grevesse N., Noels A., 1993b, 'Association Vaudoise des Chercheurs en Physique', 'La Formation des Elements Chimiques', Hauck, B., Plantani, S., Raboud, D., (eds)
- Griffin, R.F., Gunn, J.E., Zimmerman, B.A., Griffin, R.E.M., 1988, *AJ*, 96, 172
- Guenther, D.B., 1989, *ApJ* 339, 1156
- Gunn, J.E., Griffin, R.F., Griffin, R.E.M., Zimmerman, B.A., 1988, *AJ*, 96, 198
- Hanson, R.B., 1975, *AJ*, 80, 379
- Hanson, R.B., 1977, *BAAS*, 9, 585
- Hanson, R.B., 1980, In 'Star Clusters', Hesser, J.E. (ed.), *IAU Symp.* 85, Reidel, 71
- Hanson, R.B., Vasilevskis, S., 1983, *AJ*, 88, 844
- Hardorp, J., 1981, *A&A*, 105, 120
- Hauck, B., 1981, *A&A*, 99, 207
- Heckmann, O., Lübeck, K., 1956, *Z. Astrophys.*, 40, 1
- Heintz, W.D., 1988, *PASP*, 100, 839
- Helfer, H.L., 1969, *AJ*, 74, 1155
- Hénon, M., 1970, *A&A*, 9, 24
- Henry, T.J., McCarthy, D.W., Jr., 1993, *AJ*, 106, 773
- Hertzprung, E., 1909, *ApJ*, 30, 135
- Hodge, P.W., Wallerstein, G.W., 1966, *PASP*, 78, 411
- Ianna, P.A., McNamara, B.R., Greason, M.R., 1990, *AJ*, 99, 415
- Iben, I., 1967, *Ann. Rev. Astron. Ast.*, 5, 571
- Iben, I., Tuggle, R.S., 1972, *ApJ*, 173, 135
- Iglesias C. A., Rogers F. J., 1996, *ApJ* 464, 943
- Innanen, K.A., Harris, W.E., Webbink, R.F., 1983, *AJ*, 88, 338
- Jaschek, C., Jaschek, M., 1987, *The Classification of Stars*, Cambridge University Press
- Johnson, H.L., Mitchell, R.I., Iriarte, B., 1962, *ApJ*, 136, 75
- Jones, D.H.P., 1971, *MNRAS*, 152, 231
- Kholopov, P.N., 1969, *Soviet AJ*, 12, 4
- King, I.R., 1962, *AJ*, 67, 471
- King, I.R., 1966, *AJ*, 71, 64
- Klemola, A.R., Harlan, E.A., McNamara, B., Wirtanen, C.A., 1975, *AJ*, 80, 642
- Koester, D., Weidemann, V., 1973, *A&A*, 25, 437
- Kovalevsky, J., Lindegren, L., Froeschlé, M., et al., 1995, *A&A*, 304, 34
- Kroupa, P., 1995, *MNRAS*, 277, 1522
- Lebreton, Y., Michel, E., Goupil, M.J., Baglin, A., Fernandes, J., 1995, In 'Astronomical and Astrophysical Objectives of Sub-Millarcsecond Optical Astrometry', Høg, E., Seidelman, P.K., (eds), *IAU Symp.* 166, Kluwer, 135
- Lindegren, L., 1989, In 'The Hipparcos Mission', ESA SP-1111, Vol. III, Chapter 18.
- Lindegren, L., Kovalevsky, J., 1995, *A&A*, 304, 189
- Lindegren, L., 1995, *A&A*, 304, 61
- Lindegren, L., Röser, S., Schrijver, H., et al., 1995, *A&A*, 304, 44
- Loktin, A.V., Matkin, N.V., Fedorov, V.V., 1987, *Sov. Astron.*, 31, 582
- Loktin, A.V., Matkin, N.V., 1989, *Astron. Nachr.*, 310(3), 231
- Luri, X., Arenou, F., 1997, in *HIPPARCOS Venice '97*, ESA SP-402, 449
- Lutz, T.E., 1970, *AJ*, 75, 1007
- Lutz, T.E., Kelker, D.H., 1973, *PASP*, 85, 573
- Ma, C., et al., 1997, *IERS Technical Note* 24, Obs. de Paris
- Maeder, A., 1971, *A&A*, 10, 354
- Maeder, A., Mermilliod, J.-C., 1980, *A&A*, 93, 136
- Mason, B.D., McAlister, H.A., Hartkopf, W.I., Bagnuolo, W.G., 1993, *AJ*, 105, 220
- Mathieu, R.D., 1985, In 'Dynamics of Star Clusters', Goodman, J., Hut, P. (eds), *IAU Symp.* 113, Reidel, 427
- McAllister, H.A., 1977, *AJ*, 82, 487
- McClure, R.D., 1982, *ApJ*, 254, 606
- Mermilliod, J.C., 1995, In 'Information and On-line Data in Astronomy', Egret, D., Albrecht, M.A. (eds), Kluwer, 127
- Morel P., 1993, *IAU Coll.* 137, In 'Inside the Stars', Weiss, W.W., Baglin, A. (eds), *ASP Conf. Ser.*, 40, 445
- Morel, P., 1997, *A&ASS*, in press
- Morgan, B.L., Beckmann, G.K., Scaddan, R.J., Vine, H.A., 1982, *MNRAS*, 198, 817
- Morris, S.C., 1992, *JRASC*, 86, 292
- Morris, S.C., Luyten, W.J., 1983, *BAAS*, 15, 683
- Murray, C.A., 1989, *A&A*, 218, 325
- Murray, C.A., Harvey, G.M., 1976, *R. Greenwich Obs. Bull.*, 182, 15
- Nelson, B., Young, A., 1970, *PASP*, 82, 699
- Oort, J.H., 1979, *A&A*, 78, 312
- Pagel, B.E.J., 1995, In 'Astronomical and Astrophysical Objectives of Sub-Millarcsecond Optical Astrometry', Høg, E., Seidelman, P.K., (eds), *IAU Symp.* 166, Kluwer, 181
- Patterson, R.J., Ianna, P.A., 1991, *AJ*, 102, 1091
- Pearce, J.A., 1955, *PASP*, 67, 23
- Pels, G., Oort, J.H., Pels-Kluyver, H.A., 1975, *A&A*, 43, 423
- Perryman M.A.C., Lindegren, L., Kovalevsky, J., et al., 1995, *A&A*, 304, 69

- Peterson, D.M., Solensky, R., 1987, ApJ, 315, 286
- Peterson, D.M., Stefanik, R.P., Latham, D.W., 1993, AJ, 105, 2260
- Reid, N., 1992, MNRAS, 257, 257
- Reid, N., 1993, MNRAS, 265, 785
- Scarfe C.D., Batten A.H., Fletcher J.M., 1990, Publ. DAO XVIII, 21
- Schaller, G., Schaerer, D., Meynet, G., Maeder, A., 1992, A&SS, 96, 269
- Schwan, H., 1990, A&A, 228, 69
- Schwan, H., 1991, A&A, 243, 386
- Seares, F.H., 1944, ApJ, 100, 255
- Seares, F.H., 1945, ApJ, 102, 366
- Sears, R.L., Whitford, A.E., 1969, ApJ, 155, 899
- Smart, W.M., 1938, Stellar Dynamics, Cambridge University Press
- Smart, W.M., 1939, MNRAS, 99, 168
- Smith, H., Eichhorn, H., 1996, MNRAS, 281, 211
- Spitzer, L. 1975, In 'Dynamics of Stellar Systems', Hayli, A. (ed.), IAU Symp. 69, Reidel, 1
- Stefanik, R.P., Latham, D.W., 1985, In 'Stellar Radial Velocities', Davis Philip, A.G., Latham, D.W. (eds), IAU Coll. 88, L. Davis Press, 213
- Strömberg, G., 1922, ApJ, 56, 265
- Strömberg, G., 1923, ApJ, 57, 77
- Strömberg, B., Olsen, E.H., Gustafsson, B., 1982, PASP, 94, 5
- Taylor, B.J., 1980, AJ, 85, 242
- Taylor, B., 1997, In 'Fundamental Stellar Properties: the Interaction between Observation and Theory', IAU Symp. 189, in press
- Terlevich, E., 1987, MNRAS, 224, 193
- Thackeray, A.D., 1967, In 'Determination of Radial Velocities and their Application', Batten, A.H., Heard, J.F. (eds), IAU Symp. 30, Academic Press, 163
- Theuns, T., 1992a, A&A, 259, 493
- Theuns, T., 1992b, A&A, 259, 503
- Torres, G., Stefanik, R.P., Latham, D.W., 1997a, ApJ, 474, 256
- Torres, G., Stefanik, R.P., Latham, D.W., 1997b, ApJ, 479, 268
- Torres, G., Stefanik, R.P., Latham, D.W., 1997c, ApJ, in press
- Turner, D.G., Garrison, R.F., Morris, S.C., 1994, JRASC, 88, 303
- Upgren, A.R., 1974, AJ, 79, 651
- Upgren, A.R., Weis, E.W., Fu, H.-H., Lee, J.T., 1990, AJ, 100, 1642
- Upton, E.K.L., 1970, AJ, 75, 1097
- Upton, E.K.L., 1971, AJ, 76, 117
- VandenBerg, D.A., Bridges, T.A., 1984, ApJ, 278, 679
- VandenBerg, D.A., Poll, H.E., 1989, AJ, 98, 1451
- Wallerstein, G., Hodge, P.W., 1967, ApJ, 150, 951
- Wayman, P.A., 1967, PASP, 79, 156
- Wayman, P.A., Symms, L.S.T., Blackwell, K., 1965, Royal Obs. Bull., No. 98
- Weidemann, V., Jordan, S., Iben, I., Casertano, S., 1992, AJ, 104, 1876
- Wielen, R., 1967, Veroff. Astr. Rechen-Inst., Heidelberg, 19
- Wielen, R., 1974, Proc. First European Astronomical Meeting, Mavridis, L.N. (ed.), 2, 326
- Wielen, R., 1997, A&A, in press

This article was processed by the author using Springer-Verlag L<sup>A</sup>T<sub>E</sub>X A&A style file L-AA version 3.